2017-12

Theoretical study of structure, vibrational spectra and thermodynamic properties of cluster ions existing in vapours over barium dihalides

Jacob, Fortunatus

NM-AIST

THEORETICAL STUDY OF STRUCTURE, VIBRATIONAL SPECTRA AND THERMODYNAMIC PROPERTIES OF CLUSTER IONS EXISTING IN VAPOURS OVER BARIUM DIHALIDES

Fortunatus Jacob

A Dissertation Submitted in Partial Fulfillment of the Requirements for the Degree of Doctor of Philosophy in Materials Science and Engineering of the Nelson Mandela African Institution of Science and Technology

Arusha, Tanzania

December, 2017

ABSTRACT

Computational and theoretical methods were employed to study the structure, vibrational spectra and thermodynamic properties of cluster ions that were detected earlier in saturated vapour over barium dihalides. The equilibrium geometrical parameters and vibrational spectra were computed for the ions BaX_3^-, $Ba_2X_3^+$, $Ba_3X_5^+$, $Ba_4X_7^+$ and $Ba_5X_9^+$ (X= F, Br or I); the DFT/B3P86 and MP2 methods with triple-zeta valence basis sets were used. The ions BaX_3^-, $Ba_2X_3^+$, $Ba_3X_5^+$ and $Ba_5X_9^+$ were confirmed to correspond to D_{3h} point group of symmetry and $Ba_4X_7^+$ to C_{2v} configuration. Alternative structures for the cluster ions have been considered but no isomers were identified. The structural parameters and frequencies calculated with different theoretical approaches appeared to be not much sensitive regarding the methods and basis sets used.

The enthalpies of ion molecular reactions were obtained both theoretically through the total energies of participants and based on experimental data through the equilibrium constants measured earlier. The enthalpies of formation $\Delta_f H^o(0)$ of the ions have been determined (in kJ mol^{-1}): -1356 ± 4 (BaF_3^-); -1039 ± 12 ($Ba_2F_3^+$); -2179 ± 16 ($Ba_3F_5^+$); -3277 ± 35 ($Ba_4F_7^+$); -4316 ± 22 ($Ba_5F_9^+$); -858 ± 6 ($BaBr_3^-$); -293 ± 10 ($Ba_2Br_3^+$); -982 ± 20 ($Ba_3Br_5^+$); -1644 ± 30 ($Ba_4Br_7^+$); -2282 ± 17 ($Ba_5Br_9^+$); -709 ± 6, (BaI_3^-); -96 ± 12 ($Ba_2I_3^+$); -654 ± 17 ($Ba_3I_5^+$); -1177 ± 20 ($Ba_4I_7^+$); -1686 ± 20 ($Ba_5I_9^+$).

The dimer molecules existing in vapours over the respective barium dihalides were studied, the thermodynamic properties and vapour compositions of their isomers were computed. For Ba_2F_4, Ba_2Cl_4 and Ba_2Br_4, three isomers of C_{3v}, C_{2v} and C_{2h} symmetries were confirmed to exist while for Ba_2I_4 only two isomers, C_{3v} and C_{2h} were confirmed. For all isomers, the pyramidal isomer (C_{3v}), was observed to be predominant at lower temperatures up to about 700 K followed by *trans-* and *cis-*isomers. The pyramidal isomer possesses higher magnitude of enthalpy of dissociation reaction and hence more stable than other isomers at ambient temperature. The enthalpies of formation of the C_{3v} isomers were obtained (in kJ mol^{-1}): -1874 ± 2 (Ba_2F_4); -1236 ± 7 (Ba_2Cl_4); -1023 ± 8 (Ba_2Br_4); -787 ± 11 (Ba_2I_4).

DECLARATION

I, **FORTUNATUS JACOB** do hereby declare to the Senate of the Nelson Mandela African Institution of Science and Technology that this dissertation is my own original work and that it has neither been submitted nor being concurrently submitted for degree award in any other institution.

_____   _____

Name and signature of candidate   **Date**

The above declaration is confirmed

_____   _____

Name and signature of supervisor (1)   **Date**

_____   _____

Name and signature of supervisor (2)   **Date**

COPYRIGHT

CERTIFICATION

The undersigned certify that they have read dissertation titled "***Theoretical Study of Structure, Vibrational Spectra and Thermodynamic Properties of Cluster Ions Existing in Vapours over Barium Dihalides***" and recommend for examination in fulfillment of the requirements for the degree of Doctor of Philosophy of Materials Science and Engineering of the Nelson Mandela African Institution of Science and Technology.

_____

Professor Alexander M. Pogrebnoi

(Supervisor)

_____

Professor Tatiana P. Pogrebnaya

(Supervisor)

ACKNOWLEDGEMENT

DEDICATION

I dedicate this work to my parents **Jacob N. Rwabululi** & **Florentina Clemence** and my sisters **Theopista Jacob** and **Victoria Jacob**.

TABLE OF CONTENTS

LIST OF TABLES

LIST OF FIGURES

LIST OF APPENDICES

LIST OF ABBREVIATIONS AND SYMBOLS

B1	Middle size basis set
B1PW91	Becke Hartree-Fock exchange, Perdew nonlocal Perdew-Wang local correlation
B2	Extended basis set
B3LYP	Becke-Lee-Yang-Parr DFT functional
B3P86	Becke-Perdew DFT functional
BHHLYP	Becke-Hartree-Fock-exchange functional, Lee-Yang-Parr correlation functional
BSSE	Basis set superposition error
CC	Coupled cluster
cc-pVTZ	Correlation consistent, polarized valence triple zeta basis set
CCSDT	Coupled cluster single, double and triple excitations
CI	configuration interaction
CP	Counterpoise method
DFT	Density functional theory
ECP	Effective core potential
EMSL	The Environmental molecular science laboratory US
GAMESS	General Atomic and Molecular Electronic Structure System
HF	Hartee-Fock theory
MO	Molecular orbital
MP2	2nd order Møller-Plesset perturbation theory
MP3	3rd order Møller-Plesset perturbation theory
MP4	4th order Møller-Plesset perturbation theory
PES	Potential energy surface
RS-PT	Rayleigh-Schrödinger perturbation theory
SCF	Self consistent field
SDB-aug-cc-pVTZ	Stuttgart–Dresden–Bonn–augmented correlation consistent polarized valence triple zeta basis set
T	Temperature

$\Delta_f H°(0)$	Enthalpy of formation
$\Delta_r E$	Energy of dissociation reaction
$\Delta_r E_{iso}$	Energy of isomerization reaction
$\Delta_r G°(T)$	Gibbs free energy of dissociation reaction
$\Delta_r H°(0)$	Enthalpy of dissociation reaction
$K_p^°$	Equilibrium constant
$\Sigma\omega_{i\_prod}$	Sum of vibrational frequencies of the products
$\Sigma\omega_{i\_react}$	Sum of vibrational frequencies of the reactants
p_i	Partial pressure of a reactant
p_j	Partial pressure of a product
Φ_{HF}	Hartree-Fock reference configuration
$\Delta_r\Phi°(T)$	Reduced Gibbs energy of a reaction
$\Delta_r\varepsilon$	Zero point vibration energy (ZPVE) correction
Ψ	Wave function
c	Speed of light in free space
h	Planck constant
R	Gas constant

CHAPTER ONE

1.0   Introduction

1.1   Background Information

The term "alkaline earths" referred only to calcium, strontium and barium but later on the definition was extended to the entire group 2 elements (Alkali Earth Metals, 2017). The elements of this group lose two *s* orbital electrons found in their outermost shell and thus attain a positive charge of 2. The ion formed has the desired complete octet of *s* and *p* orbital electrons in its outermost energy level. When halogens like fluorine, chlorine, bromine, iodine and astatine combine chemically with alkaline-earth elements, alkaline earth halides of different species (like $M_2X_3^+$, $M_3X_5^+$) may be formed in the vapor over the solid alkaline earth halides (Pogrebnoi *et al*., 1984; Pogrebnoi, 1981).

There has been an interest in the structure of gaseous alkaline earth halide molecules as they have important practical applications, from halogen metallurgy, chemical vapor transport and deposition, to the lamp industry (Binnewies, 1998). Alkaline earth halide lamps provide more light from less power and have been applied in diverse areas, from horticulture to dermatology and dentistry (Hilpert & Niemann, 1997). The behavior of alkaline earth metals in the presence of halogens, their effect as impurities or additives in combustion systems, also warrants the knowledge of the molecules that might be formed in these processes (Devore & Gole, 1999). Recent developments in combustion syntheses of nanoscale refractory solids of high purity and controlled size distribution also call for a better understanding of vapor-phase metal halide systems (Devore & Gole, 1999; Fontijn, 1998).

Several methods for computing the structure and vibrational frequencies of different species are available (Cramer, 2004). They are based on quantum mechanics. The most common methods used for computing the geometrical structure and vibrational frequencies are: Hartree-Fock (HF) theory, Møller-Plesset (MP) perturbation theory and Density Function Theory (DFT) (Cramer, 2004; Zatula, 2012). These quantum chemical methods have been proved to be useful tools in explaining the main characteristics of cluster ions (Pogrebnaya *et al*., 2007; Pogrebnaya *et al*., 2008; Elliot *et al*., 2005). Various ionic species in vapor over MX_2 molecules were revealed

experimentally but there is little or no information on their structural and thermochemical properties.

Alkaline earth metal halides form a research area that has attracted the interests of many researchers for decades (Axten *et al.*, 1994; Hargittai *et al.*, 2001; Hargittai, 2000, 2005; Levy & Hargittai, 2000; Molntir *et al.*, 1995; Réffy *et al.*, 2005; Seijo *et al.*, 1991; Varga *et al.*, 2006). Much effort has been devoted in understanding the geometrical properties and vibrational spectra of different alkaline earth metal halides (Hargittai, 2000; Seijo *et al.*, 1991; Pogrebnoi *et al.*, 2013). These studies, both experimental and theoretical, have concentrated on neutral species; monohalides, dihalides and dimers (Calder, 1969; Donald & Hoffmann, 2006; Ehlert *et al.*, 1964; Hargittai, 2000; Kaupp *et al.*, 1991; Levy & Hargittai, 2000).

Levy and Hargittai applied density functional theory to compute the properties of six different isomers of Ca_2X_4, Sr_2X_4, and Ba_2X_4, (X = F and Cl) (Levy & Hargittai, 2000). For these isomers, they were able to identify a correlation between the linear/bent structural preference in the monomers and the D_{2h}/C_{3v} structural preference in the dimer. In their findings, they provided computational evidence that, for the dimers Ca_2F_4, Sr_2F_4, Ba_2F_4 and Ba_2Cl_4, the D_{2h} configuration is not a local minimum on the potential energy surface. To the moment, the Ba dibromide and diiodide dimers are not fully characterized experimentally or studied using reliable computational methods.

Few studies have attempted to investigate ionic species of alkaline earth metal halides (Butman *et al.*, 2001; Butman, 2002; Elliott *et al.*, 2005; Moustapher *et al.*, 2016; Pogrebnoi *et al.*, 2013 and Pogrebnoi, 1981) For instance, Elliot *et al* conducted an investigation on MX_3^- (M = Ca and Mg, X = Cl and Br) superhalogens using photoelectron spectroscopic and *ab* initio theoretical methods (Elliott *et al.*, 2005). They considered also the corresponding neutral species in order to analyze their structures and stabilities. Electron binding energies and vertical detachment energies were determined. The results show that these ions fall in the category of superhalogens. However, the tetraatomic negative ions and their corresponding neutral species of other alkaline earth metals (e.g. Ba and Sr) for all halogens are not well studied. In his work, Pogrebnoi investigated ionic species MX_3^-, $M_2X_3^+$, $M_3X_5^+$ and $M_4X_7^+$ (M = alkaline earth metal, X = halogen) using high temperature mass spectrometer and measured equilibrium constants of the

ion molecular dissociation reactions (Pogrebnoi, 1981). More detailed information on geometrical structures and vibrational spectra were not possible to obtain experimentally.

1.2 Theoretical Approaches and Computational Methods

1.2.1 An Overview of the Methods

Theoretical and computational works compliment experimental studies. The difficulties in some experimental studies intrigue application of theoretical and computational methods in studying a wide range of species (Hargittai, 2000). One of the advantages of theoretical and chemical computational methods is the ability of providing information about stable, unstable/intermediate molecules or even transition state which is difficult to study experimentally. The improvement of computational techniques and basis sets offers a possibility of producing computed structural information that is compatible with the level of precision of experimental data. Therefore, the theoretical and quantum chemical computational methods are good compliments of experimental works.

Quantum chemistry can be defined as a branch of chemistry that employs principles of quantum mechanics in the study of physical models and experiments of different chemical systems. It is sometimes referred to as molecular quantum mechanics (Quantum Chemistry, 2016). It is the branch of computational method primarily dealing with computing the properties of a system of an atom by applying quantum mechanics. The properties of an atom can be obtained by solving the Schrödinger equation. The electrons of atom can be modeled by describing how they behave and their energy can be determined from the system. The wave function (Ψ) is used in quantum mechanics to represent all the information about the particle. It is the mathematical representation of an electron or group of electrons' position with respect to the nucleus and to each other at a given time. By using the wave function (Ψ), the position of a particle at any time can be predicted, and it is given as the square of the absolute wave function (Cramer, 2004):

$$P(x,t) = |\psi(x,t)|^2 \tag{1.1}$$

It is very important to know the molecular structure of a system. Usually every system at a stable state has a minimum energy. Therefore the equilibrium structure of the molecule is obtained at the lowest energy and it corresponds to the global minimum of a Potential Energy Surface (PES). This surface is made up of points in which all points represent the possible energies of a system. Also each PES point is associated with a molecular structure. To obtain the global minimum

PES, one can apply Hamiltonian on that wave function that results to an eigen-value representing the energy of that system, given by the following equation (Cramer, 2004):

$$H\Psi = E\Psi \tag{1.2}$$

where H is the Hamiltonian operator which include the kinetic and potential energies of the nuclei and electrons, Ψ is the total wavefunction and E is the total energy.

Particles in a system do not move independently, they interact with one another through the forces of attraction and repulsion. Thus, when dealing with polyatomic system, the wave function of such systems is very difficult to express because of the correlation motions of particles. The problem was solved by splitting the wave function into electronic and nuclear components following the Born-Oppenheimer approximation (Cramer, 2004; Zatula, 2012). This approximation is based on great mass difference between electrons and nuclei. As a result, electrons are assumed to be moving with high speed while nuclei are considered to be fixed at a point. This enables the electronic wave function to be determined separately for each given nuclear configuration.

The Hamiltonian operator is comprised of five terms that contribute to the total energy: kinetic energies of the electrons (T_e), kinetic energies of the nuclei (T_n), the attraction of electrons to the nuclei (V_{en}), the interelectronic repulsion (V_{ee}) and internuclear repulsion (V_{nn}), which can be symbolically represented as:

$$H = T_e + T_n + V_{en} + V_{ee} + V_{nn} \tag{1.3}$$

If we consider a system with N_{nuclei} nuclei and N_{elec} electrons, after application of Born-Oppenheimer approximation, the electronic Hamiltonian operator is written as:

$$H_e = -\sum_{i=1}^{N_{elec}} \frac{1}{2}\nabla_i^2 - \sum_{i=1}^{N_{elec}}\sum_{A=1}^{N_{nuclei}} \frac{Z_A}{|R_A - r_i|} + \sum_{i=1}^{N_{elec}}\sum_{j>1}^{N_{elec}} \frac{1}{|r_i - r_j|} + \sum_{A=1}^{N_{nuclei}}\sum_{B=1}^{N_{nuclei}} \frac{Z_A Z_B}{|R_A - R_B|} \tag{1.4}$$

From the equation above, the first term on the right hand side represents the electronic kinetic energy of electrons, the second term is the nuclear-electron attraction, the third term stands for electron-electron repulsion and the last term on the right is the nuclei-nuclei repulsion potential energies. Furthermore, the symbols R and r represent the nuclear positions (A, B), the symbols (i,

j) stand for electronic coordinates corresponding to different centers, *Z* stands for atomic number and ∇ represents the gradient operator.

The Hamiltonian operator is determined by the number of electrons and the potential created by the nuclei in terms of charges and positions. This is because the last term in Eq. 1.4 is a constant as the nuclei are fixed. Potential Energy Surface (PES) of a molecule is given by the changes in electronic energies as a function of nuclear positions. The most stable structure of the molecule can be obtained from the global minimum of energy on the PES. The second derivatives of the energy with respect to the nuclear positions provide the Hessian which can be transformed into the harmonic vibrational modes of the molecule. This work intends to solve the Schrödinger equation in order to obtain information about the geometrical structures and vibrational properties of the molecules and ions.

It is possible to solve exactly the Schrödinger equation for only one-electron atoms like hydrogen atom. For multi-electron systems, approximation methods are required. Up to the moment, there are two different approaches for solving the Schrödinger equation: molecular orbital theory (Hartree-Fock and post-Hartree-Fock Theory) and density functional theory (DFT).

1.2.2   Hartree – Fock (HF) Method

The Hartree-Fock (HF) theory can be defined as the chemical computational method that can be used to determine the ground state wave function and corresponding energy of multi-electron system sometimes called *Ab Initio*. It is the simplest approach used in solving Schrödinger equation where each electron in *n*-electron system moves in an average field created by the *n*-1 other electrons and the nuclei. Electron correlation is neglected as the electron-electron repulsion is only included as an average of all of the electrons.

Through this method, the Schrödinger equation is iteratively solved for electronic wave function for a system of electrons that move in each other's static average potential. HF theory is based on two major approximations to solve the Schrödinger equation namely: Slater Determinant and Basis Set Expansion. The Slater determinant is a combination of one-electron orbitals that satisfy the requirement of the Pauli Exclusion Principle; the electronic wave function is ant-symmetric with respect to the exchange of two electrons. The second approximation means each electron spin orbital is expressed as a linear combination of basis set functions (Cramer, 2004; Zatula,

5

2012). The solution of the electronic Schrödinger equation is based on the variation principle, which states that any approximation solution to the Schrödinger equation has an energy above or equal to the exact energy of the system concerned.

In the HF method the Schrödinger equation is reduced to a set of Fock equations using the variation principle, the solution of which gives the Molecular Orbital coefficients. The HF equations have to be solved iteratively to optimize the coefficients to minimize the electronic energy, and this procedure is called the Self Consistent Field (SCF) method. HF method is viewed as a stepping stone on the way to exact solution of the Schrodinger equation because it provides a very well defined energy which can be converged in the limit of an infinite basis set, and the difference between that converged energy and reality is the electron correlation energy (ignoring relativity, spin–orbit coupling, etc.) (Vasiliu, 2010).

The Hartree-Fock theory has one major shortcoming which is the assumption that each electron moves in the average potential of the other electrons. The consequence of this is overestimation of the answers such as energy and other parameters computed from the energy (Leach, 2001; Zatula, 2012).

1.2.3 Møller-Plesset (MP) Perturbation Theory

The energy predicted by Hartree-Fock (HF) theory is higher than the energy that could be obtained if electron-electron interactions were fully included. This effect of electron-electron interaction was introduced by means of Rayleigh-Schrödinger perturbation theory (RS-PT). The Hamiltonian of the Schrödinger equation was split into two Hermiatian parts, one which is soluble and the other not. The soluble part is called unperturbed Hamiltonian or zeroth order and unsoluble part is termed as perturbation. The solution of perturbed term can be obtained through power series expansion theory. The theory was introduced by Christian Møller and Milton S. Plesset as a post Hartree-Fock theory. The second-order (MP2), third-order (MP3), or fourth-order (MP4) were obtained as a result of inclusion of electron-electron interaction. But MP2 recovers around 90% of the correlation energy while MP3 has no significant enhancement upon the MP2 results (Zatula, 2012). And MP4 recovers about 98% of the correlation energy hence good results are expected from this order. Hamiltonian contains pair wise attraction and repulsion terms, implying that no particle is moving independently of all of the others.

1.2.4   Density Function Theory (DFT)

Another common method used in quantum chemical calculations is Density Functional Theory (DFT) method. It is a fundamental theory based on the assumption that for an arbitrary system of electrons, moving in an external potential, the ground state electron density solely determines the external potential (Cramer, 2004; Parr & Yang, 1989; Parr *et al*., 1989; Rajagopal & Callaway, 1973). Since the total number of electrons is determined by electron density, the Hamiltonian of the system as well as the full ground-state wave function is also determined. The Density Function Theory can either be restricted or unrestricted depending on the treatment of electron spin. In the restricted approach the spatial components of the spin orbitals are assumed to be identical for each pair of electrons while for the spin unrestricted calculations, the complete sets of the molecular orbitals are used. In this method, the energy is the function of four terms. The terms which contribute energy to the total system are: the interaction between nuclei and the electrons, kinetic energy of a non-interacting system of electrons, coulombic repulsion between the electrons, and the last term is due to exchange and correlation interactions (Kohn & Sham, 1965; Zatula, 2012).

There are about five groups of functional available for use with DFT method. They are exchange functional, pure correlational functional, exchange correlational functional, hybrid functional and double hybrid functional. Each category consists of several functionals. For example the hybrid functionals are exemplified by B1P86 (Becke, 1988; Perdew & Zunger, 1981; Perdew, 1986a), B1LYP (Becke, 1988; Lee *et al*., 1988), BHHLYP (Becke, 1993a; Lee *et al*., 1988), B1PW91 (Becke, 1988; Perdew *et al*., 1992; Perdew & Wang, 1992), B3P86 (Becke, 1993; Perdew & Zunger, 1981; Perdew, 1986b), B3LYP1 (Becke, 1993; Lee *et al*., 1988), B3LYP (Becke, 1993; Lee *et al*., 1988), etc. In this work the Becke-Perdew functional (B3P86) which is a hybrid functional (Becke, 1993b, 2014; Perdew & Zunger, 1981; Perdew, 1986a) was employed for all computations where the DFT method was used.

1.2.5   Coupled-Cluster (CC) Theory

Coupled-Cluster (CC) theory is one of the best techniques/methods for estimating the electron correlation energy (Bartlett & Purvis, 1978; Bartlett, 1989; Čížek, 1966; Pople *et al*., 1978; Purvis & Bartlett, 1982; Watts *et al*., 1993). This theory is based on the assumption (Cramer, 2004) that the wave function can be approximated as:

$$\Psi_{CC} = e^T \Phi_{HF} \tag{1.6}$$

$$e^T = 1 + T + \frac{1}{2}T^2 + \frac{1}{6}T^3 + \ldots\ldots = \sum_{k=0}^{\infty} \frac{1}{k!}T^k \tag{1.7}$$

In the above equation, we have expanded the exponential in a Taylor series form. T is the cluster operator and Φ_{HF} is the HF reference configuration, and T can be defined as:

$$T = T + T^2 + T^3 + \ldots\ldots\ldots + T^n \tag{1.8}$$

From above, n describes a specific degree of excitation: n=1 are singles, n=2 are doubles, n=3 are triple excitation etc. Usually the cluster operator has to be truncated at certain levels of excitation in order to avoid scaling up as in the full-CI method.

In contrast with the CI methods, the CC methods and MP theory are consistent with size. The CC methods have demonstrated good results in terms of accuracy and correlation energy recovered as compared to MP methods. The challenge with CC methods is that they are expensive and extremely time consuming with up to N^7 scaling. Based on these factors, this study relied more on DFT, MP2 and MP4 methods. For MP methods, the Basis Set Superposition Error (BSSE) with Counterpoise (CP) correction was applied to further improve the results. Details of the methods can be found in chapter two (section 2.2).

1.3   Research Problem and Justification of Study

The knowledge of geometrical structure and vibrational frequencies is vital to fundamental research on molecules and ions. The positive and negative cluster ions have been discovered to exist in vapours over alkaline earth halides under high temperature mass spectrometry studies. These ions as well as other similar charged particles were proved to be important in advanced high technology applications such as ion thrusters, magneto-hydrodynamic (MHD) generators, ion implantation, aerospace investigations, etc. By now, there is a lack of data on structural properties and vibration spectra of these species. Quantum chemical methods are well rooted in chemical and physical problems through Schrödinger equation solution (Bartlett, 1989; Bisseling & Kosloff, 1985). A theoretical investigation of the structure, vibration frequencies and thermodynamic properties of $BaCl_3^-$, $Ba_2Cl_3^+$, $Ba_3Cl_5^+$, and $Ba_4Cl_7^+$ cluster ions have already been carried out using quantum chemical methods (Pogrebnoi *et al.*, 2013). Yet, little or no detail analyses have been reported on other barium halide ions over BaX_2 (X represents a halogen).

Therefore, there is a need of computing the geometrical structure, vibration spectra and thermodynamic properties of cluster ions existing in vapours over barium dihalides using quantum chemical calculations.

1.4 Objectives

1.4.1 Main Objective

The aim of this work is the quantum chemical study of the geometrical structure, vibrational spectra and thermodynamic properties of the ions BaX^+, $Ba_2X_3^+$, $Ba_3X_5^+$, $Ba_4X_7^+$, $Ba_5X_9^+$, BaX_3^- and dimer molecules Ba_2X_4 (where X is F, Br or I).

1.4.2 Specific Objectives

i. To evaluate the accuracy of computational methods through comparison of theoretical results and reference data available for neutral BaX_2, Ba_2X_4 molecules and diatomic BaX^+ ions.

ii. To determine the geometrical structure and vibrational frequencies of BaX-cluster ions.

iii. To identify the possible isomers among the alternative structures for the species.

iv. To calculate the thermodynamic functions of the ions like heat capacity, entropy, reduced Gibbs free energy and enthalpy increment.

v. To determine thermodynamic properties: energies, enthalpies of dissociation reactions and enthalpies of formation of the clusters.

vi. To evaluate relative abundance and thermodynamic properties of the Ba_2X_4 isomers (X = F, Cl, Br or I).

1.5 Research Questions

i. What is an accuracy of computational methods for determination of geometrical structure and vibrational frequencies of the BaX-cluster ions?

ii. What are the geometrical structures and vibrational frequencies of the BaX-ionic clusters?

iii. What are the possible isomers among the alternative structures of the species?

iv. What are the thermodynamic functions of the cluster ions considered?

v. What is the energy, enthalpy of formation and enthalpy of dissociation of the BaX- ions?

vi. What are the relative abundances and thermodynamic properties of the Ba_2X_4 isomers?

CHAPTER TWO

2.0   Cluster ions in saturated vapor over barium difluoride: structure and thermodynamic properties[1]

Abstract

Different cluster ions detected earlier in saturated vapor over barium fluoride have been studied here theoretically. The equilibrium geometrical parameters and vibrational spectra were obtained for the ions BaF_3^-, $Ba_2F_3^+$, $Ba_3F_5^+$, $Ba_4F_7^+$, and $Ba_5F_9^+$. The DFT/B3P86 and MP2 methods were implemented with the TZVP basis sets including the diffuse and polarized basis functions. The enthalpies of ion molecular reactions were obtained both theoretically and based on experimental data. The enthalpies of formation $\Delta_f H^o(0)$ of the species were determined (in kJ mol^{-1}): -1356 ± 4 (BaF_3^-); -1039 ± 12 ($Ba_2F_3^+$); -2179 ± 16 ($Ba_3F_5^+$); -3277 ± 35 ($Ba_4F_7^+$); -4316 ± 22 ($Ba_5F_9^+$).

2.1   Introduction

An interest in the structure and properties of gaseous alkaline earth halide cluster ions has not declined due to a variety of applications. Heavy ions are applicable in ion thrusters (Benson & Patterson, 2009; Patterson, 2008), where accelerated ion beams generate a propellant force. Also ion beams may be used in magneto-hydrodynamic (MHD) generators (Smirnov, 2012), ion implantation technologies (Michael & Allan, 1994) and aerospace investigations (Duncan, 2000; Huenecke, 2002). The molecular and ionic clusters may serve as building blocks of novel materials (Castleman & Khanna, 2007; Khanna & Jena, 1995; Rao *et al*., 2000), useful in assembling crystals (Khanna & Jena, 1992); and also useful in chemical vapor transport and deposition (Binnewies, 1998; Hendricks *et al*., 1998; Ottosson *et al*., 1989). The understanding of behavior of alkaline earth metals in the presence of halogens, their effect as impurities or additives in combustion systems also require information on the cluster ions in vapor phase (Devore & Gole, 1999).

Alkali earth halide cluster ions were detected experimentally by using high temperature mass spectrometry (Pogrebnoi *et al*., 1984; Pogrebnoi, 1981). However, experimental data on the geometrical structure and vibrational spectra of the species are not available. A theoretical

---

investigation of the properties of $BaCl_3^-$, $Ba_2Cl_3^+$, $Ba_3Cl_5^+$, and $Ba_4Cl_7^+$ ions had been carried out (Pogrebnoi *et al.*, 2013) using quantum chemical methods. The structural properties of similar calcium chloride cluster ions were investigated recently (Moustapher *et al.*, 2016). In equilibrium vapor over barium difluoride, the $Ba_2F_3^+$, $Ba_3F_5^+$ and $Ba_4F_7^+$ ions were detected by mass spectrometric technique, and equilibrium constants of the ion molecular reactions were measured (Pogrebnoi *et al.*, 1984; Pogrebnoi, 1981). Until now, there is no information reported regarding cluster ions in saturated vapour over barium difluoride, BaF_2. Therefore, this work intends to investigate the family of cluster ions BaF_3^-, $Ba_2F_3^+$, $Ba_3F_5^+$, $Ba_4F_7^+$ and $Ba_5F_9^+$ and achieve the following specific objectives:

(i)   to determine the geometrical structure and vibrational spectra of the species;

(ii)   to examine an existence of possible isomers for the heavier ions $BaF^+(BaF_2)_n$ with $n = 1–4$.

(iii) to calculate the thermodynamic functions on the basis of geometrical parameters and vibrational frequencies obtained;

(iv)   to determine enthalpies of dissociation reactions and enthalpies of formation of the species.

2.2   Computational details

The calculations were performed using the Firefly QC package (Granovsky, 2012), which is partially based on the GAMESS (US) (Schmidt *et al.*, 1993) source code, and implementing the following methods: the electron density functional theory (DFT) with the functional B3P86, and the second and fourth order Møller–Plesset perturbation theory (MP2 and MP4). For the barium atom, the effective core potential with the def2-TZVP basis set 6s4p3d1f (Kaupp *et al.*, 1991) has been applied while for the fluorine atom, the two full-electron basis sets, including the diffuse and polarized basis functions, have been utilized. The first one is a mid-sized basis set 6s4p1d (Dunning, 1989) denoted as B1, incorporated into the software (Granovsky, 2012; Schmidt *et al.*, 1993), and the second one is extended, aug-cc-pVTZ 5s4p3d2f (Kendall *et al.*, 1992), denoted as B2 and accessed from the EMSL library (The Environmental Molecular Sciences Laboratory, U.S.) (Feller, 1996; Schuchardt *et al.*, 2007). In calculations by MP2, MP4 methods no orbitals were 'frozen', the option NCORE=0 was applied. The combination of the two methods (DFT and MP2) and two basis sets (B1 and B2) provided us with the following four theoretical approaches: DFT B1, MP2 B1, DFT B2, and MP2 B2 which were used to optimize the geometric parameters of the species and calculate the vibrational frequencies. The

11

geometrical structures and vibrational spectra were visualized and analyzed using the Chemcraft (Zhurko, 2015) and the MacMolPlt (Bode & Gordon, 1998) software.

The theoretical values of enthalpies of the reactions $\Delta_r H°(0)$ were computed through the total energies $\Delta_r E$ and zero point vibrational energy (ZPVE) $\Delta_r \mathcal{E}$ of the reactions as follows:

$$\Delta_r H^o(0) = \Delta_r E + \Delta_r \mathcal{E} \tag{2.1}$$

$$\Delta_r E = \Sigma E_{i\_prod} - \Sigma E_{i\_react} \tag{2.2}$$

$$\Delta_r \mathcal{E} = 1/2 hc(\Sigma \omega_{i\_prod} - \Sigma \omega_{i\_react}) \tag{2.3}$$

where E_{i_prod} and E_{i_react} are the total energies of the products and reactants, respectively, h is the Planck's constant, c is the speed of light in vacuum, ω_{i_prod} and ω_{i_react} are the vibrational frequencies of the products and reactants, respectively. All theoretical approaches including the DFT, MP2, and MP4 methods with B1 and B2 basis sets were employed in calculations of the $\Delta_r H°(0)$ values. To get more accurate results for the MP2 and MP4 methods, the basis set superposition error (BSSE) was taken into account through the counterpoise (CP) correction (Boys & Bernardi, 1970; Solomonik *et al*., 2005) To illustrate the procedure, the dissociation reaction of the $Ba_2F_3^+$ ion is considered as an example:

$$Ba_2F_3^+ \rightarrow BaF^+ + BaF_2 \tag{2.4}$$

According to (Solomonik *et al*., 2005), the dissociation of each reactant and product into atomic ions are taken into account as follows:

$$Ba_2F_3^+ \rightarrow 2Ba^{2+} + 3F^- \tag{2.5}$$

$$BaF^+ \rightarrow Ba^{2+} + F^- \tag{2.6}$$

$$BaF_2 \rightarrow Ba^{2+} + 2F^- \tag{2.7}$$
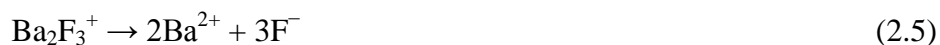
The energies of reactions (2.5) – (2.7) with the BSSE are equal to:

$$\Delta_r E(2.5) = 2E(Ba^{2+}/Ba_2F_3^+) + 3E(F^-/Ba_2F_3^+) - E(Ba_2F_3^+)$$

$$\Delta_r E(2.6) = E(Ba^{2+}/BaF^+) + E(F^-/BaF^+) - E(BaF^+)$$

$$\Delta_r E(2.7) = E(Ba^{2+}/BaF_2) + 2E(F^-/BaF_2) - E(BaF_2)$$

Since the reaction (2.4) may be presented as a combination of Eqs. (2.5) – (2.7), the BSSE corrected energy for dissociation of the $Ba_2F_3^+$ is given by

$$\Delta_r E(2.4) = \Delta_r E(2.5) - \Delta_r E(2.6) - \Delta_r E(2.7)$$

The similar procedure was used to determine the energies of dissociation reactions with BSSE correction for other cluster ions. The selection of the fragment position (Ba^{2+} or F^- within the species) was unambiguous for simple species (BaF^+, BaF_2, BaF_3^-, and $Ba_2F_3^+$). But for larger

12

clusters ($Ba_3F_5^+$, $Ba_4F_7^+$, and $Ba_5F_9^+$), alternative choices were possible. Each case was examined, the energies of the fragments were calculated, and the enthalpy of dissociation reaction $\Delta_r H°(0)$ of the cluster was found. Finally the choice of the fragment position was dictated by the better agreement of the calculated values $\Delta_r H°(0)$ with those based on experiment; the data array on the similar species was also involved in the analysis.

2.3 Results and discussion

2.3.1 Properties of simple species BaF, BaF^+, BaF_2 and BaF_2^+

The calculated values of geometrical parameters, vibrational frequencies, ionization energies, and dipole moments are presented in Table 1 for the diatomic species BaF, BaF^+, and for monomer molecule BaF_2 and BaF_2^+ ion. The BaF possesses open electronic shell, its ground state is $X\,^2\Sigma^+$.

Concerning the internuclear separations calculated through different methods, the values of R_e(Ba–F) are the same (for BaF) or slightly longer (for BaF^+ and BaF_2) for MP2 method compared to DFT. The extension of basis set from B1 to B2 results in decrease in the values of R_e(Ba–F) by 0.001–0.016 Å (within the same approach, DFT B1 → DFT B2 or MP2 B1 → MP2 B2). The magnitude of the valence angle in the BaF_2 molecule is also not much sensitive to the basis set with the same approach, the difference between DFT and MP2 values is about 2–2.5°. For BaF^+ and BaF_2, the variations in vibrational frequencies are in relationship to internuclear separations as increase in the distances corresponds to decrease in frequencies, while for BaF this tendency is not held. The magnitudes of the dipole moments follow the trend: the longer the bond length, the bigger is the dipole moment.

For the species considered, one can compare our results with some experimental data available (Table 2.1). The calculated values of R_e(Ba–F) are longer by ~0.02 Å for BaF and ~0.03– 0.05 Å for BaF^+ compared to reference. There is no reliable experimental data on the geometrical parameters of the BaF_2 molecule; our results are in reasonable agreement with the previous theoretical data [Kaupp *et al.*, 1991; Levy & Hargittai, 2000]: our DFT values are close to 118º calculated using B3LYP functional [Levy & Hargittai, 2000], while our MP2 results are close to 123º found by CISD (Kaupp *et al.*, 1991). As compared to the barium difluoride molecule BaF_2 which has a valence angle of 119.4^o (bent), the barium difluoride ion BaF_2^+ has a valence angle of 180° (linear). The two species have the same values of R_e(Ba–F) for the shorter basis set B1 while for the extended basis set B2, the value is slightly higher for BaF_2 than BaF_2^+.

Table 2.1. Theoretical and experimental properties of the BaF, BaF^+, and BaF_2 species.

Property	DFT B1	MP2 B1	DFT B2	MP2 B2	Reference
BaF					
R_e(Ba–F)	2.185	2.185	2.181	2.181	2.1595[a], 2.160[b], 2.162[c]
$-E$	125.45454	125.04488	125.45494	125.13322	
ω_e	463	469	471	478	470[b], 469[c]
μ_e	3.5		3.3		
IE_{ad}	4.95	4.70	4.92	4.67	4.7 ± 0.3[d]
					4.8034 ± 0.0004[e]
					4.59 ± 0.06[c]
					4.85[f]
IE_{ver}	4.99	4.72	4.96	4.70	4.9 ± 0.3[g]
					4.59 ± 0.06[h]
					4.7 ± 0.3[d]
BaF^+					
R_e(Ba–F)	2.110	2.127	2.109	2.118	2.077[e]
$-E$	125.27262	124.87229	125.27415	124.96166	
ω_e	534	520	542	536	535[e]
BaF_2					
R_e(Ba–F)	2.236	2.262	2.233	2.246	2.258[i], 2.236[j]
α_e(F–Ba–F)	119.4	121.9	119.5	121.4	118[j], 123[k]
$-E$	225.40756	224.82747	225.40770	225.00207	
$\omega_1 (A_1)$	442	426	448	442	416[l1], 437[l2], 421[l3], 415[m]
$\omega_2 (A_1)$	96	90	96	91	95[n]
$\omega_3 (B_1)$	422	403	429	422	392[l1], 413[l2], 398[l3]
μ_e	7.1	7.3	6.9	7.1	
IE_{ad}	10.35		10.30		
IE_{ver}	10.66	11.36	10.63	11.57	
BaF_2^+					
R_e(Ba–F)	2.236		2.227		
α_e(F–Ba–F)	180		180		
$-E$	225.02714		225.02920		

Note: R_e(Ba−F) is the equilibrium internuclear distance, Å; α_e(F−Ba−F) is the valence angle, degs; E is the total energy, au; ω_i are the vibrational frequencies, cm^{-1}; IE_{ad} and IE_{ver} are the adiabatic and vertical ionization energies, respectively, eV; μ_e is the dipole moment, D
Notes to the reference data: [a](Herzberg & Huber, 1979); [b](Kushawaha, 1973); [c]accessed from NIST (www.nist.gov); [d](Lau *et al*., 1989) accessed from NIST (www.nist.gov); [e](Jakubek *et al*., 1994); [f](Rosen, 1988); [g](Ehlert *et al*., 1964); [h](Belyaev *et al*., 1990); [i](Donald & Hoffmann, 2006); [j](Levy & Hargittai, 2000); [k](Kaupp *et al*., 1991); [l1]MI(Kr)-IR; [l2]MI(Ne)-IR; [l3]MI(Ar)-IR (l1, l2, l3 measured in (Snelson, 1966), retrieved from (Hargittai, 2000), and (Krasnov *et al*., 1979)); [m]IR, measured in (Baikov, 1969), retrieved from (Krasnov *et al*., 1979); [n]measured in (Baikov, 1968), retrieved from (Krasnov *et al*., 1979).

As for vibrational spectra of the diatomic species, the calculated frequencies correspond well to the experimental data (Knight, 1971; Kushawaha, 1973), MP2 B2 being preferable. For BaF_2, our results for ω_1 and ω_3 look slightly bigger than experimental data (Baikov, 1969) but agree

well for ω_2 with data (Baikov, 1968; Snelson, 1966). The discrepancy for the valence modes may be attributed partly to the matrix shifting effect. Note that our results closely relate to the value estimated for the gaseous phase, $\omega_1 = 440$ and $\omega_3 = 416$ cm^{-1} (Hargittai, 2000). It is worth to note that our result for BaF_2 confirms the remark by Hargittai (Hargittai, 2000) that the symmetric stretching frequency ω_1 is bigger than asymmetric ω_3 on the contrary to other alkali-earth dihalides (Hargittai, 2000; Levy & Hargittai, 2000).

The values of internuclear separations R_e(Ba–F) for BaF, BaF$^+$, and BaF$_2$ versus method of determination are plotted in Fig. 2.1; the results obtained earlier for BaCl, BaCl$^+$, BaCl$_2$ (Pogrebnoi *et al*., 2013) are shown for comparison. The plots for frequencies of the diatomic species are given in Fig. 2.2. It is seen that the tendencies for barium fluoride species are similar to those for barium chloride.
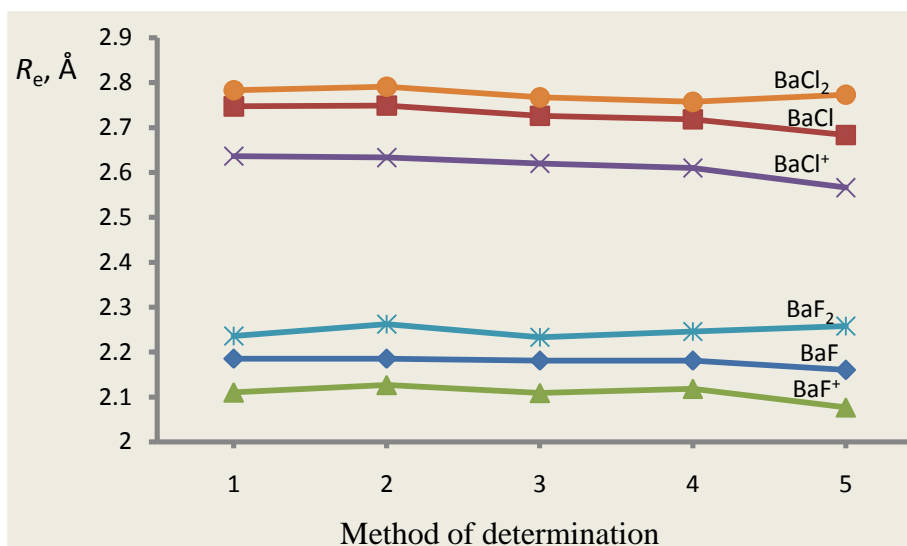
Figure 2.1. Internuclear separation versus method of determination for BaF, BaF$_2$, BaCl, BaCl$_2$, BaF$^+$, and BaCl$^+$. 1−DFT B1, 2−MP2 B1, 3−DFT B2, 4−MP2 B2 and 5−Reference.

Generally, the results obtained across all computational levels applied are in good agreement with the literature data, both theoretical and experimental. Analysis of the calculated geometrical parameters and vibrational frequencies has shown that these properties are not much sensitive to the theoretical levels applied. Therefore, the methods DFT B2 and MP2 B2 were applied for the heavier species except for Ba$_4$F$_7$$^+$ and Ba$_5$F$_9$$^+$ where MP2 was not achievable. For these exceptional species, DFT B1 and DFT B2 methods were employed.
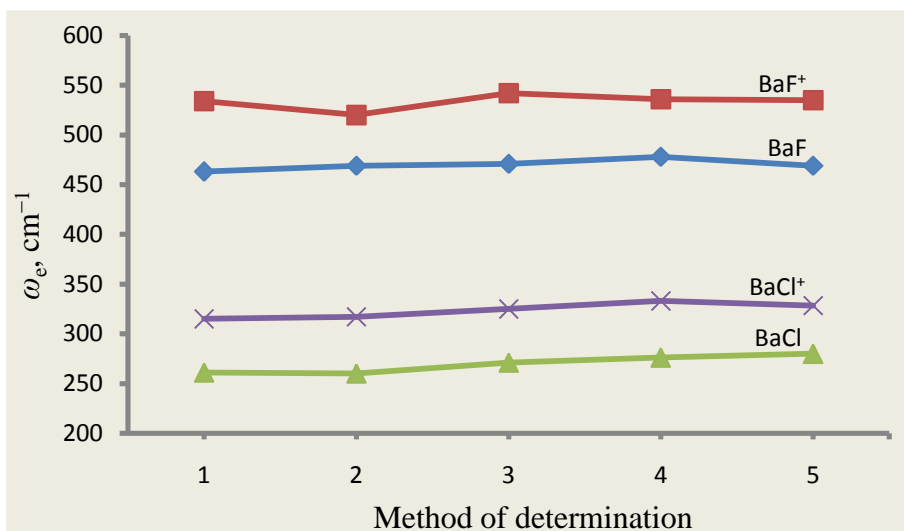
Figure 2.2. Vibrational frequencies versus computational methods for BaF, BaF$^+$, BaCl and BaCl$^+$ species. 1−DFT B1, 2−MP2 B1, 3−DFT B2, 4−MP2 B2 and 5−Reference.

Ionization energies, adiabatic IE_{ad} and vertical IE_{ver}, were calculated as the energy difference between the ionic and neutral states. For the adiabatic values, the optimized coordinates were used for both states, while for vertical values the parameters were optimized only for the neutral species and for the ions were accepted the same. As is seen the calculated magnitudes are sensitive to the methods applied (from DFT to MP2, the values of IE decrease by ~0.2–0.3 eV for BaF and increase by ~0.7–0.9 eV for BaF$_2$) but are not sensitive to the basis set used. Within the same theoretical approach, the vertical ionization energies are slightly bigger than the adiabatic, by $0.02 − 0.04$ eV for BaF, and essentially bigger, by ~0.3 eV, for BaF$_2$. If we compare our theoretical values with the experimental data available for BaF, the MP2 results are in better accordance.

2.3.2   Tetraatomic negative ion BaF$_3^-$

The geometrical structure and vibrational spectrum of the tetraatomic negative ion BaF$_3^-$ have been determined; the results are shown in Table 2.2. The equilibrium configuration of the BaF$_3^-$ ion is planar of the D_{3h} symmetry (Fig. 2.3a). The respective parameters calculated by two methods are in a good agreement between each other. Compared to the neutral BaF$_2$ molecule, the internuclear distance R_e(Ba–F) in BaF$_3^-$ is essentially bigger, by 0.14 Å, and the stretching frequencies are lower by ~80 cm^{-1} (MP2). Worth to note that the angle α(F–Ba–F) = 120º is close to that in the molecule BaF$_2$. The peculiarity of the BaF$_2$ vibrational spectrum mentioned above that the symmetric

stretching frequency is higher than asymmetric one, remains in the spectrum of BaF_3^- ion; the difference between ω_1 and ω_3 being 20 cm^{-1} (MP2) for both species. The deformational frequency $\omega_4 = 97$ cm^{-1} which corresponds to the in-plane bending mode is very close to $\omega_2 = 91$ cm^{-1} of the BaF_2 molecule. The lowest frequency 51 cm^{-1} is assigned to the out-of-plane vibration mode.

The geometrical structure and vibrational spectrum of the BaF_3^- ion are similar to those of $BaCl_3^-$ (Pogrebnoi *et al.*, 2013) and $CaCl_3^-$ (Moustapher *et al.*, 2016) ions, but for the latter two ions, the relationship between symmetric and asymmetric stretching modes differs as ω_1 is less than ω_3 ($\omega_1 = 214$ cm^{-1}, $\omega_3 = 225$ cm^{-1} for $BaCl_3^-$ and $\omega_1 = 213$ cm^{-1}, $\omega_3 = 341$ cm^{-1} for $CaCl_3^-$) which is more inherent to the alkaline earth halides species.
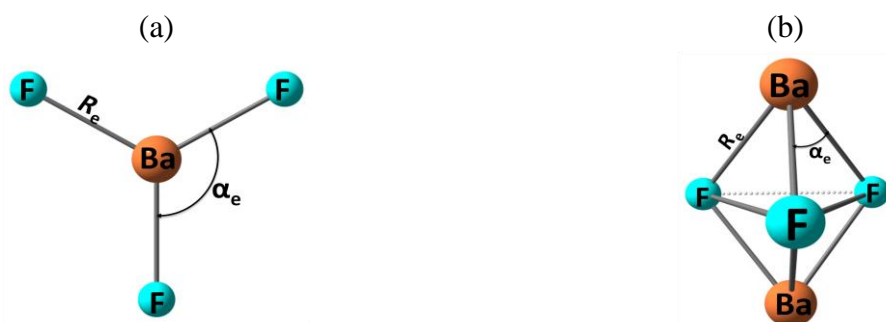
Figure 2.3. Equilibrium geometrical structures of the ions: (a) BaF_3^- (D_{3h}), (b) $Ba_2F_3^+$ (D_{3h}).

Table 2.2. Properties of the tetraatomic BaF_3^- (D_{3h}) ion.

Property	DFT B2	MP2 B2
R_e(Ba–F)	2.372	2.383
$-E$	325.38080	324.88669
$\omega_1\,(A_1')$	359 (0)	357 (0)
$\omega_2\,(A_2'')$	45 (2.1)	51 (2.2)
$\omega_3\,(E')$	335 (10.1)	337 (10.1)
$\omega_4\,(E')$	99 (1.0)	97 (1.1)

Note: R_e(Ba−F) is the equilibrium internuclear distance, Å; E is the total energy, au; ω_i are the vibrational frequencies, cm^{-1} and the values given in parenthesis near the frequencies are the intensities in IR spectrum, D^{2}amu^{-1}Å^{-2}.

2.3.3 Pentaatomic positive ion $Ba_2F_3^+$

The cyclic (kite-shaped) and bipyramidal structures were considered for the ion $Ba_2F_3^+$ but the cyclic one appeared to be not stable as the imaginary frequencies were revealed. The bipyramidal structure of D_{3h} symmetry was confirmed to be equilibrium, the barium atoms being in the vertices of the bipyramid and fluorine atoms in the horizontal plane (Fig. 2.3b). The parameters obtained by the DFT B2 and MP2 B2 methods agree well between each other, respectively (Table 2.3). The vertex angles of the bipyramid α_e(F–Ba–F) are about 71°, that is the pyramid is

stretched along the axis. The same structure (D_{3h}) was reported earlier for the ions $Ca_2Cl_3^+$ (Moustapher *et al*., 2016) and $Ba_2Cl_3^+$ (Pogrebnoi *et al*., 2013), for which three alternative configurations, linear, cyclic and bipyramidal, were considered but only the bipyramidal one was confirmed to be stable.

Table 2.3. Properties of the pentaatomic positive ion $Ba_2F_3^+$ (D_{3h}).

Property	DFT B2	MP2 B2
R_e(Ba–F)	2.411	2.413
α_e(F–Ba–F)	71.8	71.3
$-E$	350.81153	350.10662
$\omega_1\,(A_1')$	372 (0)	366 (0)
$\omega_2\,(A_1')$	159 (0)	160 (0)
$\omega_3\,(A_2'')$	364 (6.8)	370 (7.2)
$\omega_4\,(E')$	320 (4.6)	324 (4.8)
$\omega_5\,(E')$	171 (1.6)	173 (1.8)
$\omega_6\,(E'')$	227 (0)	240 (0)

Note: R_e is the equilibrium internuclear distance, Å; α_e is the valence angle, degs; E is the total energy, au; ω_i are the vibrational frequencies, cm^{-1} and the values given in parenthesis near the frequencies are the intensities in IR spectrum, D^{2}amu^{-1}Å^{-2}.

In the IR spectrum of the ion, three vibrational modes are active, asymmetric stretching $\omega_3\,(A_2'')$, $\omega_4\,(E')$ and the bending mode $\omega_5\,(E')$. No low frequencies are observed that is apparently due to the compactness of the bipyramidal structure.

It is worth to compare the properties of the $Ba_2F_3^+$ ion to those of the C_{3v} isomer of the dimeric molecule Ba_2F_4 as the latter is composed of the bipyramidal moiety Ba_2F_3 and F$^-$ atom attached as a tail. As it is mentioned above the lowest vibrational frequency of the isomer is attributed to the bending mode involving the terminal F$^-$ atom. The ion $Ba_2F_3^+$ looks more compact and stable, as far as detachment of the terminal loose F atom from the neutral dimer favours the stabilization of the ion.

2.3.4   Octaatomic positive ion $Ba_3F_5^+$

Two possible shapes of the octaatomic ion $Ba_3F_5^+$, the bipyramidal (D_{3h}) and two-cycled with the F-tail (C_{2v}), were considered. The latter appeared to be not stable as the imaginary frequencies were revealed while the bipyramidal structure was equilibrium one (Fig. 2.4). The structural parameters are given in Table 2.4. In the bipyramid, the alternating Ba and F_h atoms form the planar hexagonal Ba_3F_3 moiety with angles F_h–Ba–F_h and Ba–F_h–Ba equal to 138º and 102º, respectively. Other two fluorine atoms F_v in the vertices are triply coordinated and the angles

Ba–F_v–Ba are equal to 95º. The barium atoms are tetra-coordinated and bonded with F_v and F_h atoms. The bipyramid has a squeezed shape as the 'height' equal to the distance between two F_v atoms, 2.658 Å, is 1.7 times less than the 'width', the distance between two F_h atoms, 4.551 Å. Still the structure of this ion is rather stable and its energy is ~340 kJ mol^{-1} (MP2 B2) lower than the sum of energies of the $Ba_2F_3^+$ ion and BaF_2 molecule.

Figure 2.4. Equilibrium geometrical structure of the $Ba_3F_5^+$ ion: (a) view 1, (b) view 2.

The vibrational frequencies are in the range ~90–360 cm^{-1} thus no very low frequencies are observed. The lowest frequency ω_{12} (E'') = 89 cm^{-1} is not active in IR spectrum and corresponds to the swinging out-of-plane vibration of Ba and F_h. The most intensive vibrations are those with highest frequencies, ω_7 (E') = 360 cm^{-1} and ω_8 (E') = 311 cm^{-1}, which are assigned to the stretching vibrations of the Ba–F_v and Ba–F_h bonds, respectively.

Table 2.4. Properties of the octatomic $Ba_3F_5^+$ (D_{3h}) ion.

Property	DFT B2	MP2 B2
R_{e1}(Ba–F_h)	2.433	2.435
R_{e2}(Ba–F_v)	2.570	2.563
α_e(Ba–F_v–Ba)	94.9	95.6
β_e(Ba–F_h–Ba)	102.2	102.4
–E	576.33180	575.23894
ω_1 (A_1')	329 (0)	322 (0)
ω_3 (A_1')	275 (0)	283 (0)
ω_4 (A_1')	258 (0)	270 (0)
ω_2 (A_1')	154 (0)	159 (0)
ω_5 (A_2'')	245 (2.5)	248 (2.7)
ω_6 (A_2'')	109 (0.9)	107 (1.0)
ω_7 (E')	356 (10.2)	360 (11.6)
ω_8 (E')	314 (5.8)	311 (5.0)
ω_9 (E')	224 (1.5)	237 (1.5)
ω_{10} (E')	109 (0.3)	110 (0.2)
ω_{11} (E'')	215 (0)	225 (0)
ω_{12} (E'')	84 (0)	89 (0)

Note: R_{e1} and R_{e2} are the equilibrium internuclear distances, Å; α_e and β_e are the valence angles, degs; E is the total energy, au; ω_i are the vibrational frequencies, cm^{-1} and the values given in parenthesis near the frequencies are the intensities in IR spectrum, D^{2}amu^{-1}Å^{-2}.

2.3.5 Undecaatomic positive ion $Ba_4F_7^+$

Two computational methods, DFT B1 and DFT B2, were employed to find the geometrical parameters and vibrational spectrum of the ion $Ba_4F_7^+$. The parameters obtained are listed in Table 2.5. As is seen, the calculated internuclear separations slightly decrease or do not change from the basis set B1 to B2; the respective frequencies are in a good accordance with each other. The equilibrium configuration of the ion $Ba_4F_7^+$ corresponds to the C_{2v} point group of symmetry. Similar to $Ba_4Cl_7^+$ (Pogrebnoi $et\ al.$, 2013) the ion $Ba_4F_7^+$ may be considered as composed of $Ba_2F_3^+$ bipyramid and two molecules of BaF_2 attached (Fig. 2.5). The bipyramidal fragment $Ba_2F_3^+$ is distorted now; neither the Ba–F distances nor F–Ba–F angles are equivalent. The separation between Ba atoms in vertices is extended from 3.571 Å in $Ba_2F_3^+$ to 4.129 Å in $Ba_4F_7^+$. The BaF_2 moieties are more flattened compared to free molecule BaF_2; the angle F_3–Ba_1–F_3 is increased by ~20º, the distances Ba–F and F–F are elongated by 0.18 Å; and 0.67 Å, respectively. The Ba atoms which originated from BaF_2 fragments attached become tetra-coordinated in the $Ba_4F_7^+$ ion, while Ba atoms in the bipyramid become penta-coordinated. If we assume, the longer is the bond length, the lower is the strength, and then the new bonds formed between BaF_2 and $Ba_2F_3^+$ moieties appear to be comparable by strength with those within the moieties themselves.

(a)   (b)

Figure 2.5. Equilibrium geometrical structure of the $Ba_4F_7^+$ ion: (a) view 1; (b) view 2.

The energy of the undecaatomic $Ba_4F_7^+$ ion is ~275 kJ mol^{-1} lower than the sum of energies of octaatomic positive $Ba_3F_5^+$ ion and BaF_2 molecule or ~570 kJ mol^{-1} lower than the sum of the energies of pentaatomic positive $Ba_2F_3^+$ ion and two BaF_2 molecules. This decrease in energy may be attributed to the formation of new bonds Ba_1–F_3 and Ba_2–F_2.

Table 2.5. Properties of the undecaatomic $Ba_4F_7^+$ (C_{2v}) ion.

Property	DFT B1	DFT B2	Property	DFT B1	DFT B2
$R_{e1}(Ba_1-F_1)$	2.919	2.878	$\omega_9(A_1)$	42 (0.003)	41 (0.002)
$R_{e2}(Ba_1-F_2)$	2.588	2.587	$\omega_{10}(A_2)$	301 (0)	306 (0)
$R_{e3}(Ba_1-F_3)$	2.446	2.443	$\omega_{11}(A_2)$	263 (0)	263 (0)
$R_{e4}(Ba_2-F_1)$	2.558	2.559	$\omega_{12}(A_2)$	237 (0)	234 (0)
$R_{e5}(Ba_2-F_2)$	2.575	2.562	$\omega_{13}(A_2)$	104 (0)	102 (0)
$R_{e6}(Ba_2-F_3)$	2.432	2.427	$\omega_{14}(A_2)$	89 (0)	88 (0)
$\alpha_e(F_2-Ba_1-F_2)$	71.0	71.7	$\omega_{15}(B_1)$	189 (0.1)	189 (0.1)
$\alpha'_e(F_1-Ba_1-F_2)$	61.0	61.7	$\omega_{16}(B_1)$	173 (1.0)	176 (1.0)
$\beta_e(F_3-Ba_1-F_3)$	106.4	106.7	$\omega_{17}(B_1)$	152 (0.5)	151 (0.3)
$\gamma_e(F_3-Ba_2-F_3)$	140.2	141.5	$\omega_{18}(B_1)$	124 (0.2)	123 (0.2)
$-E$	801.85173	801.84415	$\omega_{19}(B_1)$	105 (0.2)	104 (0.3)
$\omega_1(A_1)$	367 (6.3)	367 (6.3)	$\omega_{20}(B_1)$	105 (0.1)	103 (0.1)
$\omega_2(A_1)$	354 (3.7)	361 (3.7)	$\omega_{21}(B_1)$	82 (0.1)	83 (0.03)
$\omega_3(A_1)$	342 (5.2)	342 (5.5)	$\omega_{22}(B_2)$	260 (1.0)	259 (0.8)
$\omega_4(A_1)$	298 (0.2)	320 (0.02)	$\omega_{23}(B_2)$	242 (0.6)	240 (0.6)
$\omega_5(A_1)$	303 (4.9)	308 (4.7)	$\omega_{24}(B_2)$	229 (0.3)	227 (0.3)
$\omega_6(A_1)$	293 (3.3)	295 (3.6)	$\omega_{25}(B_2)$	222 (0.4)	225 (0.4)
$\omega_7(A_1)$	270 (0.6)	271 (0.4)	$\omega_{26}(B_2)$	196 (0.7)	196 (0.7)
$\omega_8(A_1)$	85 (0.5)	83 (0.4)	$\omega_{27}(B_2)$	48 (0.2)	53 (0.2)

Note: R_{ei} are the equilibrium internuclear distances, Å; α_e, α'_e, β_e and γ_e are the valence angles, degs; E is the total energy, au; ω_i are the vibrational frequencies, cm^{-1} and the values given in parenthesis near the frequencies are the intensities in IR spectrum, D^{2}amu^{-1}Å^{-2}.

In the vibrational spectrum of the $Ba_4F_7^+$ ion, the highest frequencies assigned to the Ba–F stretching modes lie in the range 300–370 cm^{-1} that is similar to the $Ba_2F_3^+$ ion (Table 2.3). Two lowest frequencies, $\omega_9 = 41$ cm^{-1} and $\omega_{27} = 53$ cm^{-1}, correspond to the bending modes of the BaF_2 moieties. In the IR spectrum, there are five most intensive bands which relate to the stretching vibrations of the BaF_2 fragments ($\omega_1 = 367$ cm^{-1}, $\omega_2 = 361$ cm^{-1}, $\omega_5 = 308$ cm^{-1}, $\omega_6 = 295$ cm^{-1}) and of $Ba_2F_3^+$ moiety ($\omega_3 = 342$ cm^{-1}). Two frequencies of medium intensities, $\omega_{16} = 176$ cm^{-1} and $\omega_{22} = 259$ cm^{-1} are attributed to bending vibrations of the $Ba_2F_3^+$ fragment.

2.3.6 Tetradecaatomic cluster ion $Ba_5F_9^+$

In contrast to the positive ions considered above, the $Ba_5F_9^+$ ion was not detected experimentally, but its existence is feasible; it may be predicted since the attachment of three BaF_2 molecules to the core $Ba_2F_3^+$ bipyramid may result in a high symmetrical structure. This idea had been suggested previously regarding the similar $Ba_5Cl_9^+$ cluster ion but not accomplished (Pogrebnoi *et al.*, 2013).

The geometrical parameters and vibrational spectra of the tetradecaatomic cluster ion $Ba_5F_9^+$ have been studied at two computational levels, DFT B1 and DFT B2. Two configurations of the ion were considered, the polyhedron of D_{3h} (Fig. 2.6) symmetry and the chain structure composed of four cycles in mutually perpendicular planes, C_{2v} symmetry; the latter configuration appeared to be non-equilibrium. The properties of the $Ba_5F_9^+$ ion (D_{3h}) are reported in Table 2.6.

(a)   (b)
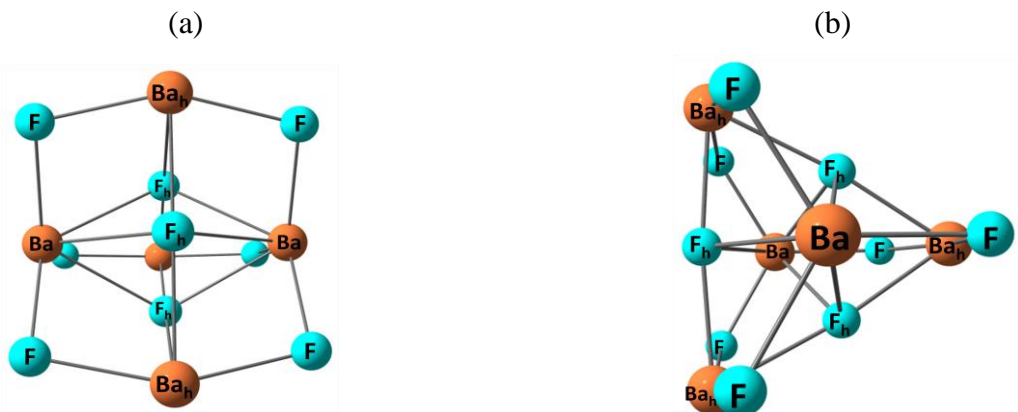
Figure 2.6. Equilibrium geometrical structure of the $Ba_5F_9^+$ ion: (a) view 1; (b) view 2.

The shape of the $Ba_5F_9^+$ ion looks like a 'three layered sandwich' (Fig. 2.6): two almost planar BaF_3 fragments on the top and bottom (the angle α_e(F–Ba–F) = 119.9°) and a hexagon $Ba_{h3}F_{h3}$ between in the middle of the polyhedron. This hexagon with six equivalent bonds Ba_h–F_h and three equivalent acute valence angles β_e(F_h–Ba_h–F_h) seems to be rather a triangle as the fragment Ba_h–F_h–Ba_h is nearly linear, $\angle Ba_h$–F_h–Ba_h = 173°. In the hexagon, the F_h and Ba_h atoms are tetra-coordinated. Other two Ba atoms originated from the bipyramid $Ba_2F_3^+$ form three new bonds with BaF_2 molecules attached and thus become hexa-coordinated. The new bonds are as strong as those within individual moieties. The formation of new bonds brings to the stabilization of the polyhedron. The energy of the tetradecaatomic $Ba_5F_9^+$ ion is ~230 kJ mol^{-1} lower than the sum of energies of undecaatomic positive $Ba_4F_7^+$ ion and BaF_2 molecule or ~800 kJ mol^{-1} lower than the sum of the energies of pentaatomic positive $Ba_2F_3^+$ ion and three BaF_2 molecules.

In the vibrational spectrum, the highest frequencies lie in the range ~260–365 cm^{-1} and attributed mostly to the stretching modes of Ba–F bonds of the BaF_2 fragments attached. The lowest frequencies are assigned to the wagging modes of BaF_2 moieties (ω_7 = 58 cm^{-1} and ω_{19} = 37 cm^{-1}), bending modes of the $Ba_2F_3^+$ moiety (ω_8 = 37 cm^{-1}) and combination of bending modes of both moieties (ω_{24} = 45 cm^{-1}). It is worth to remind that lower frequencies result in the major

impact on the thermodynamic functions. In the IR spectrum only five or six frequencies may be observed. The most intensive bands with frequencies $\omega_9 = 348$ cm^{-1}, $\omega_{10} = 295$ cm^{-1}, $\omega_{13} = 364$ cm^{-1}, $\omega_{14} = 280$ cm^{-1}, $\omega_{15} = 261$ cm^{-1} correspond to the stretching modes and $\omega_{16} = 161$ cm^{-1} to the bending mode of the $Ba_2F_3^+$ bipyramid.

Table 2.6. Properties of the cluster ion $Ba_5F_9^+$ (D_{3h}).

Property	DFT B1	DFT B2	Property	DFT B1	DFT B2
R_{e1}(Ba–F$_h$)	2.960	2.929	ω_{10} (A_2'')	290 (3.5)	295 (3.1)
R_{e2}(Ba$_h$–F$_h$)	2.613	2.605	ω_{11} (A_2'')	172 (0.8)	173 (0.8)
R_{e3}(Ba$_h$–F)	2.457	2.457	ω_{12} (A_2'')	69 (0.9)	72 (0.8)
R_{e4}(Ba–F)	2.419	2.414	ω_{13} (E')	363 (12.6)	364 (12.4)
α_e(F–Ba–F)	119.8	119.9	ω_{14} (E')	283 (4.5)	280 (6.4)
β_e(F$_h$–Ba$_h$–F$_h$)	66.4	66.8	ω_{15} (E')	258 (3.0)	261 (1.4)
$-E$	1027.34929	1027.33920	ω_{16} (E')	161 (3.1)	161 (2.9)
ω_1 (A_1')	357 (0)	356 (0)	ω_{17} (E')	108 (0.7)	109 (0.7)
ω_2 (A_1')	282 (0)	292 (0)	ω_{18} (E')	84 (0.9)	83 (0.8)
ω_3 (A_1')	218 (0)	215 (0)	ω_{19} (E')	38 (0.1)	37 (0.1)
ω_4 (A_1')	230 (0)	207 (0)	ω_{20} (E'')	302 (0)	308 (0)
ω_5 (A_1')	128 (0)	124 (0)	ω_{21} (E'')	276 (0)	274 (0)
ω_6 (A_1')	79 (0)	79 (0)	ω_{22} (E'')	166 (0)	167 (0)
ω_7 (A_1')	59 (0)	58 (0)	ω_{23} (E'')	90 (0)	89 (0)
ω_8 (A_1')	42 (0)	37 (0)	ω_{24} (E'')	35 (0)	45 (0)
ω_9 (A_2'')	348 (9.6)	348 (9.9)			

Note: R_{ei} are the equilibrium internuclear distances, Å; α_e and β_e are the valence angles, degs; E is the total energy, au; ω_i are the vibrational frequencies, cm^{-1} and the values given in parenthesis near the frequencies are the intensities in IR spectrum, D^{2}amu^{-1}Å^{-2}.

2.4 Enthalpies of dissociation reactions and enthalpies of formation of the species

The dissociation reactions with elimination of BaF_2 molecule were considered for the ions BaF_3^-, $Ba_2F_3^+$, $Ba_3F_5^+$, $Ba_4F_7^+$ and $Ba_5F_9^+$. Different levels of computation, DFT, MP2 and MP4 with the basis sets B1 and B2, were used to calculate the energies of the species. There was no optimization procedure for the MP4 method; for the ions BaF_3^-, $Ba_2F_3^+$ and $Ba_3F_5^+$ the optimized geometrical parameters were used as obtained by the MP2 method, while for $Ba_4F_7^+$ and $Ba_5F_9^+$ by DFT. Moreover in the calculation of enthalpies of dissociation reactions $\Delta_r H^o$ by the MP2 and MP4 methods the counterpoise correction (Boys & Bernardi, 1970; Solomonik *et al.*, 2005) was taken into consideration. Altogether ten computational methods, DFT B1, MP2 B1, MP4 B1, DFT B2, MP2 B2, MP4 B2, MP2^{CP} B1, MP4^{CP} B1, MP2^{CP} B2, and MP4^{CP} B2, were used.

The calculated enthalpies of reactions are given in Fig. 2.7 versus level of computation. An oscillatory behavior along the plots is observed for all ions. The increase in oscillation amplitude

is seen from the lighter to heavier clusters; for the ion BaF_3^- the deviation between the values is rather small, within 10 kJ mol^{-1}, but for the heaviest clusters the span reaches 47 kJ mol^{-1}. Note that alike oscillatory behavior was observed previously in calculated values of enthalpies of dissociation reactions for barium dichloride (Pogrebnoi *et al.*, 2013) and cesium halides [Mwanga *et al.*, 2015, 2016] clusters. As is seen in Fig. 2.7 along each plot, minimum values of $\Delta_r H^o$ correspond to the DFT and maximum to MP2 and MP4 methods. The CP corrections for the latter two methods may be estimated as the difference between MP2 and MP2^{CP} (or MP4 and MP4^{CP}) results; the values of these corrections are as follows: ~10–13 kJ mol^{-1} ($Ba_2F_3^+$ and $Ba_3F_5^+$), ~15 kJ mol^{-1} ($Ba_4F_7^+$), and ~30–40 kJ mol^{-1} ($Ba_5F_9^+$). Thus the CP corrections rise with size of the cluster, bringing an essential decrease in theoretical values $\Delta_r H^o$. The basis set superposition error was not taken into account in calculations by the DFT method because it was not much sensitive to the counterpoise correction if the basis set is sufficiently large (Perdew & Zunger, 1981). Also in previous work it was found that the CP corrections in the DFT results for dissociation reactions of CsF cluster ions were rather small and did not exceed 3 kJ mol^{-1} (Mwanga *et al.*, 2015).

Besides the theoretical results on the enthalpies of dissociation reactions, the values of $\Delta_r H^o(0)$ based on experimental equilibrium constants K^o_p, were obtained:

$$\Delta_r H^o(0) = -RT \ln K^o_p + T \Delta_r \Phi^o(T) \tag{2.9}$$

The equilibrium constants, K^o_p had been measured previously (Pogrebnoi *et al.*, 1984; Pogrebnoi, 1981) for heterophase ion-molecular reactions involving the $Ba_2F_3^+$, $Ba_3F_5^+$, and $Ba_4F_7^+$ ions (Table 2.7). In this work, the thermodynamic functions of the cluster ions have been calculated within the 'rigid rotator-harmonic oscillator' approximation; the OpenThermo software (Tokarev, 2007-2009) was used. The geometrical parameters and vibrational frequencies are implemented as obtained at the highest computational level, namely MP2 B2 for the $Ba_2F_3^+$ and $Ba_3F_5^+$, and DFT B2 for $Ba_4F_7^+$. The thermodynamic functions of the cluster ions are tabulated in Appendix A1. The thermodynamic functions of the barium difluoride in condensed phase, and BaF^+ ion were taken from the Ivtanthermo Database (Gurvich *et al.*, 2000). The enthalpy of sublimation of BaF_2, $\Delta_s H^o(0) = 396$ kJ mol^{-1} (Gurvich *et al.*, 2000) was added to the enthalpy of the heterophase reaction in order to obtain the enthalpy of the gas phase reaction. The values of $\Delta_r H^o(0)$ 'based on experiment' for the heterophase and gas phase reactions are given in Table 2.8 and for gas phase reactions are also displayed in Fig. 2.7 with horizontal lines.

Table 2.7. Equilibrium constants for heterophase ion molecular reactions measured experimentally at different temperatures (Pogrebnoi *et al.*, 1984; Pogrebnoi, 1981).

No	Reaction	$\ln K^{\circ}_p\,(T, K)$
1	$Ba_2F_3^+ = BaF^+ + BaF_2$	1.548 (1179); 1.603 (1179); 1.561(1182); 1.621 (1164); 1.421 (1213); 1.580 (1171); 1.591(1176); 1.748 (1160); 1.633 (1174); 1.578 (1191); 1.515(1203); 1.490 (1213); 1.458 (1203); 1.421 (1232); 1.437(1230); 1.573 (1198); 1.624 (1187); 1.647 (1175); 1.594(1197); 1.527 (1207); 1.690 (1158)
2	$Ba_3F_5^+ = BaF^+ + 2BaF_2$	5.394 (1291); 6.034 (1352)
3	$Ba_4F_7^+ = Ba_3F_5^+ + BaF_2$	4.786 (1352)
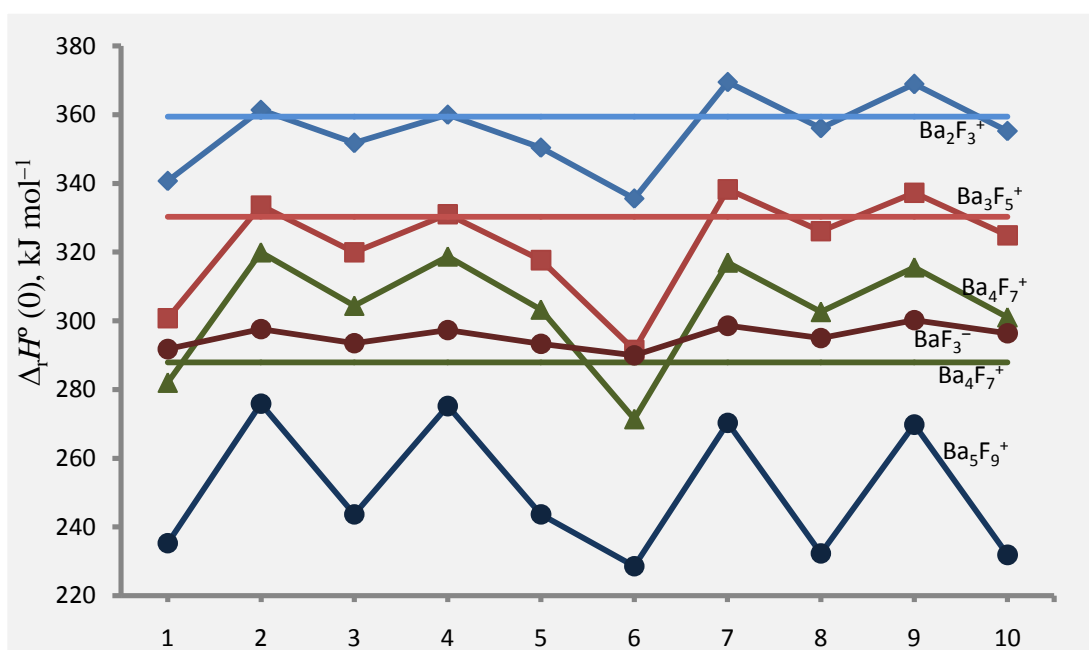
Figure 2.7. Enthalpies of dissociation reactions of the ions BaF_3^-, $Ba_2F_3^+$, $Ba_3F_5^+$, $Ba_4F_7^+$ and $Ba_5F_9^+$ versus level of computation compared with the experimental data which are shown by the horizontal lines: 1 – DFT B1, 2 – MP2 B1, 3 – MP2^{CP} B1, 4 – MP4 B1, 5 – MP4^{CP} B1, 6 – DFT B2, 7 – MP2 B2, 8 – MP2^{CP} B2, 9 – MP4 B2, 10 – MP4^{CP} B2.

The theoretical results on $\Delta_r H^{\circ}(0)$ for the ions $Ba_2F_3^+$, $Ba_3F_5^+$ and $Ba_4F_7^+$, are compared to the values 'based on experiment' in Fig. 2.7. One can see the DFT results with both basis sets, B1 and B2, are lower than experimental data by up to ~40 kJ mol^{-1}. The MP2 and MP4 methods provide rather good agreement with the 'based on experiment' data for the $Ba_2F_3^+$ and $Ba_3F_5^+$. For the ion $Ba_4F_7^+$, the accordance is not so good; the MP2 and MP4 results look essentially higher (up to 38 kJ mol^{-1}) and the value found by the highest level MP4^{CP} B2 remains still overrated by 13 kJ mol^{-1}. This discrepancy may be attributed partly to the experimental results which were not so much reliable compared to the lighter clusters; due to low intensities of $Ba_4F_7^+$ ion currents only a single measurement was carried out (Pogrebnoi *et al.*, 1984). For the BaF_3^-

and $Ba_5F_9^+$, there are no experimental data; the theoretical values of $\Delta_rH°(0)$ show similar trend as for other cluster ions.

In further processing, the data obtained by the eight methods MP2, MP2^{CP}, MP4, MP4^{CP} with both basis sets B1 and B2 were taken into account. We have disregarded the DFT results because this method did not provide an appropriate agreement with the 'based on experiment' data. The similar case, when the DFT method gave essentially underrated values, was observed for the barium chloride cluster ions $Ba_2Cl_3^+$ and $Ba_2Cl_5^+$ (Pogrebnoi et al., 2013). The accepted theoretical enthalpies of reactions were taken here as averages of the data arrays found by the MP2 and MP4 methods with both basis sets and CP corrections. The uncertainties in the accepted $\Delta_rH°(0)$ values were estimated on the base of half differences between maximum and minimum magnitudes of the $\Delta_rH°(0)$ obtained by eight methods (MP2, MP2^{CP}, MP4, MP4^{CP} with two basis sets B1 and B2); the similar approach of uncertainty estimation was used in previous works, e.g. (Pogrebnoi et al., 2013). The theoretical values of the enthalpies of reactions are given in Table 2.8 along with those 'based on experiment'. Between the theoretical and 'based on experiment' results, one can see almost coincidence for the $Ba_2F_3^+$ and for $Ba_3F_5^+$ ions and rather good agreement for the $Ba_4F_7^+$ ion.

Table 2.8. Enthalpies of dissociation reactions $\Delta_rH°(0)$ and enthalpies of formation $\Delta_fH°(0)$ of the cluster ions (in kJ mol^{-1}).

No	Reaction	$\Delta_rH°(0)$ based on experiment		Theoretical		Based on experiment
		Heterophase	Gaseous	$\Delta_rH°(0)$	$\Delta_fH°(0)$	$\Delta_fH°(0)$
1	$BaF_3^- \rightleftarrows BaF_2 + F^-$			297 ± 4	-1356 ± 4	
2	$Ba_2F_3^+ \rightleftarrows BaF^+ + BaF_2$	-36 ± 12	360 ± 12	359 ± 10	-1039 ± 10	-1039 ± 12
3	$Ba_3F_5^+ \rightleftarrows Ba_2F_3^+ + BaF_2$	-65 ± 16	331 ± 16	329 ± 10	-2177 ± 10	-2179 ± 16
4	$Ba_4F_7^+ \rightleftarrows Ba_3F_5^+ + BaF_2$	-107 ± 35	289 ± 35	310 ± 10	-3300 ± 10	-3277 ± 35
5	$Ba_5F_9^+ \rightleftarrows Ba_4F_7^+ + BaF_2$			255 ± 22	-4316 ± 22	

The theoretical enthalpies of dissociation reactions, $\Delta_rH°(0)$, for barium fluoride and chloride cluster ions are plotted versus the cluster size in Fig. 2.8. For both systems a similar trend is observed: increase of $\Delta_rH°(0)$ from the BaX_3^- to $Ba_2X_3^+$ ions, following by decrease for heavier clusters. One can suppose that the stability of the cluster may relate to the number and strength of the Ba–X bonds broken in the detachment of one BaX_2 molecule. In the BaX_3^- ions only one bond is broken, thus the lowest values of $\Delta_rH°(0)$ are seen both for BaF_3^- and $BaCl_3^-$. The highest enthalpy of dissociation is observed for the $Ba_2X_3^+$ ions which relates to the three shortest, hence strongest, Ba–X bonds to be torn. In the heavier clusters minimum four bonds are

to be broken but in spite of the bigger number of bonds, the $\Delta_r H^o(0)$ drops because the bonds weaken as it appears through the bond lengths elongation.
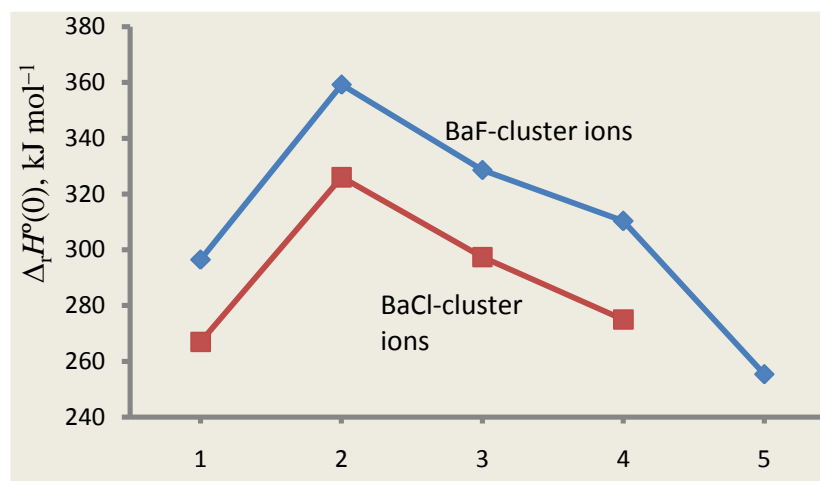
Figure 2.8. Enthalpies of dissociation reactions of the ions versus the size of the cluster: $1 - BaX_3^-$; $2 - Ba_2X_3^+$, $3 - Ba_3X_5^+$, $4 - Ba_4X_7^+$, $5 - Ba_5X_9^+$, where X = F or Cl.

The enthalpies of dissociation reactions, both theoretical and 'based on experiment', were employed to find the enthalpies of formation of the ions. The required values of $\Delta_f H^\circ(0)$ of gaseous species, 130.0 kJ mol^{-1} (BaF$^+$), -250.7 kJ mol^{-1} (F$^-$) and -809.7 kJ mol^{-1} (BaF$_2$), were taken from the Ivtanthermo Database (Gurvich *et al.*, 2000). A good agreement between the theoretical and experimental values of enthalpies of reactions $\Delta_r H^\circ(0)$ mentioned above obviously results in the same good agreement between the enthalpies of formation $\Delta_f H^\circ(0)$ of the ions accordingly (Table 2.8). As accepted magnitudes of $\Delta_f H^\circ(0)$ of the species we recommend values 'based on experiment' for the ions $Ba_2F_3^+$, $Ba_3F_5^+$ and $Ba_4F_7^+$, and theoretical values for the rest: BaF_3^- and $Ba_5F_9^+$.

The obtained enthalpies of formation of positive ions BaF$^+$(BaF$_2$)$_n$ are analyzed through the number of BaF$_2$ molecules attached (*n*); the values of $\Delta_f H^\circ(0)$ are plotted versus *n* in Fig. 2.9. For comparison a similar plot is added for the positive ions BaCl$^+$, $Ba_2Cl_3^+$, $Ba_3Cl_5^+$ and $Ba_4Cl_7^+$ reported earlier (Pogrebnoi *et al.*, 2013). Both graphs show dependences very close to linear with correlation coefficients 0.9995 for BaF$^+$(BaF$_2$)$_n$ and 0.9998 for BaCl$^+$(BaCl$_2$)$_n$, still the energy of the consequent detachment of one BaX$_2$ molecule slightly diminishes with increase in cluster size, from BaF$^+$ to $Ba_5F_9^+$ and from BaCl$^+$ to $Ba_4Cl_7^+$. The values of $\Delta_f H^\circ(0)$ for clusters ions of barium fluoride are lower and the slope of the plot is steeper compared to that of barium chloride which reflect more strong bonding in the family of BaF$^+$(BaF$_2$)$_n$ cluster ions.
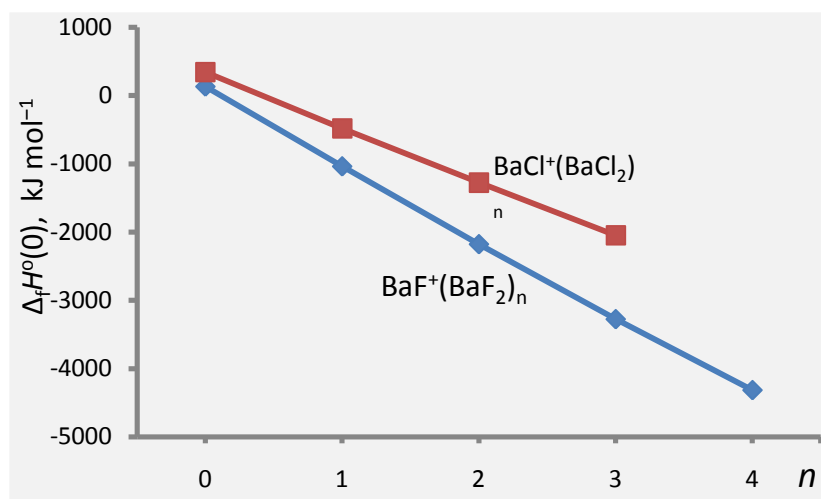
Figure 2.9. Enthalpies of formation of the ions $BaX^+(BaX_2)_n$, X = F or Cl, versus number of BaX_2 molecules attached (n).

2.5 Conclusion

The ions BaF^+, $Ba_2F_3^+$, $Ba_3F_5^+$, and $Ba_4F_7^+$ have been detected earlier in vapors over barium difluoride by a high temperature mass spectrometry technique. In this work the theoretical study of the $BaF^+(BaF_2)_n$ ions (with $n = 0$–4) is performed; the properties of the negative BaF_3^- ion also are determined. The structures of the positive ions are designed through the consequent attachment of BaF_2 molecules to BaF^+ ion. The equilibrium geometrical configurations of the ions $Ba_2F_3^+$, $Ba_3F_5^+$, and $Ba_5F_9^+$ are confirmed to be compact and highly symmetrical (D_{3h}). The $Ba_4F_7^+$ ion, being less symmetrical by its shape (C_{2v}), possesses also rather high stability and compactness. Alternative structures for the cluster ions have been considered but no isomers identified. The structural parameters and frequencies calculated with different theoretical approaches appeared to be not much sensitive regarding the method used (DFT/B3P86 or MP2) and basis sets (B1 or B2).

The geometrical properties and vibrational frequencies of the species have been implemented in the calculations of the thermodynamic functions and the latter employed in the treatment of the available experimental equilibrium constants. Thus the enthalpies $\Delta_r H°(0)$ of the ion molecular reactions 'based on experiment' have been determined. Also the theoretical values of $\Delta_r H°(0)$ have been scrutinized applying a number of DFT, MP2, MP4 approaches. A comparison between the theoretical and 'based on experiment' magnitudes of $\Delta_r H°(0)$ has shown that the DFT results exhibit insufficient accuracy, while the values found both by MP2 and MP4 methods are more reliable as they demonstrate a good accordance with the experimental data.

28

CHAPTER THREE

3.0 Structure and thermodynamic properties of cluster ions in saturated vapor over barium dibromide[2].

ABSTRACT
The structure and thermodynamic properties of cluster ions detected earlier in saturated vapour over barium dibromide were studied theoretically. The equilibrium geometrical parameters and vibrational spectra were computed for the ions $BaBr_3^-$, $Ba_2Br_3^+$, $Ba_3Br_5^+$, $Ba_4Br_7^+$ and $Ba_5Br_9^+$; the DFT and MP2 methods with triple-zeta valence basis sets were used. The enthalpies of ion molecular reactions were obtained both theoretically through the total energies of participants and based on experimental data. The theoretical results were scrutinized with respect to methods of computation (DFT, MP2, and MP4). The enthalpies of formation $\Delta_f H^o(0)$ of the ions have been determined (in kJ mol^{-1}): -858 ± 6 ($BaBr_3^-$); -293 ± 10 ($Ba_2Br_3^+$); -982 ± 20 ($Ba_3Br_5^+$); -1644 ± 30 ($Ba_4Br_7^+$); -2282 ± 17 ($Ba_5Br_9^+$).

Key words: barium dibromide, cluster ions, DFT, MP2, MP4, geometrical structure, vibrational spectra, enthalpies of ion molecular reactions, enthalpies of formation, thermodynamic functions.

3.1 Introduction

Cluster ions are formed by the combination via noncovalent forces of two or more atoms or molecules of one or more chemical species with an ion (Murray *et al*., 2013). They attract the interests of many researchers due to their unique electronic, optical and magnetic properties (Khanna & Jena, 1992, 1995; Rao *et al*., 2000). They have been identified as potential candidates in numerous applications as explained in section 2.1.

Different cluster ions had been proved to exist in saturated vapour over alkaline earth halides by means of high temperature mass spectrometric technique (Pogrebnoi *et al*., 1984; Pogrebnoi, 1981). Positive and negative ionic species were produced through thermal emission from crystalline $SrCl_2$ and BaF_2 at elevated temperatures under the conditions of free-surface and

Knudsen cell evaporation (Butman *et al*., 2001; Butman, 2002); the ions $SrCl^+$, $Sr_2Cl_3^+$, and $SrCl_3^-$ and BaF^+, $Ba_2F_3^+$, BaF_3^- were detected. Negative tetraatomic ions MgX_3^- and CaX_3^- (X = Cl, Br) were generated by electrospray technique and electron vertical detachment energy (VDE) values were measured using photoelectron spectroscopy (Elliott *et al*., 2005). Also the theoretical investigation of structural properties and stability of the ions MX_3^- and respective neutral species MX_3 had been performed (Elliott *et al*., 2005). Regarding barium dibromide, positively charged cluster ions $Ba_2Br_3^+$, $Ba_3Br_5^+$ and $Ba_4Br_7^+$ had been registered, and the intensities of the ion currents and equilibrium constants of ion molecular reactions had been measured (Pogrebnoi et al., 1984; Pogrebnoi, 1981).

Recently, theoretical studies of the properties of the cluster ions existing in vapours over $BaCl_2$ (Pogrebnoi *et al*., 2013), BaF_2 (chapter two) and $CaCl_2$ (Moustapher *et al*., 2016) have been conducted. In continuation of these works, this work intends to determine the geometrical structure, vibrational spectra, thermodynamic (TD) functions, enthalpies of dissociation and enthalpies of formation of the ions $BaBr_3^-$ and $BaBr^+(BaBr_2)_n$ (n = 1–4) using quantum chemical methods. The other target is the treatment of the equilibrium constants measured previously (Pogrebnoi *et al*., 1984; Pogrebnoi, 1981) applying the TD functions calculated in this work.

3.2   Computational details

The computations of geometrical parameters and vibrational spectra were carried out using two methods: electron density functional theory (DFT) with the functional B3P86 and the Møller-Plesset perturbation theory (MP2). For the barium atom, the effective core potential with def2-TZVP basis set 6s4p3d1f (Kaupp *et al*., 1991) has been utilized while for the bromine atom, two basis sets were employed. The first one with effective core potential was SDB-aug-cc-pvtz 4s4p3d2f (Martin & Sundermann, 2001) denoted as B1 and the second one was all-electron aug-cc-pvtz 7s6p4d2f (Dunning *et al*., 2001) denoted as B2. Both basis sets for bromine were accessed from the EMSL library (The Environmental Molecular Sciences laboratory, US) (Feller, 1996; Schuchardt *et al*., 2007). In calculations by the MP2 method with the small basis set B1, no orbitals were frozen, the option NCORE=0 was used. For the extended basis set B2, the option NCORE=0 also was implemented for the lighter species (BaBr, $BaBr^+$, $BaBr_2$, $BaBr_3^-$, $Ba_2Br_3^+$), while for the heavier clusters five core orbitals (1s, 2s, 2p) of each Br atom were frozen. The DFT and MP2 methods together with the two basis sets B1 and B2 formed four

theoretical levels in the following combinations: DFT/B1, MP2/B1, DFT/B2, and MP2/B2. Similar software described in section 2.2 were employed in the computations and analyses of the results.

As concerns the thermodynamic properties, the dissociation reactions of the cluster ions with elimination of $BaBr_2$ molecule have been considered. Two approaches have been implemented to determine the enthalpies of the reactions $\Delta_r H^o(0)$: (i) theoretical (through the energies of the species) and (ii) based on experiment (using equilibrium constants measured previously (Pogrebnoi *et al.*, 1984; Pogrebnoi, 1981)). The theoretical values of $\Delta_r H^o(0)$ were calculated employing the procedure described in section 2.2. In addition to DFT and MP2 methods with both basis sets, MP4 was employed using the geometrical parameters optimized by MP2 method. Based on our experience on systematic quantum chemical investigations of cluster ions of alkaline and alkaline earth halides (Jacob *et al.*, 2016; Mwanga *et al.*, 2015; Pogrebnoi *et al.*, 2013), we could state that the MP4 method improves the calculated values approaching experimental data. Besides, for the MP2 and MP4 methods, the superposition error (BSSE) was taken into account through counterpoise correction (CP) as described in the previous chapter.

The values of $\Delta_r H^o(0)$ 'based on experiment' were obtained using equation 2.9 following the procedure described in section 2.4. The thermodynamic functions of the cluster ions, entropy $S^\circ(T)$, enthalpy increment $H^\circ(T)-H^\circ(0)$, reduced Gibbs energy $\Phi^\circ(T) = -[H^\circ(T)-H^\circ(0)-TS^\circ(T)]/T$, have been calculated within the 'rigid rotator-harmonic oscillator' approximation on the base of the geometrical parameters and vibrational frequencies obtained; the OpenThermo software (Tokarev, 2007-2009) was used. Equilibrium constants had been measured previously for heterophase ion molecular reactions involving the $Ba_2Br_3^+$, $Ba_3Br_5^+$, and $Ba_4Br_7^+$ ions (Pogrebnoi *et al.*, 1984; Pogrebnoi, 1981). The enthalpies of the heterophase reactions were converted to gas phase. The required TD functions and enthalpies of formation of the simple species Br^-, $BaBr_{2(g)}$ and $BaBr_{2(c)}$ were retrieved from Ivtanthermo database (Gurvich *et al.*, 2000). For the $BaBr^+$, the TD functions were calculated by us, the enthalpy of formation was found through the ionization energy of BaBr (Belyaev *et al.*, 1990) and the enthalpy of formation of gaseous BaBr (Gurvich *et al.*, 2000).

3.3 Results and discussion on the properties of the species

3.3.1 BaBr, BaBr$^+$, BaBr$_2$ and BaBr$_2^+$

Four computational levels DFT/B1, MP2/B1, DFT/B2, and MP2/B2 were used to calculate geometrical parameters, vibrational frequencies, ionization energies and dipole moments for the simple species BaBr, BaBr$^+$, BaBr$_2$ and BaBr$_2^+$. The ground state symbol of the BaBr is $X^2\Sigma^+$. The results are compared with literature data (Table 3.1) in order to validate the methods and basis sets for computation of properties of cluster ions.

As is seen, the values of internuclear separations R_e(Ba–Br) calculated through different methods are close to one another, the maximum difference between the highest (by MP2/B2) and lowest (by DFT/B1) being 0.014 Å (BaBr$^+$), 0.027 Å (BaBr) and 0.015 Å (BaBr$_2$). A slight increase in the values of R_e from DFT to MP2 (for the same basis set) as well as from B1 to B2 (for the same method) can be observed. The magnitude of bond angle α_e(Br–Ba–Br) in the BaBr$_2$ molecule is more sensitive to the method rather than to basis set, and it is about 5° bigger as found by MP2 method compared to DFT. The calculated values of R_e(Ba–Br) through all methods are in a good accordance with electron diffraction data (Hargittai *et al*., 2001), while for the bond angle the MP2/B2 level shows better agreement with the experiment. The dipole moment values of the BaBr$_2$ molecule obtained through different theoretical levels are related rather to the bond angle than bond length, the smaller is the α_e(Br–Ba–Br) the bigger μ_e. In the diatomic species, the dipole moment values correlate with the bond lengths: the longer is the bond the bigger the dipole moment. It is noted that the BaBr$_2^+$ ion is linear (α_e(Br–Ba–Br) = 180°) while its corresponding neutral molecule BaBr$_2$ is bent (α_e(Br–Ba–Br) ≈ 130°). The two species BaBr$_2$ and BaBr$_2^+$ have comparable values of R_e(Ba–Br) at both basis sets.

The calculated vibrational frequencies of the species are not much sensitive to the method across all computational levels and generally agree well with the available literature data (Hargittai *et al*., 2001). Regarding the parameters in the series of three species BaBr$^+$→BaBr→BaBr$_2$, the vibrational frequencies decrease, 232 cm^{-1}→188 cm^{-1}→170 cm^{-1}, while the R_e(Ba−Br) values increase, 2.771 Å→2.893 Å→2.919 Å (MP2/B2 results). When comparing the frequencies in the row of the barium dihalides BaF$_2$→BaCl$_2$→BaBr$_2$ one can see that a relationship between symmetrical and asymmetrical vibration frequencies, $\omega_1 > \omega_3$, observed for BaF$_2$ (chapter two),

is not held for other two halides where ω_1 is less than ω_3 by ~10 cm^{-1} (BaCl$_2$ (Pogrebnoi *et al.*, 2013)) and ~30 cm^{-1} (BaBr$_2$).

Table 3.1. Properties of BaBr, BaBr$^+$ and BaBr$_2$.

Property	DFT/B1	MP2/B1	DFT/B2	MP2/B2	Reference
BaBr					
R_e(Ba–Br)	2.866	2.880	2.872	2.893	
$-E$	39.02994		2599.90224		
ω_e	190	191	191	188	193.8[a]
IE_{ad}	5.15	4.95	5.16	4.95	5.04 ± 0.04[b]
IE_{ver}	5.20	4.99	5.21	5.00	
μ_e	5.48		5.53		
BaBr$^+$					
R_e(Ba–Br)	2.757	2.769	2.762	2.771	
$-E$	38.84071	38.18554	2599.71275	2597.95876	
ω_e	232	232	231	232	
μ_e	10.36	11.16	10.43	11.20	
BaBr$_2$					
R_e(Ba–Br)	2.904	2.917	2.908	2.919	2.899 ± 0.007[c]
α_e(Br–Ba–Br)	130.3	134.9	130.7	135.5	137.1 ± 4.9[c]
$-E$	52.56759	52.13868	5174.31244	5171.02844	
ω_1 (A$_1$)	173	171	174	170	178[d]
ω_2 (A$_1$)	31	27	31	27	28[d]
ω_3 (B$_1$)	199	201	199	200	206[d]
IE_{ad}	9.1		9.3		
IE_{ve}	9.5	9.9	9.5	9.9	9.40 ± 0.02[e]
μ_e	7.01	6.85	7.02	6.80	
BaBr$_2$$^+$					
R_e(Ba–Br)	2.888		3.076		
α_e(Br–Ba–Br)	180		179.9		
$-E$	52.23328		5173.97174		

Note: R_e(Ba−Br) is the equilibrium internuclear distance, Å; α_e(Br−Ba−Br) is the valence angle, degrees; ω_i are the vibrational frequencies, cm^{-1}; IE_{ad} and IE_{ver} are the adiabatic and vertical ionization energies, respectively, eV; and μ_e is the dipole moment, D.
Notes to the reference data: [a]emission spectra in flames (Bradford, 1975), retrieved from NIST (www.nist.gov); [b]emission spectra in flames (Belyaev *et al.*, 1990), retrieved from NIST (www.nist.gov); [c]electron diffraction (Hargittai *et al.*, 2001); [d]MP2 calculation (Hargittai *et al.*, 2001); [e]photoelectron spectroscopy (Lee & Potts, 1979).

The ionization energies, adiabatic IE_{ad} and vertical IE_{ver}, were found following the procedure described in section 2.3.1. As is seen in Table 3.1 for BaBr, both IE_{ad} and IE_{ver} found by the DFT method are bigger by ~0.2 eV than MP2 results, that actually exceeds greatly the difference between adiabatic and vertical values (~0.05 eV). Compared to the experimental data, the DFT results on IE_{ad} are higher by ~0.09 eV, while the MP2 results are lower by the same value. For BaBr$_2$ the trend in the DFT and MP2 data is different; the IE_{ver} values by DFT are lower (by ~0.4

eV) than MP2 and agree better with experimental magnitude (Lee & Potts, 1979). The experimental IE_{ad} of the $BaBr_2$ molecule is not available in literature, though our results on IE_{ad}, 9.1 eV (DFT/B1) and 9.3 eV (DFT/B2), are in accordance with 9.2 eV reported as the appearance energy of $BaBr_2^+/BaBr_2$ in (Horlbeck, 1982).

In general, the properties of the simple species, $BaBr$, $BaBr^+$, $BaBr_2$, obtained across all theoretical approaches employed are in agreement with the literature data. The calculated geometrical parameters and vibrational frequencies are not much sensitive to the level of computation. For heavier species we tried to implement all four methods considered, except most heavy ions, $Ba_3Br_5^+$, $Ba_4Br_7^+$, $Ba_5Br_9^+$, where the MP2 method was not achievable, so we were constrained by DFT.

3.3.2 Tetraatomic negative ion $BaBr_3^-$ and neutral species $BaBr_3$

The equilibrium configuration of the ion $BaBr_3^-$ is planar of D_{3h} symmetry (Fig. 3.1a); the structural properties are presented in Table 3.2. It is observed that the values of the internuclear separation R_e(Ba–Br) as well as vibrational frequencies obtained by four computational methods are in a good accordance between each other.

Figure 3.1. Equilibrium geometrical structures of the tetraatomic species: (a) $BaBr_3^-$ (D_{3h}, $^1A_1'$), (b) $BaBr_3$ (C_s, $^2A''$).

In the IR spectrum of the $BaBr_3^-$ ion, the most intensive band ω_3 (E') corresponds to the asymmetric stretching mode Ba–Br. Two bending vibrational frequencies, out-of-plane ω_2 (A_2'') and in-plane ω_4 (E') modes, are approximately equal to each other and exceed slightly the deformational frequency ω_2 in the neutral dihalide $BaBr_2$. It is worth to mention that the same geometrical equilibrium structure of the D_{3h} symmetry was proved earlier for the similar tetraatomic negative ions MX_3^- (M = Be, Mg, Ca; X= Cl, Br) (Elliott *et al*., 2005), $BaCl_3^-$

(Pogrebnoi *et al.*, 2013), $CaCl_3^-$ (Moustapher *et al.*, 2016) and BaF_3^- (section 2.3.3). In the spectra of the BaF_3^- and $BaCl_3^-$ ions, the bending frequencies ω_2 (A_2'') were much lower than ω_4 (E'); and if compare with the neutral dihalides, the following relationships were observed: ω_4 (E', BaF_3^-) $\approx \omega_2$ (A_1, BaF_2) and ω_2 (A_2'', $BaCl_3^-$) $\approx \omega_2$ (A_1, $BaCl_2$).

Table 3.2. Properties of tetraatomic $BaBr_3^-$ (D_{3h}, $^1A_1'$) ion.

Property	DFT/B1	MP2/B1	DFT/B2	MP2/B2
R_e(Ba–Br)	3.028	3.015	3.031	3.032
ω_1 (A_1')	126 (0)	135 (0)	130 (0)	132 (0)
ω_2 (A_2'')	33 (0.5)	31 (0.6)	33 (0.5)	38 (0.6)
ω_3 (E')	161 (2.9)	170 (2.9)	161 (2.9)	166 (2.9)
ω_4 (E')	35 (0.1)	35 (0.1)	37 (0.1)	37 (0.1)
q(Ba)	1.648	1.723	1.660	1.731
$-q$(Br)	0.883	0.908	0.887	0.910

Note: R_e(Ba−Br) is the equilibrium internuclear distance, Å; ω_i are the vibrational frequencies, cm^{-1}; q(Ba) and q(Br) are atomic charges, au; the values given in parenthesis near the frequencies are the intensities in IR spectrum, D^{2}amu^{-1}Å^{-2}.

The enthalpy $\Delta_r H^o(0)$ of the dissociation reaction

$$BaBr_3^- = Br^- + BaBr_2 \qquad (3.2)$$

was calculated through the total energies and ZPVE of the species; ten methods were employed: DFT/B1, MP2/B1, MP2^{CP}/B1, MP4B1, MP4^{CP}/B1, DFT/B2, MP2/B2, MP2^{CP}/B2, MP4/B2, and MP4^{CP}/B2. The results are given in Fig. 3.2 together with the values of $\Delta_r H^o(0)$ for $BaCl_3^-$ (Pogrebnoi *et al.*, 2013) and BaF_3^- (chapter two) studied earlier. All three ions display an oscillatory behavior across the methods; the lowest values of $\Delta_r H^o(0)$ are found by the DFT method, while the highest by MP2. The oscillation span increases in series BaF_3^- (~10 kJ mol^{-1}) $\rightarrow BaCl_3^-$ (~15 kJ mol^{-1}) $\rightarrow BaBr_3^-$ (~20 kJ mol^{-1}). The average magnitude of $\Delta_r H^o(0)$ calculated by eight computational levels (MP2, MP4, MP2^{CP} and MP4^{CP} for both basis sets B1 and B2) is 254 ± 6 kJ mol^{-1} for $BaBr_3^-$; the uncertainty is accepted as a half difference between maximum and minimum values of $\Delta_r H^o(0)$. The results show that stability of the species decreases in the order $BaF_3^- \rightarrow BaCl_3^- \rightarrow BaBr_3^-$. It is also worth to compare our result for $BaBr_3^-$ with the available data for $BeBr_3^-$, $MgBr_3^-$, $CaBr_3^-$ (Elliott *et al.*, 2005): 229 kJ mol^{-1}, 265 kJ mol^{-1}, and 267 kJ mol^{-1}, respectively. The observed nonmonotonic change of the $\Delta_r H^o(0)$ magnitudes in the series of the tetraatomic negative ions may be attributed to a steric factor, due to which the arrangement of atoms in heavier species favors the higher stability of the ions compared to the $BeBr_3^-$.

To estimate the electron detachment energy of the ion $BaBr_3^-$, the properties of the neutral radical $BaBr_3$ were calculated. We have considered configurations of C_{2v} symmetry similar to those reported in (Elliott *et al.*, 2005) for MX_3 (M = Be, Mg, Ca; X = Cl, Br): T-shaped Van der Waals complex $BaBr...Br_2$ and $BaBr_2$–Br structure; but imaginary frequencies were revealed in the vibrational spectra for both of these structures. The equilibrium configuration of the $BaBr_3$ appeared to be pyramidal C_s with electronic state $^2A''$ (Fig. 3.1b). The parameters are given in Table 3.3. As is seen the bonds Ba–Br are not equivalent; compared to the ion $BaBr_3^-$ the bond length Ba–Br_1 is shorter whereas other two bonds Ba–Br are longer. The electron density distribution in the neutral molecule also is non-uniform; the atomic charge of Br_1 atom is almost twice bigger than each of other two. The height of the pyramid is about 1.8 Å and the dipole moment of the $BaBr_3$ is ~5 D.

Figure 3.2. Enthalpies of dissociation reactions $BaX_3^- \rightleftarrows X^- + BaX_2$ (X = F, Cl, Br) versus computational method: 1–DFT/B1, 2–MP2/B1, 3–MP2^{CP}/B1, 4–MP4/B1, 5–MP4^{CP}/B1, 6–DFT/B2, 7–MP2/B2, 8–MP2^{CP}/B2, 9–MP4/B2, 10–MP4^{CP}/B2.

The electron affinity (*EA*) for $BaBr_3$ that is equal to the electron detachment energy of the ion $BaBr_3^-$, was found as energy difference between the neutral $BaBr_3$ and anion $BaBr_3^-$. The value of *EA* ≈ 5 eV is high enough to categorize the $BaBr_3$ as a superhalogen. This magnitude is comparable to the VDE values of MX_3^-: 6.60 ± 0.04 eV ($MgCl_3^-$), 6.00 ± 0.04 eV ($MgBr_3^-$), 6.62 ± 0.04 eV ($CaCl_3^-$), and 6.10 ± 0.04 eV ($CaBr_3^-$) measured by photoelectron spectroscopy

(Elliott *et al.*, 2005), the respective neutral species were also identified to belong to the class of superhalogens (Elliott *et al.*, 2005).

The frontier molecular orbitals of the neutral and ionic species $BaBr_3$ and $BaBr_3^-$ are presented in Fig. 3.3. One can observe from the diagrams that the electron density is unequally distributed between bromine atoms in both HOMO and LUMO of the neutral $BaBr_3$ while it is evenly apportioned in the HOMO of the ion $BaBr_3^-$. This different character of the frontier MOs of the $BaBr_3$ and $BaBr_3^-$ correlates well with the magnitudes of the bromine atomic charges given in Tables 3.2 and 3.3. It implies that when an electron is added to the radical it evidently occupies the *p*-orbitals of two Br-atoms with smaller magnitude of charge of about 0.4*e*, which results both in rise of the $q(Br)$ magnitude up to 0.9*e* in the $BaBr_3^-$ and redistribution of electron density between the Br-atoms.

Table 3.3. Properties of tetraatomic neutral species $BaBr_3$ (C_s, $^2A''$).

Property	DFT/B1	DFT/B2
$R_e(Ba–Br)$	3.111	3.113
$R_{e1}(Ba–Br_1)$	2.905	2.909
$\alpha_e(Br–Ba–Br)$	55.6	55.8
$\beta_e(Br–Ba–Br_1)$	135.4	135.4
EA_{ad}	4.84	4.90
$\omega_1 (A')$	192 (1.7)	193 (1.8)
$\omega_2 (A')$	152 (0.1)	156 (0.1)
$\omega_3 (A')$	115 (0.2)	115 (0.2)
$\omega_4 (A')$	18 (0.2)	21 (0.2)
$\omega_5 (A'')$	114 (0.05)	114 (0.05)
$\omega_6 (A'')$	22 (0.2)	22 (0.2)
$q(Ba)$	1.603	1.616
$-q(Br)$	0.414	0.422
$-q(Br_1)$	0.774	0.772
μ_e	4.97	5.00

Note: $R_i(Ba−Br)$ are the equilibrium internuclear distances, Å; α_e and β_e are the valence angles, degs; ω_i are the vibrational frequencies, cm^{-1}; $q(Ba)$ and $q(Br)$ are atomic charges, au; EA_{ad} is adiabatic electron affinity, eV; the values given in parenthesis near the frequencies are the intensities in IR spectrum, $D^2amu^{-1}Å^{-2}$.

Figure 3.3. Frontier molecular orbitals of the neutral and ionic species (DFT/B2): (a) $BaBr_3$ neutral, HOMO α-58 (a″), ε = −7.3 eV; (b) $BaBr_3$ neutral, LUMO β-58 (a″), ε = −5.0 eV; (c) $BaBr_3^-$ ion, HOMO 58 (a′₂), ε =−3.8 eV.

3.3.3 Pentaatomic positive ion $Ba_2Br_3^+$

The structural parameters are presented in Table 3.4 as computed by DFT and MP2 methods with both basis sets B1 and B2. The bipyramidal three-bridged structure of the D_{3h} symmetry is found to be the equilibrium configuration (Fig. 3.4); barium atoms are at the vertices of the bipyramid while the bromine atoms form a horizontal plane. The bipyramidal structure has a vertex angle of about 82° which indicates the bipyramid is stretched along the axis. The similar pyramidal structure was confirmed for $Ba_2Cl_3^+$ (Pogrebnoi *et al*., 2013), $Ca_2Cl_3^+$ (Moustapher *et al*., 2016) and $Ba_2F_3^+$ (see section 2.3.4). The vertex angle increases in series $Ba_2F_3^+$ (71°) → $Ba_2Cl_3^+$ (78°) → $Ba_2Br_3^+$ (82°); the internuclear separation R_e(Ba–X) also increases, 2.41 Å → 2.95 Å → 3.06 Å. Apparently this trend is attributed to enlarging of atomic size of the halogens from fluorine to bromine.

Figure 3.4. Equilibrium geometrical structure of the pentaatomic $Ba_2Br_3^+$ ion (D_{3h}).

In the IR spectrum of the $Ba_2Br_3^+$ ion, there are two most intensive bands, ω_3 (A_2'') = 153 cm^{-1} and ω_4 (E') = 150 cm^{-1} which correspond to the stretching Ba-Br modes. As the structure is compact, there are no low vibrational frequencies, the lowest value is ω_5 (E') = 60 cm^{-1}.

Table 3.4. Properties of pentaatomic positive ion $Ba_2Br_3^+$ (D_{3h}).

Property	DFT/B1	MP2/B1	DFT/B2	MP2/B2
R_e(Ba–Br)	3.065	3.051	3.069	3.063
α_e(Br–Ba–Br)	82.3	82.7	81.3	80.6
ω_1 (A_1')	160 (0)	167 (0)	162 (0)	165 (0)
ω_2 (A_1')	89 (0)	86 (0)	86 (0)	86 (0)
ω_3 (A_2'')	149 (1.6)	155 (1.8)	149 (1.6)	153 (1.8)
ω_4 (E')	145 (2.0)	153 (2.0)	145 (2.0)	150 (2.0)
ω_5 (E')	60 (0.2)	58 (0.3)	60 (0.2)	60 (0.4)
ω_6 (E'')	101 (0)	110 (0)	101 (0)	108 (0)

Note: R_e is the equilibrium internuclear distance, Å; α_e is the valence angle, degs; ω_i are the vibrational frequencies, cm^{-1} and the values given in parenthesis near the frequencies are the intensities in IR spectrum, D^{2}amu^{-1}Å^{-2}.

The dissociation reaction of the $Ba_2Br_3^+$ cluster ion to form $BaBr_2$ molecule and $BaBr^+$ ion was considered

$$Ba_2Br_3^+ = BaBr^+ + BaBr_2. \tag{3.3}$$

The enthalpy of the reaction was calculated through the total energies of the individual species by implementing DFT, MP2 and MP4 methods with both basis sets B1 and B2. The enthalpies obtained with the aforementioned methods are plotted versus the methods of computation in Fig. 3.5; the data obtained earlier for $Ba_2Cl_3^+$ (Pogrebnoi *et al.*, 2013) and $Ba_2F_3^+$ (chapter two) are given for comparison. The horizontal lines represent the values 'based on experiment' obtained through the treatment of experimental equilibrium constants (Pogrebnoi *et al.*, 1984; Pogrebnoi, 1981) which are given in Table 3.5.

It is observed that for different computational levels, all three cluster ions show an oscillatory trend; the MP2 and MP4 results are in a good agreement with the values 'based on experiment'. However, the DFT results are essentially lower than the experimental values: by ~ 20 kJ mol^{-1} for $Ba_2F_3^+$ and ~35–40 kJ mol^{-1} for $Ba_2Cl_3^+$ and $Ba_2Br_3^+$. The theoretical magnitude of $\Delta_r H^o(0) = 317 \pm 16$ kJ mol^{-1} for $Ba_2Br_3^+$ obtained as average of the values found by MP2, MP4, MP2^{CP} and MP4^{CP} for both basis sets B1 and B2, coincides practically with the value 'based on experiment'[3], 317 ± 10 kJ mol^{-1}. The enthalpies of the dissociation reactions decrease in the order $Ba_2F_3^+$ (360 ± 12 kJ mol^{-1}) → $Ba_2Cl_3^+$ (326 ± 10 kJ mol^{-1}) → $Ba_2Br_3^+$ (317 ± 10 kJ mol^{-1}) which correlates with the reduction of the bond strength from fluoride to bromide.

---

[3] The uncertainties of the 'based on experiment' data for the $Ba_2Br_3^+$ ion are taken from the original work (Pogrebnoi *et al.*, 1984) and reduced by factor ~1.5 due to more accurate thermodynamic functions obtained in present work. The same approach of the uncertainty estimation was used for heavier ions $Ba_3Br_5^+$ and $Ba_4Br_7^+$.

Figure 3.5. Enthalpies of dissociation reactions $Ba_2X_3^+ \rightleftarrows BaX^+ + BaX_2$ (X = F, Cl, Br) versus computational method: 1–DFT/B1, 2–MP2/B1, 3–MP2^{CP}/B1, 4–MP4/B1, 5–MP4^{CP}/B1, 6–DFT/B2, 7–MP2/B2, 8–MP2^{CP}/B2, 9–MP4/B2, and 10–MP4^{CP}/B2. The horizontal lines represent the values 'based on experiment'.

Table 3.5. Equilibrium constants for heterophase ion molecular reactions measured experimentally at different temperatures (Pogrebnoi *et al.*, 1984; Pogrebnoi, 1981).

No	Reaction	$\ln K^o_p$ (*T*, K)
1	$Ba_2Br_3^+ = BaBr^+ + [BaBr_2]$	0.200 (1170); 0.272 (1156); 0.200 (1192); 0.281 (1211); 0.322 (1221); 0.364 (1237); 0.362 (1216); 0.322 (1204); 0.272 (1189); 0.286 (1180); 0.272 (1156); 0.299 (1168); 0.198 (1157); 0.203 (1147); 0.226 (1144); 0.230 (1152); 0.207 (1134); 0.246 (1156); 0.256 (1165); 0.281 (1182); 0.322 (1200); 0.343 (1220); 0.336 (1234); 0.371 (1250); 0.357 (1227); 0.355 (1206); 0.304 (1191); 0.297 (1169); 0.332 (1147); 0.244 (1132)
2	$Ba_3Br_5^+ = BaBr^+ + 2[BaBr_2]$	4.394 (1195); 4.357 (1208); 4.332 (1229); 4.297 (1242); 4.256 (1259); 4.226 (1272); 4.263 (1246); 4.304 (1232); 4.297 (1216); 4.316 (1201); 4.295 (1205); 4.233 (1237); 4.219 (1248); 4.217 (1263); 4.221 (1272); 4.235 (1257); 4.263 (1237); 4.247 (1229); 4.286 (1218); 4.330 (1207); 4.343 (1190); 4.330 (1188)
3	$Ba_4Br_7^+ = Ba_3Br_5^+ + [BaBr_2]$	4.605 (1200)

3.3.4 Octaatomic positive ion $Ba_3Br_5^+$

The geometrical parameters and vibrational frequencies of the $Ba_3Br_5^+$ cluster ion computed by DFT/B1 and DFT/B2 methods are in a good accordance between each other (Table 3.6). The equilibrium configuration of this ion is bipyramidal of D_{3h} symmetry (Fig. 3.6). The similar bipyramidal structure was found earlier for the ions $Ba_3Cl_5^+$ (Pogrebnoi *et al.*, 2013), $Ca_3Cl_5^+$

(Moustapher *et al*., 2016) and $Ba_3F_5^+$ (section 2.3.5). Note that the bipyramids are squeezed along the 3-fold axis. In series of barium halide species $Ba_3F_5^+ \rightarrow Ba_3Cl_5^+ \rightarrow Ba_3Br_5^+$, the 'width-to-height' ratio is decreasing gradually, $1.7 \rightarrow 1.6 \rightarrow 1.5$; the vertex angle $\alpha_e(Ba–X_v–Ba)$ also decreases, $96° \rightarrow 89° \rightarrow 86°$.

In the IR vibrational spectrum of the $Ba_3Br_5^+$ ion, the most intensive band ω_7 (E') = 154 cm^{-1} is assigned to the stretching mode of Ba–Br$_h$ bonds. Other bands active in IR spectrum, ω_5 (A_2'') = 123 cm^{-1} and ω_8 (E') = 133 cm^{-1} relate also to stretching vibrations of Ba–Br$_v$ and Ba–Br$_h$ bonds, respectively. The lowest frequencies, ω_6 =42 cm^{-1} and ω_{12} = 40 cm^{-1} correspond to wagging and rocking modes respectively and are smaller compared to ω_5 = 60 cm^{-1} of the pentaatomic bipyramid $Ba_2Br_3^+$ (Table 3.4), this indicates the lower rigidity of the octaatomic ion than pentaatomic.

(a)   (b)

Figure 3.6. Equilibrium geometrical structure of the ion $Ba_3Br_5^+$ (D_{3h}): (a) top view, (b) side view.

Table 3.6. Properties of octaatomic ion $Ba_3Br_5^+$ (D_{3h}).

Property	DFT/B1	DFT/B2
R_{e1}(Ba–Br$_h$)	3.113	3.115
R_{e2}(Ba–Br$_v$)	3.208	3.210
α_e(Ba–Br$_v$–Ba)	85.8	86.0
β_e(Ba–Br$_h$–Ba)	89.1	89.2
ω_1 (A_1')	137 (0)	139 (0)
ω_2 (A_1')	116 (0)	120 (0)
ω_3 (A_1')	114 (0)	117 (0)
ω_4 (A_1')	84 (0)	88 (0)
ω_5 (A_2'')	123 (0.8)	123 (0.9)
ω_6 (A_2'')	42 (0.2)	42 (0.2)
ω_7 (E')	154 (3.6)	154 (3.8)
ω_8 (E')	134 (1.4)	133 (1.1)
ω_9 (E')	87 (0.1)	90 (0.1)
ω_{10} (E')	65 (0.1)	63 (0.1)
ω_{11} (E'')	92 (0)	93 (0)
ω_{12} (E'')	40 (0)	40 (0)

Note: R_{e1} and R_{e2} are the equilibrium internuclear distances, Å; α_e and β_e are the valence angles, degs; ω_i are the vibrational frequencies, cm^{-1} and the values given in parenthesis near the frequencies are the intensities in IR spectrum, D^{2}amu^{-1}Å^{-2}.

The dissociation reaction of the $Ba_3Br_5^+$ cluster ion with elimination of $BaBr_2$ molecule

$$Ba_3Br_5^+ = Ba_2Br_3^+ + BaBr_2 \qquad (3.4)$$

was considered. The theoretical enthalpy of the reaction $\Delta_rH^o(0)$ was computed employing the DFT, MP2 and MP4 methods with basis sets B1 and B2; in calculations by MP2 and MP4 methods the geometrical parameters optimized at DFT level were implemented. Similarly to the pentaatomic $Ba_2Br_3^+$ ion, the values of $\Delta_rH^o(0)$ are plotted in Fig. 3.7 against the method of computation and compared with the results for $Ba_3Cl_5^+$ (Pogrebnoi et al., 2013) and $Ba_3F_5^+$. The magnitudes of $\Delta_rH^o(0)$ 'based on experiment' are represented by horizontal lines. For all species, the DFT results show considerable underrating, by 40–55 kJ mol^{-1}, compared to the 'based on experiment' values. The accepted theoretical enthalpy of the reaction (3.4) is obtained as average magnitude found by all methods except DFT: $\Delta_rH^o(0) = 291 \pm 21$ kJ mol^{-1}; the latter is in excellent agreement with the 'based on experiment' result 292 ± 20 kJ mol^{-1}.

Figure 3.7. Enthalpies of dissociation reactions $Ba_3X_5^+ \rightleftarrows Ba_2X_3^+ + BaX_2$ (X = F, Cl, Br) versus computational method: 1–DFT/B1, 2–MP2/B1, 3–MP2^{CP}/B1, 4–MP4/B1, 5–MP4^{CP}/B1, 6–DFT/B2, 7–MP2/B2, 8–MP2^{CP}/B2, 9–MP4/B2, and 10–MP4^{CP}/B2. Horizontal lines represent the values 'based on experiment'.

3.3.5   Undecaatomic $Ba_4Br_7^+$ and tetradecaatomic $Ba_5Br_9^+$ ions

The undecaatomic cluster ions had been registered experimentally in the equilibrium vapour over barium dihalides (Pogrebnoi et al., 1984; Pogrebnoi, 1981), whereas the tetradecaatomic ions were not detected but may be predicted to exist similarly as it was suggested earlier for the ions $Ba_5Cl_9^+$ (Pogrebnoi et al., 2013) and $Ba_5F_9^+$ (section 2.3.7). The geometrical parameters and vibrational spectra of the $Ba_4Br_7^+$ and $Ba_5Br_9^+$ ions were computed in this work and listed in

42

Table 3.7. Two theoretical levels, DFT/B1 and DFT/B2 were used for the $Ba_4Br_7^+$ ion whereas only DFT/B1 was affordable for $Ba_5Br_9^+$ ion. The equilibrium structures of the ions correspond to the C_{2v} ($Ba_4Br_7^+$) and D_{3h} ($Ba_5Br_9^+$) groups of symmetry (Fig. 3.8) and can be imagined as attachment products of two or three $BaBr_2$ molecules to the central core, $Ba_2Br_3^+$ bipyramid[4]. In the undecaatomic $Ba_4Br_7^+$ ion, $Ba_2Br_3^+$ bipyramidal fragment becomes slightly distorted due to non-symmetrical surroundings.

Figure 3.8. Equilibrium geometrical structures of the ions: (a) $Ba_4Br_7^+$ (C_{2v}); (b) $Ba_5Br_9^+$ (D_{3h}).

Compared to the individual $Ba_2Br_3^+$ ion (Table 3.4), geometrical parameters of the $Ba_2Br_3^+$-core moiety in both $Ba_4Br_7^+$ and $Ba_5Br_9^+$ ions differ; the internuclear separations Ba–Br are longer by 0.3–0.4 Å and the vertex angle smaller by ~10°–13°. Compared to the free $BaBr_2$ molecules (Table 3.1), in the attached $BaBr_2$-fragments of the ions, internuclear separations Ba–Br are elongated by ~0.2 Å, the Br–Ba–Br units are straightened as the bond angles Br–Ba–Br increased by ~30–35°. Therefore the moieties, $Ba_2Br_3^+$ and $BaBr_2$, being structural components within the cluster ions, are subjected to essential alteration with respect to the free species. The new bonds are formed in the ions: (i) bonds between Ba-atoms of the bipyramid and Br-atoms of the $BaBr_2$ units; (ii) bonds between Br-atoms of the bipyramid and Ba-atoms of the $BaBr_2$ units. The first type of these bonds appeared to be stronger than second, that can be seen through the respective internuclear separations, e.g. in the $Ba_5Br_9^+$, the distance R_{e4}(Ba–Br) = 3.158 Å is shorter than R_{e3}(Ba_h–Br_h) = 3.223 Å.

---

[4] For the $Ba_5Br_9^+$ ion, the chain structure composed of four cycles in mutually perpendicular planes, C_{2v} symmetry, was also considered but not confirmed to be equilibrium due to imaginary frequencies revealed.

Table 3.7. Properties of undecaatomic $Ba_4Br_7^+$ (C_{2v}) and tetradecaatomic $Ba_5Br_9^+$ (D_{3h}) ions.

	Ba$_4$Br$_7^+$		Ba$_5$Br$_9^+$	
Property	DFT/B1	DFT/B2	Property	DFT/B1
R_{e1}(Ba$_1$–Br$_1$)	3.347	3.350	R_{e1}(Ba–Br$_h$)	3.478
R'_{e1}(Ba$_1$–Br$_2$)	3.291	3.288		
R_{e2}(Ba$_2$–Br$_3$)	3.094	3.097	R_{e2}(Ba$_h$–Br)	3.081
R_{e3}(Ba$_2$–Br$_1$)	3.294	3.288	R_{e3}(Ba$_h$–Br$_h$)	3.223
R'_{e3}(Ba$_2$–Br$_2$)	3.159	3.162		
R_{e4}(Ba$_1$–Br$_3$)	3.125	3.128	R_{e4}(Ba–Br)	3.158
α_e(Br$_2$–Ba$_1$–Br$_2$)	74.1	74.0	α_e(Br$_h$–Ba–Br$_h$)	68.6
α'_e(Br$_1$–Ba$_1$–Br$_2$)	73.2	72.9		
β_e(Br$_3$–Ba$_2$–Br$_3$)	155.1	155.1	βe(Br–Ba$_h$–Br)	159.3
γ_e(Br$_3$–Ba$_1$–Br$_3$)	114.4	114.3	γ_e(Br–Ba–Br)	118.5
ω_1 (A_1)	153 (2.9)	154 (2.9)	ω_1 (A_1')	129 (0)
ω_2 (A_1)	152 (0)	154 (0)	ω_2 (A_1')	116 (0)
ω_3 (A_1)	145 (2.7)	145 (2.7)	ω_3 (A_1')	113 (0)
ω_4 (A_1)	137 (1.2)	138 (1.3)	ω_4 (A_1')	102 (0)
ω_5 (A_1)	135 (0.4)	138 (0.4)	ω_5 (A_1')	83 (0)
ω_7 (A_1)	120 (0.2)	122 (0.2)	ω_6 (A_1')	50 (0)
ω_8 (A_1)	118 (0)	118 (0)	ω_7 (A_1')	33 (0)
ω_{25} (A_1)	30 (0.01)	36 (0.01)	ω_8 (A_1')	31 (0)
ω_{27} (A_1)	28 (0)	31 (0)	ω_9 (A_2'')	158 (3.9)
ω_6 (A_2)	128 (0.04)	147 (0.01)	ω_{10} (A_2'')	112 (0.04)
ω_9 (A_2)	116 (0.05)	121 (0.002)	ω_{11} (A_2'')	84 (0.3)
ω_{12} (A_2)	99 (0.2)	99 (0.2)	ω_{12} (A_2'')	53 (0.1)
ω_{23} (A_2)	38 (0.1)	38 (0.1)	ω_{13} (E')	149 (3.6)
ω_{16} (B_1)	80 (0.03)	81 (0.02)	ω_{14} (E')	136 (2.4)
ω_{17} (B_1)	78 (0.1)	79 (0.1)	ω_{15} (E')	109 (0.001)
ω_{18} (B_1)	76 (0.0002)	68 (0.002)	ω_{16} (E')	83 (0.01)
ω_{19} (B_1)	68 (0.2)	68 (0.2)	ω_{17} (E')	66 (0.9)
ω_{20} (B_1)	56 (0.1)	59 (0.1)	ω_{18} (E')	39 (0.0001)
ω_{21} (B_1)	53 (0)	56 (0)	ω_{19} (E')	36 (0.4)
ω_{22} (B_1)	51 (0.03)	53 (0.04)	ω_{20} (E'')	155 (0)
ω_{24} (B_1)	34 (0.01)	35 (0.01)	ω_{21} (E'')	118 (0)
ω_{10} (B_2)	108 (0.0005)	110 (0.002)	ω_{22} (E'')	78 (0)
ω_{11} (B_2)	103 (0.2)	104 (0.2)	ω_{23} (E'')	49 (0)
ω_{14} (B_2)	94 (0.01)	101 (0.0002)	ω_{24} (E'')	30 (0)
ω_{13} (B_2)	94 (0.02)	100 (0.003)		
ω_{15} (B_2)	82 (0)	83 (0)		
ω_{26} (B_2)	30 (0.1)	34 (0.1)		

Note: R_{ei} are the equilibrium internuclear distances, Å; α_e, α'_e, β_e and γ_e are the valence angles, degs; ω_i are the vibrational frequencies, cm^{-1} and the values given in parenthesis near the frequencies are the intensities in IR spectrum, D^{2}amu^{-1}Å^{-2}.

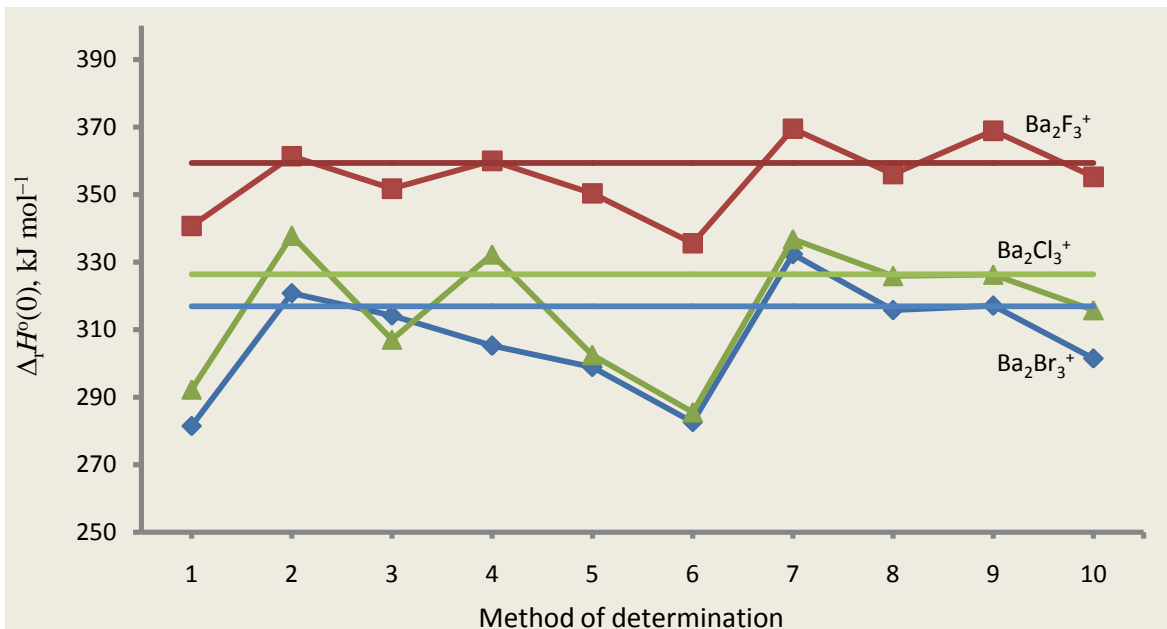Structurally, the $Ba_5Br_9^+$ ion may be considered also as composed of three layers, the $Ba_{h3}Br_{h3}$ hexagonal fragment in the middle between two $BaBr_3$ units. The similar three-layered structure was described earlier in chapter two for $Ba_5F_9^+$ ion. In the six-atomic middle fragment $Ba_{h3}Br_{h3}$, the Ba_h–Br_h–Ba_h units are slightly bent with angle α_e(Ba_h–Br_h–Ba_h) $\approx 165°$ but in the $Ba_5F_9^+$ ion the similar six-atomic fragment looks like triangle since the Ba_h–F_h–Ba_h units are almost linear,

$\alpha_e(Ba_h–F_h–Ba_h) \approx 173°$. In the $BaBr_3$ units, the angle $\alpha_e(Br–Ba–Br)$ is about 118.5°, whereas the similar units of the $Ba_5F_9^+$ ion are almost planar, $\alpha_e(F–Ba–F) = 119.9°$.

In the vibrational spectra of both cluster ions, the highest frequencies, about 150 cm^{-1}, are assigned to the stretching modes of the $BaBr_2$ moieties, but these frequencies are less than those in $BaBr_2$ molecule itself (Table 3.1). The lowest frequencies of the ions $Ba_4Br_7^+$ and $Ba_5Br_9^+$ are about 30 cm^{-1} and correspond to a swinging motion of the $BaBr_2$ units regarding bipyramids.

Figure 3.9. Enthalpies of dissociation reactions versus computational method: 1 – DFT/B1, 2 – MP2/B1, 3 – MP2^{CP}/B1, 4 – MP4/B1, 5 – MP4^{CP}/B1, 6 – DFT/B2, 7 – MP2/B2, 8 – MP2^{CP}/B2, 9 – MP4/B2, and 10 – MP4^{CP}/B2; (a) $Ba_4X_7^+ \rightleftarrows Ba_3X_5^+ + BaX_2$ (X = F, Br), horizontal lines represent the values 'based on experiment'; (b) $Ba_5X_9^+ \rightleftarrows Ba_4X_7^+ + BaX_2$ (X = F, Br).

The dissociation reactions of the $Ba_4Br_7^+$ and $Ba_5Br_9^+$ cluster ions with elimination of $BaBr_2$ molecule

$$Ba_4Br_7^+ = Ba_3Br_5^+ + BaBr_2 \qquad (3.5)$$

$$Ba_5Br_9^+ = Ba_4Br_7^+ + BaBr_2 \qquad (3.6)$$
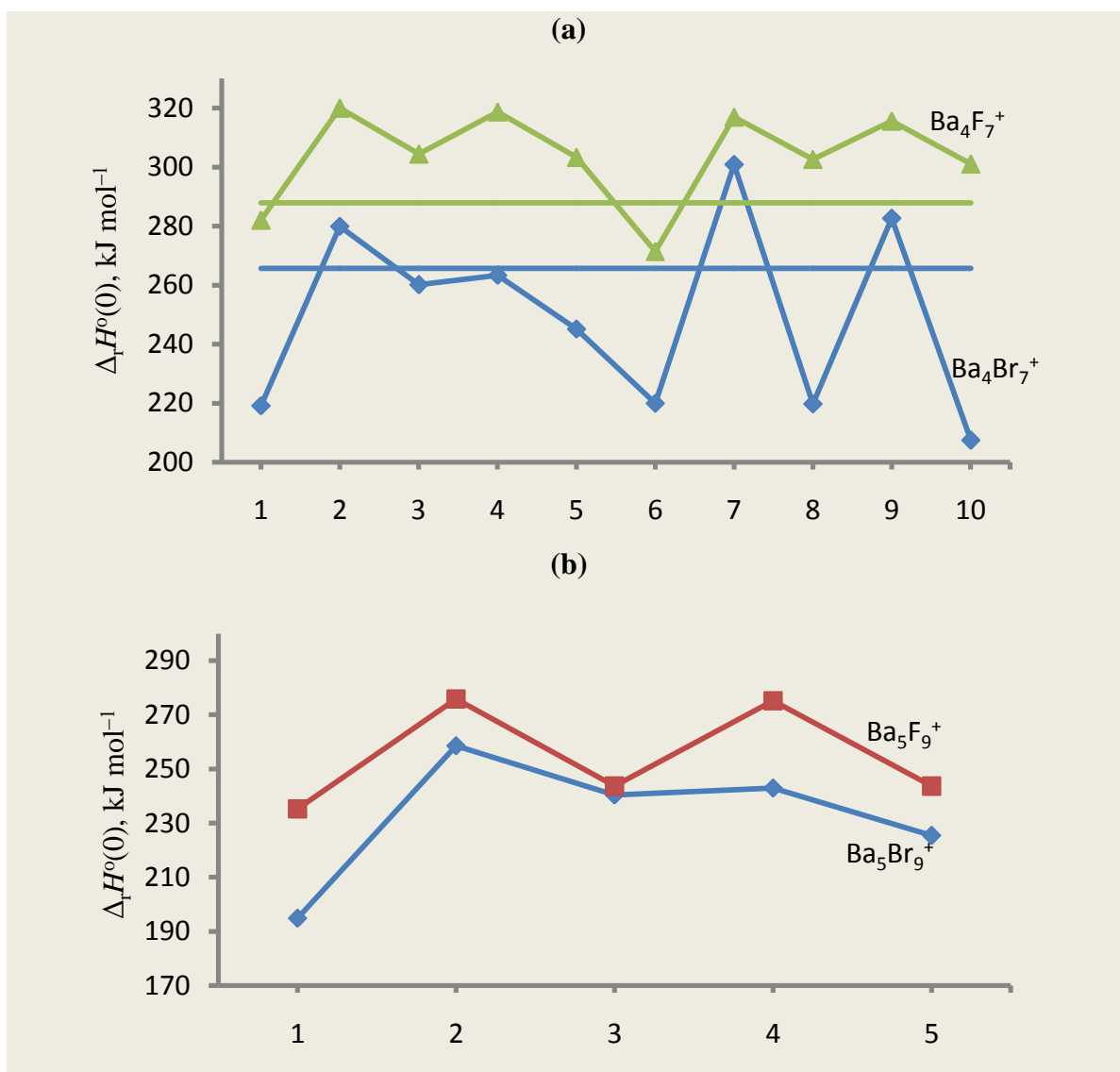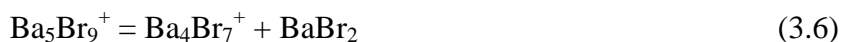
are considered. The theoretical enthalpies of the reactions, $\Delta_r H°(0)$ are displayed versus method of determination in Fig. 3.9. The enthalpies of similar reactions for the ions $Ba_4F_7^+$ and $Ba_5F_9^+$ are shown for comparison. Alike saw-shaped plots are observed for each couple of species across computational methods, but a bigger span may be seen for the $Ba_4Br_7^+$ ion in the right hand side of the plot. For the ion $Ba_4Br_7^+$ the average value of $\Delta_r H°(0) = 257 \pm 47$ kJ mol^{-1} was obtained between all methods with the exception of DFT; this result agrees well with the magnitude 'base on experiment': 266 ± 30 kJ mol^{-1}. For the ion $Ba_5Br_9^+$ the theoretical value $\Delta_r H°(0) = 242 \pm 17$ kJ mol^{-1} was obtained as average between four methods, MP2/B1, MP2^{CP}/B1, MP4/B1 and MP4^{CP}/B1.

3.4 Analysis of thermodynamic properties of the cluster ions

For all cluster ions studied, the dissociation reactions (3.2–3.6) with elimination of $BaBr_2$ molecule were considered above. The accepted theoretical values of enthalpies of the reactions are gathered in Table 3.8. On the base of the enthalpies of reactions $\Delta_r H°(0)$, the enthalpies of formation $\Delta_f H°(0)$ of the gaseous species are also obtained. For three positive ions $Ba_2Br_3^+$, $Ba_3Br_5^+$ and $Ba_4Br_7^+$, the values of $\Delta_r H°(0)$ and $\Delta_f H°(0)$ 'based on experiment' are given as well. A good agreement may be observed between theoretical and 'based on experiment' results, both for enthalpies of the reactions and enthalpies of formation of the ions. Finally we recommend the data 'based on experiment' available for $Ba_2Br_3^+$, $Ba_3Br_5^+$ and $Ba_4Br_7^+$ions and theoretical results for the rest two species $BaBr_3^-$ and $Ba_5Br_9^+$.

Table 3.8. Enthalpies of dissociation reactions $\Delta_r H°(0)$ and enthalpies of formation $\Delta_f H°(0)$ of the cluster ions (in kJ mol^{-1}).

No	Reaction	Theoretical		'Based on experiment'		
		$\Delta_r H°(0)$	$\Delta_f H°(0)$	$\Delta_r H°(0)$, heterophase	$\Delta_r H°(0)$, gaseous	$\Delta_f H°(0)$
1	$BaBr_3^- \rightleftarrows Br^- + BaBr_2$	254 ± 6	-858 ± 6			
2	$Ba_2Br_3^+ \rightleftarrows BaBr^+ + BaBr_2$	317 ± 16	-293 ± 16	-26 ± 10	317 ± 10	-293 ± 10
3	$Ba_3Br_5^+ \rightleftarrows Ba_2Br_3^+ + BaBr_2$	291 ± 21	-981 ± 21	-51 ± 20	292 ± 20	-982 ± 20
4	$Ba_4Br_7^+ \rightleftarrows Ba_3Br_5^+ + BaBr_2$	257 ± 47	-1636 ± 47	-77 ± 30	266 ± 30	-1644 ± 30
5	$Ba_5Br_9^+ \rightleftarrows Ba_4Br_7^+ + BaBr_2$	242 ± 17	-2282 ± 17			

The enthalpies of dissociation reactions, $\Delta_r H^\circ(0)$, are plotted versus cluster size for the ions BaX_3^-, $Ba_2X_3^+$, $Ba_3X_5^+$, $Ba_4X_7^+$ and $Ba_5X_9^+$ (X = F, Cl, Br) as shown in Fig. 3.10. As is seen in the graph, the values of $\Delta_r H^\circ(0)$ increase from the BaX_3^- to $Ba_2X_3^+$ then gradually decrease in series $Ba_2X_3^+ \rightarrow Ba_3X_5^+ \rightarrow Ba_4X_7^+ \rightarrow Ba_5X_9^+$. Evidently the reason for smaller $\Delta_r H^\circ(0)$ of BaX_3^- compared to $Ba_2X_3^+$ is related to less number and lower strength of the bonds disrupted; one bond is broken in BaX_3^- but three shorter bonds in $Ba_2X_3^+$. It is reasonable to suppose that the bigger is the number of bonds and shorter the bond lengths, the higher the energy required to break bonds. For the heavier clusters, the values of $\Delta_r H^\circ(0)$ drop in spite of bigger number of bonds to be destroyed, which relates here to elongation and hence weakening of the bonds.

The enthalpies of formation of the positive cluster ions $BaX^+(BaX_2)_n$, X = F, Cl or Br (n =0–4) are plotted against the number of BaX_2 molecules attached (Fig. 3.11). A similar trend is observed for three families of the ions, the values of $\Delta_f H^\circ(0)$ tend to decrease linearly with increase of the size. As is seen, the values of $\Delta_f H^\circ(0)$ for cluster ions $BaF^+(BaF_2)_n$ are lower and the slope of the plot is steeper followed by $BaCl^+(BaCl_2)_n$ and then $BaBr^+(BaBr_2)_n$ family which reflects a strengthening of the bonds from bromide to fluoride.
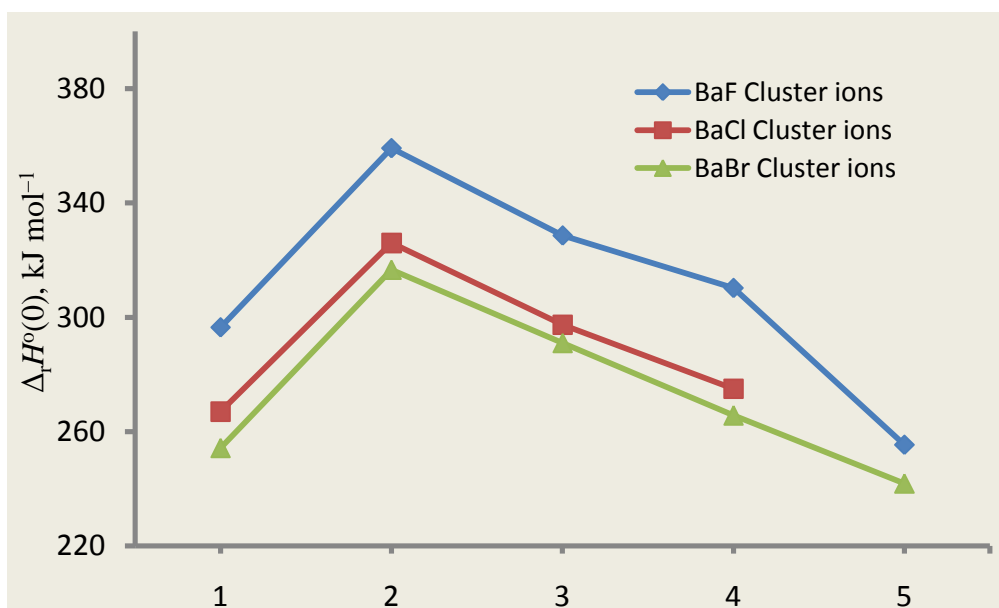
Figure 3.10. Enthalpies of dissociation reactions of the ions versus size of the cluster: 1 – BaX_3^-; 2 – $Ba_2X_3^+$, 3 – $Ba_3X_5^+$, 4 – $Ba_4X_7^+$, 5 – $Ba_5X_9^+$ (X = F, Cl or Br).
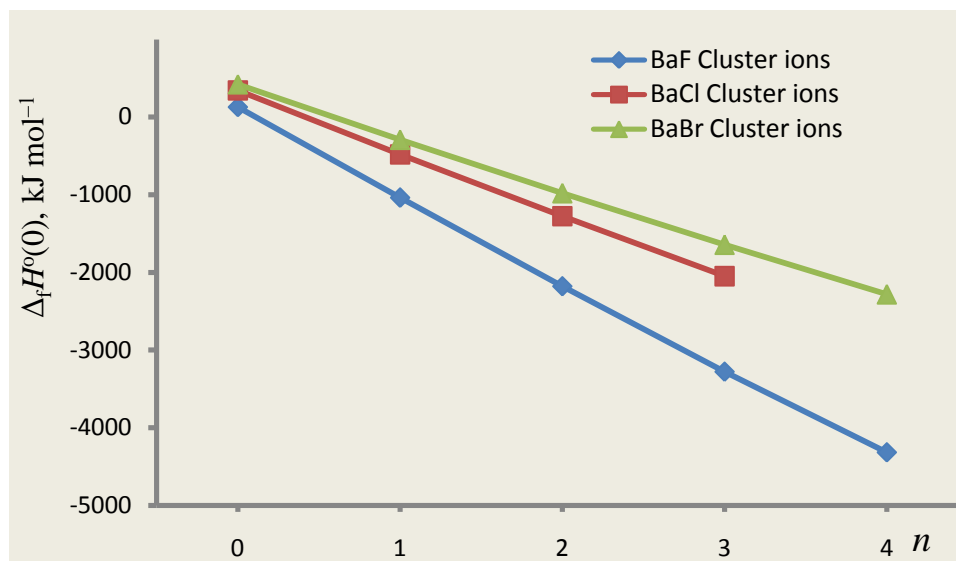
Figure 3.11. Enthalpies of formation of the ions $BaX^+(BaX_2)_n$, X = F, Cl or Br, versus number of BaX_2 molecules attached (n).

3.5　Conclusions

Different cluster ions had been registered earlier in vapour over barium dibromide. In this work the ions have been studied theoretically; the geometrical parameters, vibrational spectra and thermodynamic properties have been obtained. The equilibrium geometrical structures of the ions $BaBr_3^-$, $Ba_2Br_3^+$, $Ba_3Br_5^+$ and $Ba_5Br_9^+$ correspond to the D_{3h} and $Ba_4Br_7^+$ to C_{2v} group of symmetry. Alternative structures for the ions have been taken into consideration but no isomers were identified.

The thermodynamic functions of the species have been calculated using the geometrical parameters and vibrational frequencies obtained. The enthalpies of dissociation reactions $\Delta_r H°(0)$ and enthalpies of formation $\Delta_f H°(0)$ of the ions were computed. The thermodynamic functions for $Ba_2Br_3^+$, $Ba_3Br_5^+$ and $Ba_4Br_7^+$ were used for the treatment of the equilibrium constants measured earlier; the values of $\Delta_r H°(0)$ and $\Delta_f H°(0)$ 'based on experiment' have been found. The analysis of the results has shown that the DFT method systematically underrates the enthalpies of reactions, while MP2 and MP4 methods bring more reliable data which are in a good agreement with values 'based on experiment'.

48

CHAPTER FOUR

4.0 Ionic species in vapour over barium diiodide: quantum chemical study of structure and thermodynamic properties[5]

ABSTRACT

The cluster ions $Ba_2I_3^+$, $Ba_3I_5^+$ and $Ba_4I_7^+$ were detected earlier in saturated vapour over barium diiodide using high temperature mass spectrometric technique. In this work the structure and thermodynamic properties of the species BaI_3^-, $Ba_2I_3^+$, $Ba_3I_5^+$, $Ba_4I_7^+$, and $Ba_5I_9^+$ have been studied theoretically by using the density functional theory (DFT/B3P86) and Møller–Plesset perturbation theory (MP2 and MP4) with triple-zeta valence basis sets. The enthalpies of ion molecular reactions have been determined both theoretically and based of available experimental data; the enthalpies of formation of the cluster ions are found as follows (in kJ mol^{-1}): -709 ± 6, (BaI_3^-), -96 ± 10 ($Ba_2I_3^+$), -654 ± 15 ($Ba_3I_5^+$), -1177 ± 20 ($Ba_4I_7^+$) and -1686 ± 20 ($Ba_5I_9^+$).

4.1 Introduction

Structure of alkaline earth metal halides has been the captivating subject for many researchers and therefore this group of halides is extensively studied (Hargittai, 2000; Spoliti *et al*., 1980; Seijo *et al*., 1991; Pogrebnoi *et al*., 2013); most efforts were focused on the neutral molecular species. Much fewer investigations were devoted to the ionic vapour composition. Different cluster ions were revealed in equilibrium vapours over alkaline earth dihalides using high temperature mass spectrometric technique: $M_2X_3^+$, $M_3X_5^+$ $M_4X_7^+$ (Pogrebnoi *et al*., 1984; Pogrebnoi, 1981), and $BaCl_3^-$ (Kudin *et al*., 1990). The cluster ions $Ba_2I_3^+$, $Ba_2I_5^+$ and $Ba_4I_7^+$ were detected in vapours over barium diiodide.

In the previous theoretical work (Pogrebnoi *et al*., 2013) and previous chapters (chapters 2&3), the structure and properties of the cluster ions of the halides $BaCl_2$, BaF_2 and $BaBr_2$ were studied theoretically. This chapter focuses on the BaI_2-containing ions, BaI_3^- and $BaI^+(BaI_2)_n$ (n = 1–4). The properties to be considered are the geometrical structures, vibrational spectra, and thermodynamic functions, enthalpies of dissociation reactions and enthalpies of formation of the

ionic species. Furthermore, in this chapter we intend to apply the obtained thermodynamic functions for the treatment of previously measured equilibrium constants of ion molecular reactions (Pogrebnoi *et al*., 1984; Pogrebnoi, 1981) so as to obtain thermodynamic properties which are named below as 'based on experiment' values.

4.2   Computational details

Two methods were employed to compute the geometrical parameters and vibrational spectra of the species: the first one was electron density function theory (DFT) with the Becke–Perdew functional (B3P86) (Becke, 1993b; Perdew & Zunger, 1981; Perdew, 1986a) and the second one was Møller–Plesset perturbation theory of second order (MP2). The computations were performed using similar software as described in section 2.2. The basis sets used was SDB-aug-cc-pvtz 4s4p3d2f with relativistic ECP for iodine atom (Martin & Sundermann, 2001); this basis set with ECPs was accessed from the EMSL library (The Environmental Molecular Sciences laboratory, US) (Feller, 1996; Schuchardt *et al*., 2007). For calculations where the MP2 method was employed, no orbitals were frozen, the script NCORE = 0 was used. The geometrical structures of the species were visualized using ChemCraft (Zhurko, 2015) and MacMolPlt (Bode & Gordon, 1998) software. The vibrational spectra were computed and analysis was done to assign the frequencies to certain normal modes and confirm the geometrical structures to be equilibrium.

The enthalpies of dissociation reactions $\Delta_r H^o(0)$ and and enthalpies of formation $\Delta_f H^o(0)$ of the cluster ions have been determined applying two approaches as described earlier. Three methods, DFT, MP2 and MP4, were used to calculate theoretical enthalpies of dissociation reactions of the species. In addition the correction for the basis set superposition error (BSSE) (Boys & Bernardi, 1970) with counterpoise (CP) method (Solomonik & Smirnov, 2005) was performed for MP2 and MP4 results. The details of this procedure can be found in chapter two. The required TD functions and enthalpies of formation of the $I^-_{(g)}$, $BaI_{2(g)}$ and $BaI_{2(c)}$ were retrieved from Ivtanthermo database (Gurvich *et al*., 2000). For the BaI^+, the enthalpy of formation was found through the ionization energy of BaI (Belyaev *et al*., 1990) and the enthalpy of formation of gaseous BaI (Gurvich *et al*., 2000).

4.3 Results and discussion

4.3.1 Geometrical structure and vibrational spectra of the species

Simple species BaI, BaI⁺, BaI₂ and BaI₂⁺. The geometrical parameters, vibrational frequencies, ionization energies, total energies and dipole moments were calculated for the simple species BaI, BaI^+, BaI_2 and BaI_2^+ using the DFT and MP2 methods. BaI possesses open shell, its ground state symbol is $X\,^2\Sigma^+$. The results are compared with the available reference data as presented in Table 4.1. One can see that the calculated internuclear separations R_e(Ba–I) are shorter for DFT method as compared to MP2, by 0.046 Å, 0.022 Å and 0.026 Å for BaI, BaI^+ and BaI_2, respectively. For the valence angle α_e(I–Ba–I) of the BaI_2 molecule, the value by DFT is larger by 7.5° than that by MP2 method. The value of α_e(I–Ba–I) obtained by DFT method for BaI_2 (≈134°) shows that it is bent while its corresponding ion, BaI_2^+ is linear (α_e(I–Ba–I) = 180°). The magnitude of R_e(Ba–I) is slightly higher for neutral BaI_2 than for the ion BaI_2^+. Similar trend for the calculated geometrical parameters in general was observed for respective other halides, the increase from DFT to MP2 being about 0.01–0.02 Å for the R_e(Ba-X) values and 2°–10° for the angle as shown in (Pogrebnoi *et al*., 2013) and previous chapters.

There are no reliable reference data for internuclear separation R_e(Ba–I) of the species BaI and BaI^+. For the BaI_2, the experimental geometrical parameters obtained by electron diffraction method are available in (Spiridonov *et al*., 1981); our calculated parameters both by DFT and MP2 methods do not contradict the experimental data. The computed vibrational frequencies of the species BaI and BaI_2 are generally in a good agreement with available literature data, both theoretical and experimental. For the BaI and BaI_2 molecules, the frequencies calculated by two methods are very close to each other and in accordance with the experimental data (Bradford, 1975; Spiridonov *et al*., 1981).

The Mulliken atomic charges shown in Table 4.1 indicate a highly ionic nature of the species. As is seen the excessive negative charge on the iodine atoms rises in the series BaI^+ – BaI – BaI_2: $0.526e - 0.663e - 0.734e$ that indicates an increase in ionicity of the Ba-I bonds.

We have analyzed the frontier MOs of the species (Fig. 4.1). One can see that for BaI^+ and BaI_2 the HOMOs are composed of *p*-AOs of the iodine atom(s) which are perpendicular to the bond(s) Ba-I; they look like non-bonding orbitals. The LUMO orbitals of BaI^+ ion and BaI_2

molecule are composed mostly of the Ba s-AOs. When an electron attaches the BaI^+ ion resulting in BaI neutral molecule, this unpaired electron occupies the Ba s-AO (Figs. 4.1 b, c). When one more iodine atom is added to BaI to form the BaI_2 molecule, then the electron density redistribution occurs and doubly occupied HOMO is built from p_z-AOs of the I-atoms (Fig. 4.1d). Apparently the shape and orientation of the frontier orbitals illustrate the polar nature of bonds in the simple species considered.

Table 4.1. Properties of BaI, BaI^+ and BaI_2.

Property	DFT	MP2	Reference
BaI			
$R_e(Ba–I)$	3.111	3.157	
$-E$	37.06614	36.71099	
ω_e	148	146	152.3[a]; 150.05[b]
$q(Ba)$	0.663		
$-q(I)$	0.663		
IE_{ad}	5.18	5.00	5.08 ± 0.04[c]
IE_v	5.24	5.07	
μ_e	6.0		
BaI^+			
$R_e(Ba–I)$	2.987	3.009	
$-E$	36.87578	36,52737	
ω_e	185	183	
$q(Ba)$	1.526	1.619	
$-q(I)$	0.526	0.619	
BaI_2			
$R_e(Ba–I)$	3.140	3.166	3.150 ± 0.007[d]
$\alpha_e(I–Ba–I)$	134.2	141.7	148.0 ± 0.9[d]
$-E$	48.64184	48.17090	
$\omega_1(A_1)$	129	125	106 ± 12[d]
$\omega_2(A_1)$	22	18	~16[d]
$\omega_3(B_1)$	164	167	145 ± 21[d]
$q(Ba)$	1.467	1.574	
$-q(I)$	0.734	0.787	
IE_{ad}	8.62		8.6[e];
IE_v	8.88	9.2	8.74 ± 0.01[f]
μ_e	6.6	6.0	
BaI_2^+			
$R_e(Ba–I)$	3.127		
$\alpha_e(I–Ba–I)$	180		
$-E$	48.32494		

Note: $R_e(Ba−I)$ is the equilibrium internuclear distance, Å; $\alpha_e(I−Ba−I)$ is the valence angle, degrees; ω_i are the vibrational frequencies, cm^{-1}; IE_{ad} and IE_{ver} are the adiabatic and vertical ionization energies, respectively, eV; and μ_e is the dipole moment, D.
Notes to reference data: [a]emission spectra in flames (Bradford, 1975), [b]laser excitation spectra (Dagdigian *et al*., 1976) retrieved from NIST (www.nist.gov); [c]evaluation (Belyaev *et al*., 1990), retrieved from NIST (www.nist.gov); [d]electron diffraction (Spiridonov *et al*., 1981); [e]appearance energy (Emons *et al*., 1982); [f]photoelectron spectroscopy (Lee & Potts, 1979).
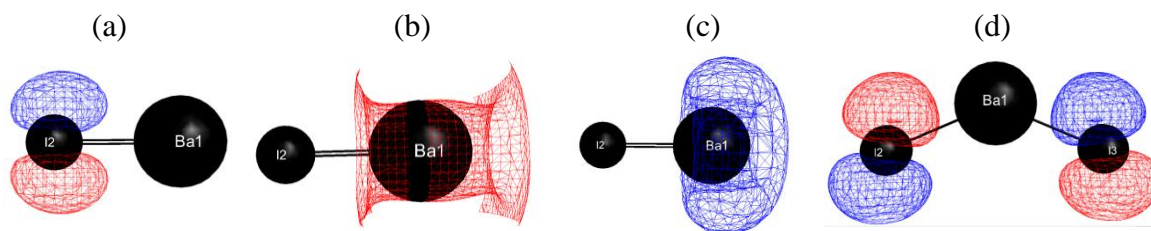
Figure 4.1. Frontier orbitals of the simple species: (a) BaI$^+$ HOMO; (b) BaI$^+$ LUMO; (c) BaI HOMO; (d) BaI$_2$ HOMO.

The values of the ionization energies, IE_{ad} and IE_{ver}, of the BaI molecule, obtained by DFT method are higher than those by MP2 method, respectively, while for BaI$_2$ it is otherwise. Note that the difference between the results found by two methods is bigger than that between vertical and adiabatic ionization energies themselves. Note that the similar relationship was observed for other halides BaX$^+$ and BaX$_2$ (X = F, Cl, Br) as mentioned in chapters 2 & 3. As for comparison with the experimental data, the computed IE_{ad} by MP2 method for BaI agrees better with that from (Belyaev *et al*., 1990) retrieved from NIST (www.nist.gov) than the DFT result. For the BaI$_2$, the IE_{ad} obtained by DFT method is in a very good accordance with the experimental data by photoelectron spectroscopy (Lee & Potts, 1979), the difference is 0.02 eV. As for the IE_{ver} of BaI$_2$ a fair agreement with the experimental data (Lee & Potts, 1979) is observed for the DFT result with the difference ~0.14 eV, while for the MP2 the discrepancy is rather high, 0.46 eV.

At the end of this section we can conclude that the calculations performed for the simple species validate the appropriateness of the methods applied; the results obtained are needed in further calculations for the complicated species considered below. The two methods, DFT and MP2, have been employed in computation of the properties of the cluster ions BaI$_3^-$, Ba$_2$I$_3^+$, Ba$_3$I$_5^+$, while for the heavier Ba$_4$I$_7^+$ and Ba$_5$I$_9^+$ only DFT method appeared to be affordable.

Tetraatomic negative ion BaI$_3^-$. The ion BaI$_3^-$ was not detected experimentally so far but its existence may be anticipated by analogy with similar alkaline earth halide anions MX$_3^-$ mentioned in introduction. The calculated properties of the ion are shown in Table 4.2. The equilibrium geometrical structure was confirmed to be planar of D_{3h} symmetry (Fig. 4.2 a). The structural parameters obtained are in a good agreement between two computational levels; the value of R_e(Ba-I) by the MP2 method is increased by ~0.01 Å from DFT to MP2, the corresponding vibrational modes almost coincide. The same D_{3h} configuration was confirmed for

other alkaline earth halide anions, CaX_3^- (Elliott *et al.*, 2005; Moustapher *et al.*, 2016), $BaCl_3^-$ (Pogrebnoi *et al.*, 2013) and BaF_3^- and $BaBr_3^-$ in the previous chapters.

Table 4.2. Properties of tetraatomic BaI_3^- (D_{3h}) ion.

Property	DFT	MP2
R_e(Ba–I)	3.260	3.269
$-E$	60.28483	59.69434
q(Ba)	1.549	1.635
$-q$(I)	0.850	0.878
ω_1 (A_1')	95 (0)	96 (0)
ω_2 (A_2'')	31 (0.3)	30 (0.4)
ω_3 (E')	136 (2.1)	138 (2.1)
ω_4 (E')	27 (0.05)	27 (0.07)

Note: R_e(Ba−I) is the equilibrium internuclear distance, Å; E is the total energy, au; ω_i are the vibrational frequencies, cm^{-1}; q(Ba) and q(I) are atomic charges and the values given in parenthesis near the frequencies are the intensities in IR spectrum, D^{2}amu^{-1}Å^{-2}.

Compared to the diiodide molecule BaI_2, the internuclear separation R_e(Ba–I) of the ion BaI_3^- is longer than that in the diiodide molecule, by ~0.1 Å, valence modes ω_2 and ω_3 are lower by frequencies, however the bending modes ω_2 and ω_4 in the BaI_3^- are remarkably higher than ω_2 in BaI_2. It seems that attachment of the I^- anion to the neutral BaI_2 molecule brings to a stabilization and rigidity of the structure of the BaI_3^- ion. To favor this stabilization and high symmetry, the extra electron gained is redistributed equally among three iodine atoms. A slight increase, by ~0.1e, of the atomic charges is observed compared to the BaI_2 molecule which facilitates the barium atom to attract iodine atoms and hold them around in the plane. The electron density distribution in the BaI_3^- ion is similar to that in BaI_2 molecule regarding the frontier orbitals; in both species, the HOMOs are composed of the iodine *p*-orbitals oriented perpendicular to the bonds and lying in the horizontal plane and LUMOs are formed mostly of *s*-AOs of Ba atoms (Fig. 4.2 b, c).
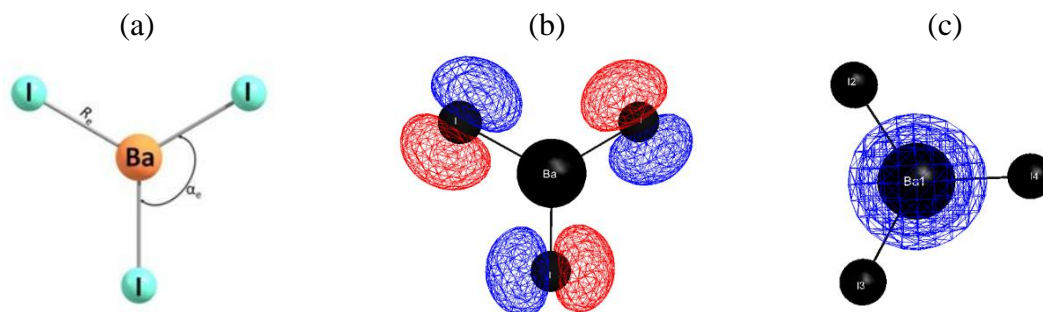
Figure 4.2. Tetraatomic negative ion BaI_3^-: (a) equilibrium geometrical structure, (b) HOMO, (c) LUMO.

Pentaatomic positive ion Ba₂I₃⁺. Different alternative geometrical configurations have been considered for the $Ba_2I_3^+$ ion but only the bipyramidal one of the D_{3h} symmetry (Fig. 4.3 a) was proved to be equilibrium. The calculated properties are presented in Table 4.3. The bipyramid $Ba_2I_3^+$ is composed of two barium atoms at the vertices and three iodine atoms in the horizontal plane. A vertex angle is about 84° that is the bipyramid is stretched along the axis. The bipyramid $Ba_2I_3^+$ is contains six bridged bonds which are longer by ~0.2 Å than those within the simple species, and the valence modes are lower respectively at the same time the bending modes ω_2 and ω_5 in $Ba_2I_3^+$ are not less than 40 cm⁻¹ that is higher compared to $\omega_2 \approx 20$ cm⁻¹ in the BaI_2 molecule. Thus the structure of the ion is compact and quite rigid. Alike equilibrium structures were confirmed for other alkaline earth halides; $Ba_2F_3^+$ (chapter two), $Ba_2Br_3^+$ (chapter three), $Ba_2Cl_3^+$ (Pogrebnoi *et al.*, 2013) and $Ca_2Cl_3^+$ (Moustapher *et al.*, 2016).

Table 4.3. Properties of pentaatomic positive ion $Ba_2I_3^+$ (D_{3h})

Property	DFT	MP2
R_e(Ba–I)	3.299	3.305
α_e (I–Ba–I)	84.2	83.6
$-E$	85.62008	84.81604
q(Ba)	1.486	1.592
$-q$(I)	0.657	0.728
ω_1 (A_1')	134 (0)	133 (0)
ω_2 (A_1')	68 (0)	69 (0)
ω_3 (A_2'')	119 (1.1)	121 (1.2)
ω_4 (E')	121 (1.5)	123 (1.6)
ω_5 (E')	43 (0.2)	41 (0.2)
ω_6 (E'')	84 (0)	88 (0)

Note: R_e is the equilibrium internuclear distance, Å; α_e is the valence angle, degs; ω_i are the vibrational frequencies, cm⁻¹; E is the total energy, au; q(Ba) and q(I) are atomic charges and the values given in parenthesis near the frequencies are the intensities in IR spectrum, $D^2amu^{-1}Å^{-2}$.

Comparatively, in the series of barium halides ions $Ba_2X_3^+$, the vertex angle increases in the order $Ba_2F_3^+$ (71°) → $Ba_2Cl_3^+$ (78°) → $Ba_2Br_3^+$ (82°) → $Ba_2I_3^+$ (84°), as well as the internuclear separation R_e(Ba–X), 2.41 Å, 2.94 Å, 3.06 Å and 3.30 Å, respectively. This ascending trend in the parameters evidently follows the increase of the halogen size in the sequence.

In the $Ba_2I_3^+$ ion, the atomic charges q(Ba) are almost equal to that in BaI_2 molecule, while the magnitudes of q(I) by ~0.06e are smaller than in the molecule providing the proper positive net charge +1e of the cluster ion. The frontier orbitals of the $Ba_2I_3^+$ ion are shown in the Figs 4.3 b,c. The HOMO is formed entirely of the iodine *p*-orbitals which are directed perpendicular to the bonds and lying in the horizontal plane. The character of these orbitals is similar to that in the

BaI_2 and BaI_3^- species; moreover the top view in Fig. 4.3 b looks exactly like the HOMO of BaI_3^- shown in Fig. 4.2b. The LUMO is composed mostly of AOs of barium atoms with a small contribution from iodine atoms.

(a)   (b)   (c)
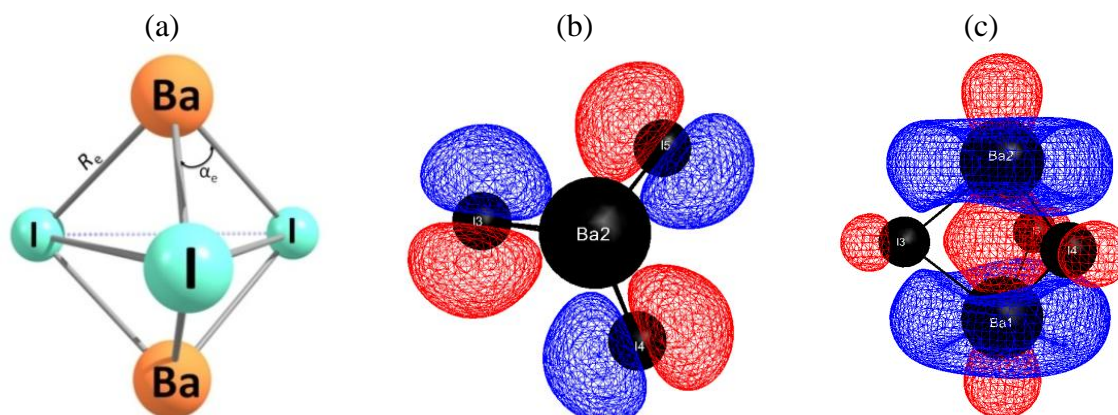
Figure 4.3. Pentaatomic positive ion $Ba_2I_3^+$: (a) equilibrium geometrical structure; (b) HOMO, top view; (c) LUMO, side view.

Octaatomic positive ion $Ba_3I_5^+$. Two different configurations, the bipyramidal and two cycle-chain structure with a I-tail were considered in this study but only the bipyramidal structure appeared to be equilibrium (Fig. 4.4a, b). The properties of the ion are presented in Table 4.4.

(a)   (b)   (c)
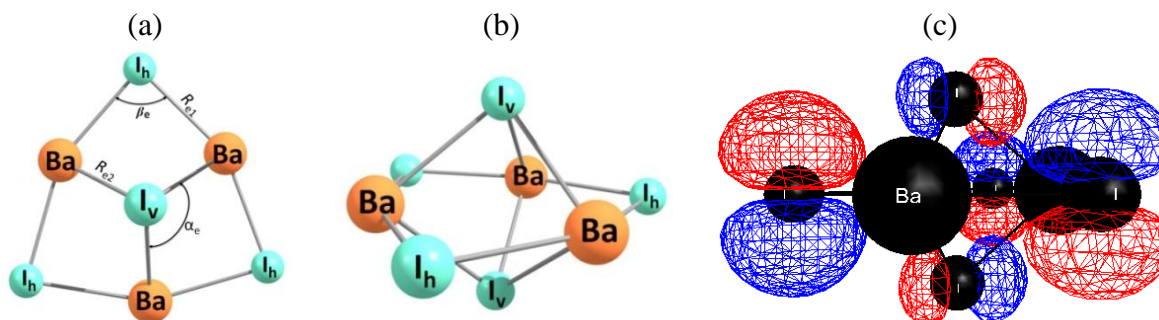
Figure 4.4. Octaatomic positive ion $Ba_3I_5^+$: (a) equilibrium geometrical structure, top view, (b) side view; (c) HOMO.

There is a good correspondence between DFT and MP2 results. Within the bipyramid, there are two types of the iodine atoms; tridentate coordinated I_v in vertices and bidentate I_h in the horizontal hexaatomic moiety. The bonds in the horizontal plane $Ba–I_h$ are shorter, by ~0.04 Å, than the vertical bridged bonds $Ba–I_v$, the ratio between two separations, $I_h–I_h$ and $I_v–I_v$, being equal to ~1.5. Therefore the bipyramid $Ba_3I_5^+$ is squeezed along the vertical axis.

56

Table 4.4. Properties of octaatomic $Ba_3I_5^+$ ion.

Property	DFT	MP2
$R_{e1}(Ba–I_h)$	3.353	3.343
$R_{e2}(Ba–I_v)$	3.436	3.404
$\alpha_e(Ba–I_v–Ba)$	82.8	82.6
$\beta_e(Ba–I_h–Ba)$	85.3	84.5
$-E$	134.34625	133.09548
$q(Ba)$	1.355	1.465
$-q(I_h)$	0.624	0.683
$-q(I_v)$	0.597	0.672
$\omega_1\ (A_1')$	113 (0)	122 (0)
$\omega_2\ (A_1')$	96 (0)	105 (0)
$\omega_3\ (A_1')$	86 (0)	92 (0)
$\omega_4\ (A_1')$	64 (0)	70 (0)
$\omega_5\ (A_2'')$	102 (0.7)	109 (0.7)
$\omega_6\ (A_2'')$	31 (0.1)	30 (0.2)
$\omega_7\ (E')$	128 (2.6)	134 (2.6)
$\omega_8\ (E')$	103 (1.2)	109 (1.3)
$\omega_9\ (E')$	64 (0.04)	70 (0.03)
$\omega_{10}\ (E')$	50 (0.07)	54 (0.06)
$\omega_{11}\ (E'')$	73 (0)	81 (0)
$\omega_{12}\ (E'')$	32 (0)	32 (0)

Note: R_{e1} and R_{e2} are the equilibrium internuclear distances, Å; α_e and β_e are the valence angles, degs; ω_i are the vibrational frequencies, cm^{-1}; E is the total energy, au; $q(Ba)$ and $q(I)$ are atomic charges and the values given in parenthesis near the frequencies are the intensities in IR spectrum, D^{2}amu^{-1}Å^{-2}.

Compared to the pentaatomic ion $Ba_2I_3^+$, the octaatomic bipyramid possessing the same high symmetry (D_{3h}) becomes less rigid due to the elongated bonds, by 0.04 Å (Ba–I$_v$) and 0.15 Å (Ba–I$_h$), and the lower bending frequencies approaching 30 cm^{-1}. Atomic charges are smaller than in $Ba_2I_3^+$ indicating reducing polarity of bonds, note that the charges on I$_v$ and I$_h$ do not differ much. The HOMO (Fig. 4.4 c) is mostly composed of p_z AOs of the horizontal iodine atoms I$_h$, and also of p_x AOs of I$_v$ atoms but in much less extent. Apparently the shape of the p_z-orbitals oriented perpendicular to the plane of the hexagonal ring favor a strengthening of the Ba-I$_h$ bonds within the ring and hence its rigidity.

Note that the identical pyramidal configuration of D_{3h} symmetry was determined for other octaatomic cluster ions of barium halides $Ba_3X_5^+$; $Ba_3Cl_5^+$ (Pogrebnoi *et al.*, 2013), $Ba_3F_5^+$ (chapter two) and $Ba_3Br_5^+$ (chapter three). Regarding the shape of the bipyramid, in the order $Ba_3F_5^+\rightarrow Ba_3Cl_5^+\rightarrow Ba_3Br_5^+\rightarrow Ba_3I_5^+$, the vertex angle $\alpha_e(Ba–X_v–Ba)$ decreases, $95^\circ\rightarrow 89^\circ\rightarrow 86^\circ\rightarrow 83^\circ$; and the angle in the ring $\beta_e(Ba–X_h–Ba)$ also decreases, $102^\circ\rightarrow 94^\circ\rightarrow 89^\circ\rightarrow 85^\circ$. Thus a slight stretching of the bipyramid along the vertical axis is observed from fluoride to iodide and a transformation of the six-atomic horizontal moiety from a hexagon to close to triangle shape.

Undecaatomic positive ion Ba₄I₇⁺. Like other positive ions described above the undecaatomic ion $Ba_4I_7^+$ was also detected earlier experimentally in saturated vapors over barium diiodide (Pogrebnoi *et al.*, 1984; Pogrebnoi, 1981). The calculated properties of the ion are presented in Table 4.5; the equilibrium geometrical configuration corresponds to the C_{2v} point group of symmetry (Fig. 4.5a). Similar to other halide cluster ions $Ba_4X_7^+$; $Ba_4Cl_7^+$ (Pogrebnoi *et al.*, 2013), $Ba_4F_7^+$ (section 2.3.6) and $Ba_4Br_7^+$ (section 3.3.5), the structure of the ion $Ba_4I_7^+$ can be presented as composed of a pentaatomic bipyramidal moiety Ba_2I_3 and two molecules BaI_2 attached along the faces of the bipyramid. Compared to the individual ion $Ba_2I_3^+$, the respective parameters of the moiety become nonequivalent; moreover the internuclear distances are essentially elongated (by ~0.23–0.25 Å) and the vertex angles decrease by 7–10°. Compared to the free molecule, the BaI_2-units are straightened, the valence angles increased by 24° and the internuclear distances lengthened by 0.19 Å. It must be emphasized that the new bonds Ba_1-I_3 and Ba_2-I_1 formed between the bipyramid Ba_2I_3 and two molecules attached are comparable by length (and hence by strength) with the Ba_2–I_3 in the BaI_2-unit and Ba_1-I_1/Ba_1-I_2 in Ba_2I_3-unit, respectively.

In the vibrational spectrum, there are five low frequencies, below 40 cm^{-1}, relate to swinging motions of the BaI_2-units around the Ba_2I_3 moiety. The highest frequencies, ~130 cm^{-1} correspond to stretching vibrational modes of the BaI_2-units; frequencies of ~120 cm^{-1} are assigned to the new-formed bonds, and those of about 60 cm^{-1} correspond to the bipyramidal moiety.

The atomic charges in the $Ba_4I_7^+$ ion are distributed non-uniformly between the Ba/I atoms, thus the charges on the iodine atoms vary approximately from $-0.3e$ to $-0.6e$. The frontier orbitals are shown in Fig. 4.5 b & c. The highest occupied orbitals, HOMO, HOMO–1 up to HOMO–10 have almost the same energies, about –0.36 eV, and are attributed to AOs from the iodine atoms; the major input comes from the BaI_2-units and the minor from the Ba_2I_3-moiety. The lowest unoccupied orbitals have almost equal energies up to LUMO+2 and composed mostly of combination of *s*-, *p*-, *d*-AOs of the Ba atoms.

Table 4.5. Properties of the undecaatomic $Ba_4I_7^+$ (C_{2v}) ion.

Property	DFT	Property	DFT
$R_{e1}(Ba_1–I_1)$	3.551	$\omega_7(A_1)$	41 (0.01)
$R_{e2}(Ba_1–I_2)$	3.534	$\omega_8(A_1)$	31 (0.01)
$R_{e3}(Ba_1–I_3)$	3.366	$\omega_9(A_1)$	27 (0.001)
$R_{e4}(Ba_2–I_1)$	3.531	$\omega_{10}(A_2)$	130 (0)
$R_{e5}(Ba_2–I_2)$	3.374	$\omega_{11}(A_2)$	97 (0)
$R_{e6}(Ba_2–I_3)$	3.332	$\omega_{12}(A_2)$	57 (0)
$\alpha_e(I_2–Ba_1–I_2)$	73.6	$\omega_{13}(A_2)$	45 (0)
$\alpha'_e(I_1–Ba_1–I_2)$	76.9	$\omega_{14}(A_2)$	23 (0)
$\beta_e(I_3–Ba_1–I_3)$	115.4	$\omega_{15}(B_1)$	120 (1.52)
$\gamma_e(I_3–Ba_2–I_3)$	158.5	$\omega_{16}(B_1)$	108 (0.87)
$-E$	183.06588	$\omega_{17}(B_1)$	88 (0.002)
$q(Ba_1)$	1.212	$\omega_{18}(B_1)$	74 (0.0005)
$q(Ba_2)$	1.263	$\omega_{19}(B_1)$	58 (0.12)
$-q(I_1)$	0.298	$\omega_{20}(B_1)$	54 (0.17)
$-q(I_2)$	0.557	$\omega_{21}(B_1)$	26 (0.06)
$-q(I_3)$	0.635	$\omega_{22}(B_2)$	129 (2.11)
$\omega_1(A_1)$	113 (0.8)	$\omega_{23}(B_2)$	92 (0.16)
$\omega_2(A_1)$	101 (0.02)	$\omega_{24}(B_2)$	84 (0.22)
$\omega_3(A_1)$	93 (0.2)	$\omega_{25}(B_2)$	63 (0.001)
$\omega_4(A_1)$	79 (0.02)	$\omega_{26}(B_2)$	49 (0.05)
$\omega_5(A_1)$	73 (0.001)	$\omega_{27}(B_2)$	27 (0.001)
$\omega_6(A_1)$	60 (0)		

Note: R_{ei} are the equilibrium internuclear distances, Å; α_e, α'_e, β_e and γ_e are the valence angles, degs; E is the total energy, au; $q(Ba)$ and $q(I)$ are atomic charges; ω_i are the vibrational frequencies, cm^{-1} and the values given in parenthesis near the frequencies are the intensities in IR spectrum, $D^2amu^{-1}Å^{-2}$.
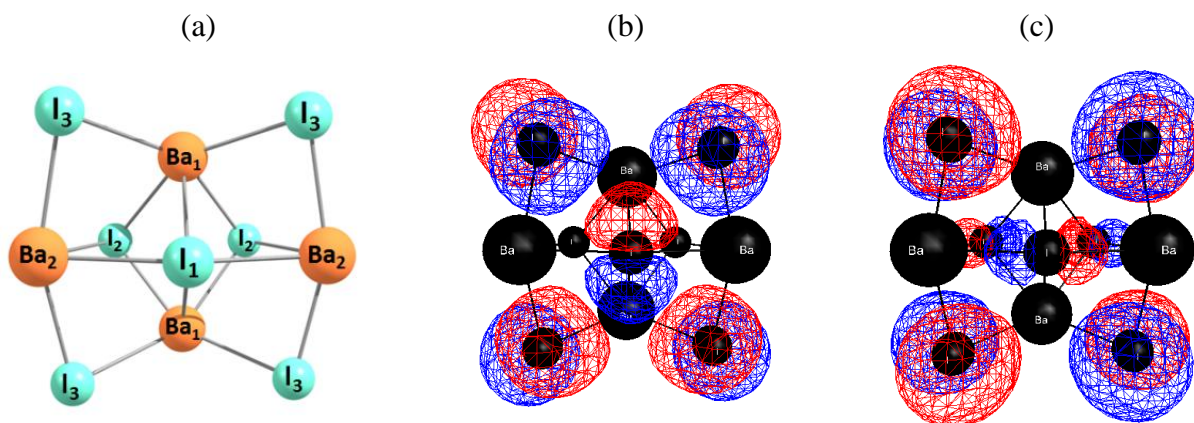
Figure 4.5. Undecaatomic positive ion $Ba_4I_7^+$: (a) equilibrium geometrical structure; (b) HOMO; (c) HOMO–1.

Concluding this section on the structural properties of the species one can note the different types of Ba–I bonds in the positive ions $BaI^+(BaI_2)_n$; single bond in the BaI^+, three equivalent bridged bonds Ba-I-Ba in $Ba_2I_3^+$, two types of bonds in $Ba_3I_5^+$ (the shorter Ba-I_h and longer Ba-I_v), and three types of bonds in $Ba_4I_7^+$ (within the BaI_2- and Ba_2I_3-units and between them). From the

first member of the series, BaI^+, to the last, $Ba_4I_7^+$, the internuclear separations vary from 3.00 Å up to 3.55 Å and maximal stretching vibrational frequencies from 185 cm^{-1} to 129 cm^{-1}. The bending modes relate to the rigidity of the cluster structure, the lowest frequencies of about 23–40 cm^{-1} are found, one in $Ba_2I_3^+$, two in $Ba_3I_5^+$, and five in $Ba_4I_7^+$, thus increase in this number leads to decrease of the rigidity and hence the stability of the clusters. The electron density distribution within the ions can be observed through the atomic charges and the frontier orbitals character. The charges of the Ba atoms, $q(Ba)$, decrease gradually from 1.53e (BaI^+) to 1.21e ($Ba_4I_7^+$). The magnitudes of $q(I)$ vary from –0.66e ($Ba_2I_3^+$) up to –0.30e (I_1 in $Ba_4I_7^+$), but the change is not monotonic in the series. Thus the ionicity, in general, decreases with increase of the ion size. The common features of the frontier orbitals in the ions are as follows: the HOMOs are degenerated orbitals attributed to the p-AOs of the iodine atoms which are perpendicular to the bonds Ba–I, the lowest unoccupied orbitals are formed by Ba-AOs. The ionic character of the Ba–I bonds is evident through the composition of the HOMOs which indicate the excessive negative charge on the iodine atoms and lack of electrons on barium atoms.

Tetradecaatomic positive ion $\mathbf{Ba_5I_9^+}$. Computations of geometrical parameters and vibrational spectrum were done for the tetradecaatomic positive ion by employing DFT method only; MP2 method was not achievable. This ion has never been detected experimentally but its existence can be predicted in a similar way that $Ba_5Cl_9^+$ was predicted by Pogrebnoi et al. (Pogrebnoi *et al*., 2013). Furthermore, in previous chapters the similar ions $Ba_5F_9^+$ and $Ba_5Br_9^+$ were studied and predicted to exist. Table 4.6 presents the results of this computation for the properties of $Ba_5I_9^+$ ion. Similar to the previous studies as presented earlier for $Ba_5F_9^+$ and $Ba_5Br_9^+$, this ion also was confirmed to correspond to D_{3h} point group of symmetry (Fig. 4.6).

The $Ba_5I_9^+$ ion can be considered as composed of $Ba_2I_3^+$ pyramidal core with three BaI_2 molecules attached along the faces of the $Ba_2I_3^+$ moiety. In the $Ba_2I_3^+$-core, the bonds Ba–I_h are equivalent similar to free $Ba_2I_3^+$ ion but being longer by 0.40 Å and the angle α_e more acute, by 12°. In the $Ba_5I_9^+$ ion, the attached BaI_2 molecules have also longer Ba_h–I bonds, by 0.18 Å, and the valence angle β_e(I–Ba_h–I) is flatter by 27° as compared to free BaI_2 molecules.

As shown in Table 4.6, the magnitude of the atomic charge on the barium atom $q(Ba_h)$, is 1.12e in $Ba_5I_9^+$. This value is lower than the values for the smaller cluster ions; the trend shows that the magnitude of the charge on barium atom decreases with increase in cluster size starting from

BaI^+ to $Ba_5I_9^+$. Similarly for the charge on iodine atom, the magnitude of the charge for iodine atom in $Ba_5I_9^+$ is lower ($-0.2e$) compared to $q(I)$ in BaI^+. The frontier MOs are presented in Fig. 4.6.

Table 4.6. Properties of the positive cluster ion $Ba_5I_9^+$ (D_{3h}).

Property[a]	DFT/B3P86	Property[a]	DFT/B3P86
$R_{e1}(Ba–I_h)$	3.700	$\omega_8\,(A_1')$	22 (0)
$R_{e2}(Ba_h–I_h)$	3.431	$\omega_9\,(A_2'')$	131 (2.9)
$R_{e3}(Ba_h–I)$	3.318	$\omega_{10}\,(A_2'')$	76 (0.005)
$R_{e4}(Ba–I)$	3.405	$\omega_{11}\,(A_2'')$	68 (0.3)
$\alpha_e(I–Ba–I)$	117.4	$\omega_{12}\,(A_2'')$	38 (0.01)
$\beta_e(I_h–Ba_h–I_h)$	78.6	$\omega_{13}\,(E')$	115 (4.4)
$-E$	231.47803	$\omega_{14}\,(E')$	107 (0.1)
$q(Ba_1)$	1.1199	$\omega_{15}\,(E')$	79 (0.01)
$q(Ba_2)$	1.0870	$\omega_{16}\,(E')$	69 (0.00002)
$-q(I_1)$	0.1878	$\omega_{17}\,(E')$	46 (0.6)
$-q(I_2)$	0.6562	$\omega_{18}\,(E')$	35 (0.00008)
$\omega_1\,(A_1')$	97 (0)	$\omega_{19}\,(E')$	20 (0.1)
$\omega_2\,(A_1')$	94 (0)	$\omega_{20}\,(E'')$	130 (0)
$\omega_3\,(A_1')$	87 (0)	$\omega_{21}\,(E'')$	95 (0)
$\omega_4\,(A_1')$	71 (0)	$\omega_{22}\,(E'')$	52 (0)
$\omega_5\,(A_1')$	52 (0)	$\omega_{23}\,(E'')$	38 (0)
$\omega_6\,(A_1')$	46 (0)	$\omega_{24}\,(E'')$	20 (0)
$\omega_7\,(A_1')$	25 (0)		

Note: R_{ei} are the equilibrium internuclear distances, Å; α_e and β_e are the valence angles, degs; E is the total energy, au; $q(Ba)$ and $q(I)$ are atomic charges; ω_i are the vibrational frequencies, cm^{-1} and the values given in parenthesis near the frequencies are the intensities in IR spectrum, $D^2amu^{-1}Å^{-2}$.

The energy of the tetradecaatomic $Ba_5I_9^+$ ion is about 170 kJ mol^{-1} lower than the sum of the energies of $Ba_4I_7^+$ and BaI_2, 380 kJ mol^{-1} lower than the sum of the energies of $Ba_3I_5^+$ and two BaI_2 molecules, or 600 kJ mol^{-1} lower than the sum of energies of $Ba_2I_3^+$ and three BaI_2 molecules (according to the DFT results). This implies that the formation of tetradecaatomic $Ba_5I_9^+$ ion from the lower cluster ions is a feasible process and thus the existence of this ion can be predicted.

Concluding this section on the structural properties of the species one can note the different types of Ba–I bonds in the positive ions $BaI^+(BaI_2)_n$: single bond in the BaI^+, three equivalent bridged bonds Ba–I–Ba in $Ba_2I_3^+$, two types of bonds in $Ba_3I_5^+$ (the shorter Ba–I_h and longer Ba–I_v), four types of bonds in $Ba_4I_7^+$ and $Ba_5I_9^+$ (within the BaI_2- and Ba_2I_3-units and two types between them). Also if the shape of the $Ba_5I_9^+$ ion is imagined as three-layered sandwich, the BaI_3-

fragments on top and bottom and the hexagon $Ba_{h3}I_{h3}$ in the central horizontal plane, then bonds can be distinguished within each fragment and between.
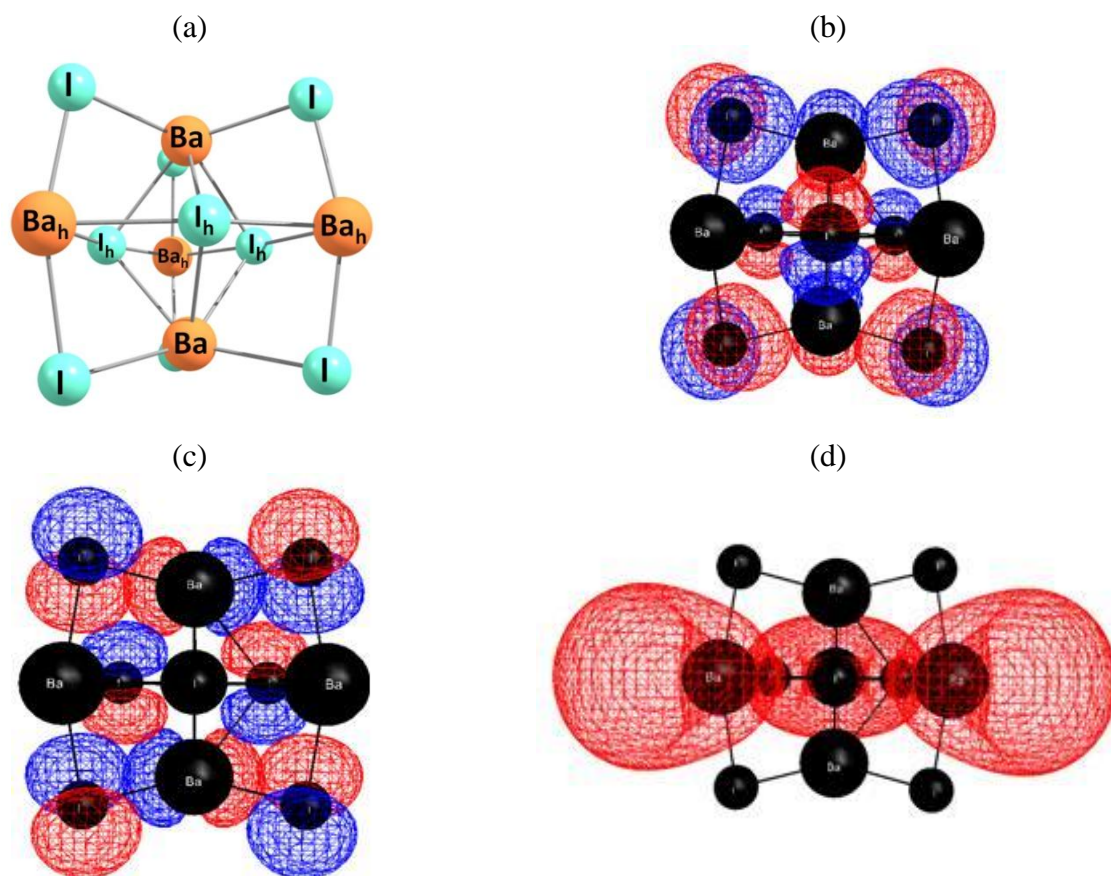
Figure 4.6. Tetradecaatomic positive ion, $Ba_5I_9^+$: (a) equilibrium geometrical structure; (b) HOMO 56; (c) HOMO-1 55; (d) LUMO 57.

From the first member of the series, BaI^+, to the last, $Ba_5I_9^+$, the internuclear separations $Ba-I$ vary from 3.00 Å up to 3.70 Å and maximal stretching vibrational frequencies from 185 cm^{-1} to 131 cm^{-1}. The bending modes relate to the rigidity of the cluster structure, the lowest frequencies below ~40 cm^{-1} are found, one in $Ba_2I_3^+$, two in $Ba_3I_5^+$, five in $Ba_4I_7^+$, and seven in $Ba_5I_9^+$, thus increase in this number leads to decrease of the rigidity and hence the stability of the clusters. The electron density distribution within the ions can be observed through the atomic charges and the frontier orbitals character. The charges of the Ba atoms, $q(Ba)$, decrease gradually from 1.53e (BaI^+) to 1.11e ($Ba_5I_9^+$). The magnitudes of $q(I)$ vary from −0.66e ($Ba_2I_3^+$) up to −0.19e (I_h in $Ba_5I_9^+$), but the change is not monotonic in the series. Thus the ionicity, in general, decreases with increase of the ion size. The common features of the frontier orbitals in the ions are as

follows: the HOMOs are degenerated orbitals attributed to the *p*-AOs of the iodine atoms, the lowest unoccupied orbitals are formed by Ba-AOs. The ionic character of the Ba–I bonds is evident through the composition of the HOMOs which indicate the excessive negative charge on the iodine atoms and lack of electrons on barium atoms.

4.3.2   Enthalpies of dissociation reactions and enthalpies of formation of the species

The dissociation reactions of the cluster ions with elimination of BaI_2 molecule were considered as follows:

$$BaI^+(BaI_2)_n \rightleftarrows BaI^+(BaI_2)_{n-1} + BaI_2 \tag{4.1}$$

$$BaI_3^- \rightleftarrows I^- + BaI_2 \tag{4.2}$$
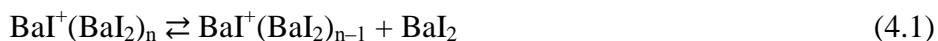
The theoretical enthalpies of the reactions $\Delta_r H^o(0)$ were calculated using the DFT, MP2 and MP4 methods; the BSSE correction with counterpoise (CP) method was used as well; altogether five methods, DFT, MP2, MP2^{CP}, MP4, and MP4^{CP} were employed[6]. There was no optimization of geometries for the MP4 method, the coordinates optimized by MP2 method for the BaI^+, BaI_2, $Ba_2I_3^+$ and $Ba_3I_5^+$ species and by DFT method for $Ba_4I_7^+$ and $Ba_5I_9^+$ ions were used. The theoretical results are displayed versus method of computation in Fig. 7. Alike tendency of the plots can be seen as a leap from minimum quantities by DFT to maximum by MP2 with the descent to the MP4^{CP} followed by; the span between maximum and minimum values varies from 13 kJ mol^{-1} (BaI_3^-) to 70 kJ mol^{-1} ($Ba_5I_9^+$).

In addition, the 'based on experiment' values of $\Delta_r H^o(0)$ were found using the equilibrium constants K_p° which had been measured previously (Pogrebnoi *et al.*, 1984; Pogrebnoi, 1981) for the heterophase ion molecular reactions involving the positive ions $Ba_2I_3^+$, $Ba_3I_5^+$, and $Ba_4I_7^+$; the values of K_p° at different temperatures are given in Table 4.7. The enthalpies of the heterophase reactions were converted to gas phase reactions using the reference data from Ivtanthermo database (Gurvich *et al.*, 2000). The TD functions were calculated using geometrical parameters and vibrational frequencies obtained by the MP2 method for all ions with the exception of the heaviest, $Ba_4I_7^+$ and $Ba_5I_9^+$, for which the DFT results were employed. The obtained TD

---

[6]The couple cluster method, CCSD(T) was employed in ORCA software (version 3.0.3) using the contracted basis sets: Ba – Def2-TZVP (6s4p3d1f), I – aug-cc-pvtz (6s5p3d2f) for pentaatomic cluster ion ($Ba_2I_3^+$) to calculate $\Delta_r H^o(0)$, the value (290 kJ mol^{-1}) obtained was compared with the based on experiment result (295 ± 10 kJ mol^{-1}), no significant difference in the results. Note: The CCSD(T) method requires more time of computation and is not affordable for heavier species.

functions of the ions are given in Appendix A1. The 'based on experiment' values of $\Delta_r H^o(0)$ for the gas phase reactions are displayed with horizontal lines in Fig. 4.7 together with the theoretical results.
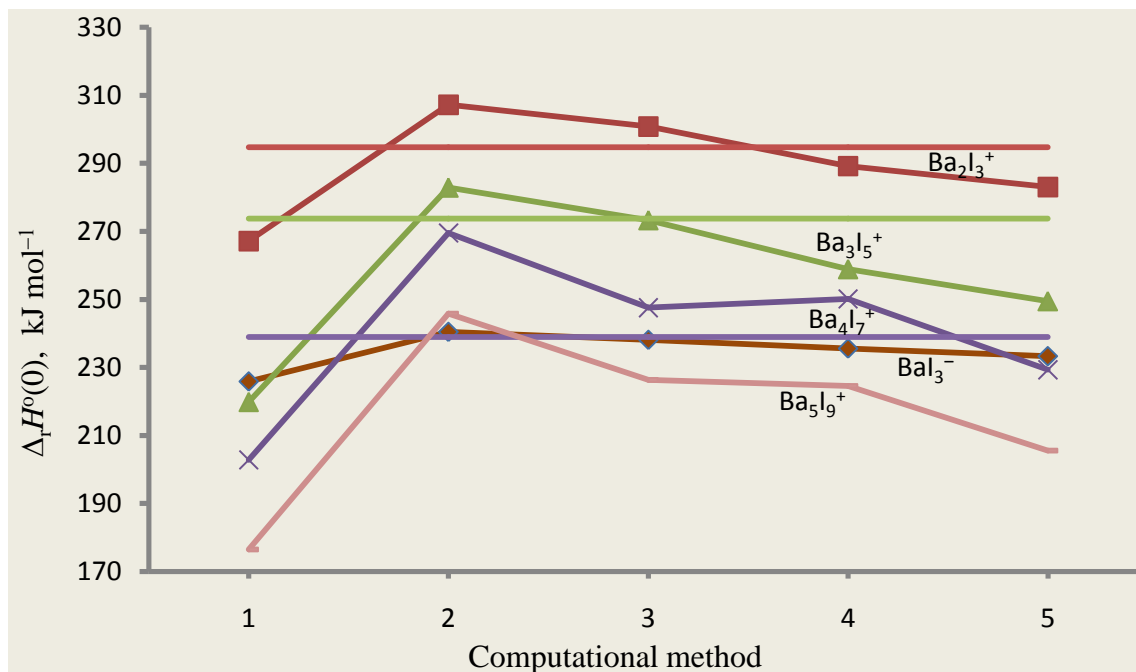
Figure 4.7. Enthalpies of dissociation reactions $\Delta_r H^o(0)$ versus computational method: 1– DFT, 2– MP2, 3 – MP2^{CP}, 4 – MP4 and 5 – MP4^{CP}. The horizontal lines represent the 'based on experiment' results for positively charged ions. For the negative BaI$_3^-$ ion and positive Ba$_5$I$_9^+$ ion the experimental data are not available.

As is seen, the species demonstrate in general a similar trend across all methods (with minimum for the DFT results and maximum for MP2); the DFT results are essentially underrated compared to the values 'based on experiment'; by ~28 kJ mol^{-1} (Ba$_2$I$_3^+$), ~50 kJ mol^{-1} (Ba$_3$I$_5^+$) and ~36 kJ mol^{-1} (Ba$_4$I$_7^+$). The results by MP-methods are in better accordance with the 'based on experiment' data. Worth to note that for other halide cluster ions BaX$^+$(BaX$_2$)$_n$ (n = 1–3, X = F, Cl, Br) similar observations were made in the previous studies (Pogrebnoi *et al.*, 2013) and chapters 2&3. Thus we disregarded the DFT magnitudes of $\Delta_r H^o(0)$ and took into account only MP-results for further considerations. The averaged values by four methods, MP2, MP2^{CP}, MP4 and MP4^{CP}, are accepted as 'theoretical' and presented in Table 4.8. The 'based on experiment' results of $\Delta_r H^o(0)$ both for the heterophase and gaseous reactions are shown in Table 4.8 as well.

Table 4.7. Equilibrium constants for heterophase ion molecular reactions measured experimentally at different temperatures (Pogrebnoi *et al.*, 1984; Pogrebnoi, 1981).

No.	Reaction	$\ln K^{\circ}_p$ (*T*, K)
1	$Ba_2I_3^+ = BaI^+ + [BaI_2]$	0.468 (1019); 0.525 (1010); 0.557 (1008); 0.548 (1023);0.548 (1023); 0.502 (1036); 0.525 (1052); 0.527 (1054);0.456 (1071); 0.440 (1086); 0.481 (1071); 0.479 (1066);0.509 (1055); 0.504 (1045); 0.539 (1036); 0.562 (1028); 0.567 (1015); 0.573 (1004); 0.523 (1010); 0.562 (1009); 0.590 (1023); 0.573 (1034); 0.564 (1049); 0.514 (1062); 0.458 (1074); 0.461 (1083); 0.405 (1100); 0.322 (1130); 0.341 (1114); 0.398 (1097); 0.447 (1074); 0.474 (1055); 0.530 (1042); 0.479 (1028); 0.507 (1061); 0.454 (1075); 0.382 (1079); 0.544 (1034); 0.567 (1022); 0.613 (1022); 0.580 (1035); 0.527 (1061); 0.520 (1066); 0.442 (1106); 0.433 (1114); 0.405 (1124); 0.359 (1129); 0.371 (1107); 0.486 (1088); 0.486 (1074); 0.553 (1063); 0.592 (1049); 0.613 (1040); 0.613 (1026); 0.649 (1014); 0.670 (1004); 0.643 (1011); 0.654 (1017); 0.601 (1044); 0.544 (1056); 0.299 (1067); 0.339 (1095); 0.295 (1106); 0.281 (1113); 0.292 (1116); 0.274 (1125); 0.272 (1134); 0.318 (1099); 0.371 (1092); 0.304 (1124); 0.387 (1058); 0.364 (1072); 0.336 (1082); 0.299 (1098); 0.281 (1113); 0.269 (1115); 0.260 (1124); 0.336 (1108); 0.355 (1065); 0.292 (1087); 0.299 (1095); 0.279 (1112); 0.240 (1120); 0.240 (1136); 0.207 (1141); 0.249 (1123); 0.272 (1111); 0.299 (1101); 0.364 (1066); 0.309 (1065); 0.299 (1085); 0.288 (1100); 0.336 (1087); 0.339 (1076); 0.401 (1062); 0.368 (1072); 0.272 (1091); 0.336 (1081); 0.267 (1103); 0.281 (1115); 0.244 (1130); 0.226 (1122); 0.286 (1112); 0.246 (1104); 0.537 (991); 0.560 (986); 0.534 (997); 0.624 (989); 0.633 (1003); 0.663 (996); 0.622 (981); 0.610 (987); 0.606 (992); 0.601 (1001); 0.643 (1011); 0.654 (1017)
2	$Ba_3I_5^+ = BaI^+ + 2[BaI_2]$	4.620 (1056); 4.468 (1064); 4.509 (1085); 4.385 (1099); 4.413 (1087); 4.523 (1076); 4.493 (1062); 4.491 (1072); 4.413 (1091); 4.445 (1077); 4.357 (1103); 4.417 (1115); 4.463 (1130); 4.468 (1122); 4.456 (1104); 4.542 (1067); 4.500 (1095); 4.406 (1106); 4.410 (1113); 4.357 (1116); 4.334 (1125); 4.302 (1134); 4.544 (1092); 4.337 (1124); 4.569 (1058); 4.489 (1073); 4.399 (1082); 4.337 (1098); 4.468 (1113); 4.281 (1124); 4.380 (1108); 4.505 (1064); 4.394 (1087); 4.380 (1095); 4.378 (1112); 4.486 (1120); 4.383 (1137); 4.380 (1141); 4.350 (1123); 4.456 (1111); 4.537 (1101)
3	$Ba_4I_7^+ = Ba_3I_5^+ + [BaI_2]$	4.605 (1100)

On the base of the enthalpies of reactions the enthalpies of formation $\Delta_f H^{\circ}(0)$ of the gaseous cluster ions are obtained. For the ion $Ba_2I_3^+$ a coincidence between the theoretical and 'based on experiment' results is observed and good agreement for two other clusters $Ba_3I_5^+$ and $Ba_4I_7^+$; the agreement holds both for enthalpies of reactions and enthalpies of formation. Finally we accept the data 'based on experiment' when available otherwise we use the theoretical values.

Table 4.8. Enthalpies of dissociation reactions $\Delta_r H°(0)$ and enthalpies of formation $\Delta_f H°(0)$ of the cluster ions (in kJ mol^{-1}).

No	Reaction	Theoretical		'Based on experiment'		
		$\Delta_r H°(0)$	$\Delta_f H°(0)$	$\Delta_r H°(0)$, heterophase	$\Delta_r H°(0)$, gaseous	$\Delta_f H°(0)$
1	$BaI_3^- \rightleftarrows I^- + BaI_2$	237 ± 6	-709 ± 6			
2	$Ba_2I_3^+ \rightleftarrows BaI^+ + BaI_2$	295 ± 12	-96 ± 12	-26 ± 12	295 ± 12	-96 ± 12
3	$Ba_3I_5^+ \rightleftarrows Ba_2I_3^+ + BaI_2$	266 ± 17	-646 ± 17	-73 ± 17	274 ± 17	-654 ± 17
4	$Ba_4I_7^+ \rightleftarrows Ba_3I_5^+ + BaI_2$	249 ± 20	-1187 ± 20	-82 ± 20	239 ± 20	-1177 ± 20
5	$Ba_5I_9^+ \rightleftarrows Ba_4I_7^+ + BaI_2$	226 ± 20	-1686 ± 20			

One can see that the values of $\Delta_r H°(0)$ increase from BaI_3^- to $Ba_2I_3^+$ and then decrease continuously with the cluster size growth in the series $Ba_2I_3^+ \rightarrow Ba_3I_5^+ \rightarrow Ba_4I_7^+ \rightarrow Ba_5I_9^+$. Apparently the magnitude of $\Delta_r H°(0)$ relates to the strength and number of bonds to be broken in the detachment of the BaI_2 molecule. This observation was discussed previously in details (chapter two). We can note additionally that among the bonds tear, a rearrangement of the ionic product may occur. For example, in the dissociation of the octaatomic cluster ion, the formed 'unclosed' pentaatomic product curls into the bipyramid gaining an energy which finally brings a decrease of the enthalpy of dissociation reaction of $Ba_3I_5^+$ compared to $Ba_2I_3^+$ ion. Similar speculations may be suggested for the heavier clusters. For the $Ba_2I_3^+$ no rearrangement may occur as the dissociation products are the simple species BaI^+ and BaI_2, therefore the enthalpy of this reaction is the highest.

The enthalpies of dissociation reactions are plotted versus cluster size in Fig. 4.8; the results found previously for other halides are given for comparison as well. The cluster ion $Ba_5Cl_9^+$ was optimized and then the frequencies of normal vibration were computed by employing DFT method. The results of geometrical parameters of this ion are presented in Appendix Table A2.12. Also the thermodynamic functions of this ion were calculated and are shown in Appendix Table A1.18. The enthalpies of dissociation reaction and formation of $Ba_5Cl_9^+$ ion were calculated following similar procedure as for other ions. Alike behavior can be observed for all halides; rise of $\Delta_r H°(0)$ from BaX_3^- to $Ba_2X_3^+$ and then descending to $Ba_5X_9^+$. As for the halogen nature, the stability of the cluster decreases in the order $F \rightarrow Cl \rightarrow Br \rightarrow I$. Evidently, with the growth of the halide atom size the respective chemical bonds are elongated and hence weakened that brings to lower stability of the cluster. The exception can be noted for the case of the $Ba_5F_9^+$ and $Ba_5Cl_9^+$ ions. The higher value of $\Delta_r H°(0)$ for the latter might be attributed to a steric factor, as the Cl-ion matches better by size with barium than F-ion. Furthermore, an increase in

steepness of the slope from $Ba_4F_7^+$ to $Ba_5F_9^+$ seems also relates to the bigger difference in size of Ba and F ions compared to other halides. For lower clusters, the symbatic lines are kept on for all halides, thus the steric factor appears to be crucial for the biggest, tetradecaatomic ions $Ba_5X_9^+$.
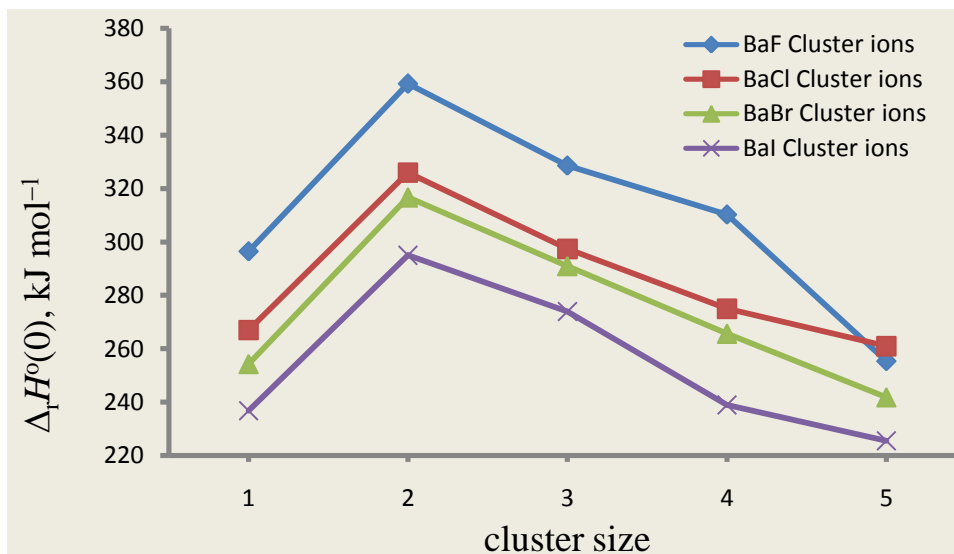
Figure 4.8. Enthalpies of dissociation reactions versus cluster size: $1-BaX_3^-$, $2-Ba_2X_3^+$, $3-Ba_3X_5^+$ and $4-Ba_4I_7^+$ (X= F, Cl, Br or I).
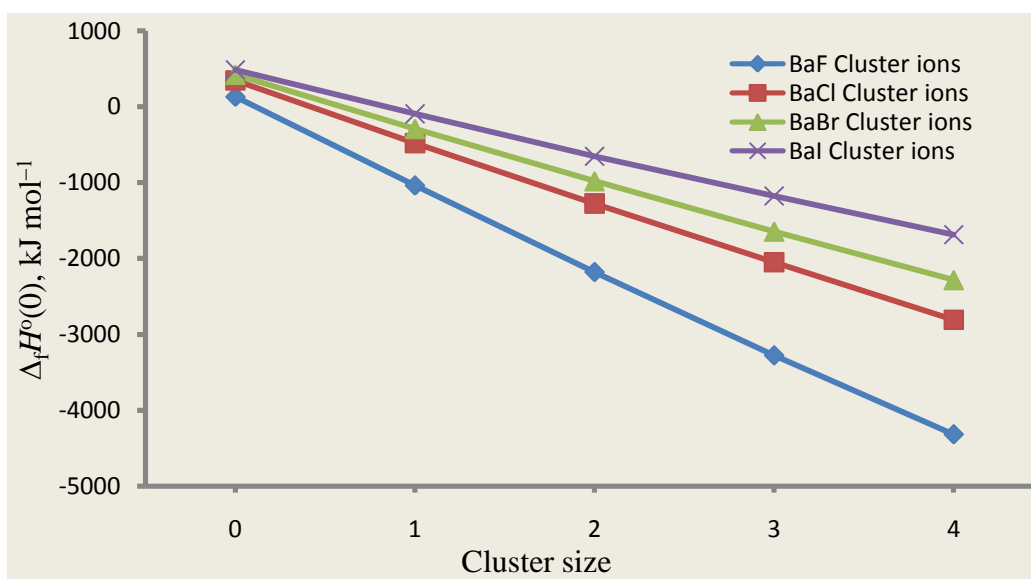
Figure 4.9. Enthalpies of formation of the ions versus size of species: $0 - BaX^+$, $1-Ba_2X_3^+$, $2 - Ba_3X_5^+$, $3 - Ba_4X_7^+$, and $4 - Ba_5X_9^+$ (X= F, Cl, Br or I).

The enthalpies of formation of positive ions $BaI^+(BaI_2)_n$ (n = 0-4) are plotted versus the number of BaI_2 molecules attached (Fig. 4.9) together with the results for other barium halides. The enthalpies of formation of the ions increase by magnitude with the size of the species. The plots

are close to linear for all halides but the slopes are different increasing subsequently from the iodide to fluoride. Apparently the increase in the slope corresponds to rise of the enthalpies of respective dissociation reactions from BaI- to BaF-clusters (Fig. 4.9). That reflects that for the most electronegative halogen, the strongest bonding occurs within the clusters.

4.4 Conclusion

The structural properties of the cluster ions BaI_3^-, $Ba_2I_3^+$, $Ba_3I_5^+$, $Ba_4I_7^+$ and $Ba_5I_9^+$ have been calculated by DFT/B3P86 and MP2 methods. The equilibrium shape of the ions BaI_3^-, $Ba_2I_3^+$, $Ba_3I_5^+$ and $Ba_5I_9^+$ has been confirmed to be compact and highly symmetrical (D_{3h}), while the structure of the $Ba_4I_7^+$ ion corresponds to C_{2v} symmetry. No isomers were revealed for all cluster ions. The calculated Mulliken atomic charges and the frontier orbitals analysis indicate the high polarity of the bonds.

The theoretical enthalpies of dissociation reactions of the ions, $\Delta_r H^o(0)$, have been calculated by the DFT, MP2 and MP4 methods and the BSSE correction employed for the MP methods. For the ions $Ba_2I_3^+$, $Ba_3I_5^+$ and $Ba_4I_7^+$, the values of $\Delta_r H^o(0)$ were compared with those calculated on the base of available experimental data. It was observed that the values obtained by DFT method were underrated essentially regarding the values based on experiment; the MP results with BSSE correction provided a better agreement. This observation is in accordance with our previous results on other barium halides cluster ions. It is worth to emphasize that to ensure the results are reliable, high theoretical level together with thorough analysis of the calculated values is required, moreover experimental data are highly desirable as reference points at least for few species considered.

The enthalpies of the BaI_2 molecules detachment reactions have been analyzed for the BaI-clusters and compared to other halides in series $BaX_3^- - Ba_2X_3^+ - Ba_3X_5^+ - Ba_4X_7^+ - Ba_5X_9^+$ (X = F, Cl, Br, I). The increase in stability from BaX_3^- to $Ba_2X_3^+$ with further descending to $Ba_5X_9^+$ followed by was discussed.

CHAPTER FIVE

5.0 Isomers of the dimer molecules Ba$_2$X$_4$ (X = F, Cl, Br or I)[7]

Abstract

Geometrical parameters and vibrational spectra of the dimer Ba$_2$X$_4$ molecules were calculated; different isomeric structures were revealed. For the Ba$_2$F$_4$, Ba$_2$Cl$_4$ and Ba$_2$Br$_4$, three isomers of C_{3v}, C_{2v} and C_{2h} symmetries were confirmed to exist while for Ba$_2$I$_4$ only two isomers, C_{3v} and C_{2h}, were confirmed. For all halides, the bipyramidal C_{3v} isomers possessed the lowest energy. The structural parameters and vibrational frequencies were employed in calculation of thermodynamic functions and enthalpies of dissociation reactions of the species. The enthalpies of formation $\Delta_f H°(0)$ of the C_{3v} isomers were obtained (in kJ mol^{-1}): -1859 ± 7 (Ba$_2$F$_4$); -1236 ± 7 (Ba$_2$Cl$_4$); -1023 ± 8 (Ba$_2$Br$_4$); -787 ± 11 (Ba$_2$I$_4$). The relative abundance of the isomeric forms was evaluated for a broad temperature range, between 200 and 2000 K. It was shown that the concentrations of different isomers appeared to be comparable in saturated vapours at temperatures close to experimental conditions.

5.1 Introduction

Alkaline earth dihalides have been investigated by using different experimental techniques and found to contain certain amount of dimeric species in the vapour phase (Lesiecki & Nibler, 1976; Ramondo *et al*., 1989; Ramondo *et al*., 1988; Snelson *et al*., 1974). The geometrical properties have been obtained experimentally for the dimers Be$_2$Cl$_4$ (Girichev *et al*., 1996) and Mg$_2$Cl$_4$ (Molntir *et al*., 1995). Data from computational studies are available for Be$_2$F$_4$ and Mg$_2$F$_4$ (Ramondo *et al*., 1992), Mg$_2$F$_4$, Mg$_2$Cl$_4$ and Mg$_2$Br$_4$ (Ystenes & Westberg, 1995), all four Mg$_2$X$_4$ dimers (Axten *et al*., 1994), Mg$_2$Cl$_4$ (Molntir *et al*., 1995), Be$_2$F$_4$, Mg$_2$F$_4$ and Ca$_2$F$_4$ (Pogrebnaya *et al*., 1997) and Ca$_2$X$_4$, Sr$_2$X$_4$ Ba$_2$X$_4$ (X = F or Cl) (Levy & Hargittai, 2000) and M$_2$X$_4$ (M = Be, Mg, Ca, Sr and Ba; X = F, Cl, Br and I) (Donald & Hoffmann, 2006).

Different configurations have been considered in computational studies of the alkaline earth dihalides dimeric species. It was found that the dimers of beryllium and magnesium dihalides prefer D_{2h} symmetry with a halogen bridged structure consisting of two halogen bridges. Other

---

[7] Manuscript

configurations such as C_{3v}, C_{2v} and C_{2h} were also confirmed to be stable but have relatively higher energy. Dimers of the heavier dihalides prefer triply bridged geometry of C_{3v} symmetry (Donald & Hoffmann, 2006; Gigli, 1990; Guido & Gigli, 1976; Hargittai, 2000, 2005; Kaupp, 2001; Levy & Hargittai, 2000; Pogrebnaya *et al*., 1997).

Regarding barium halides, the dimer molecules Ba_2F_4 and Ba_2Cl_4 were studied and different configurations including C_{3v}, C_{2v}, C_{2h} and D_{2h} were confirmed to exist (Hargittai, 2000; Levy & Hargittai, 2000); the geometrical parameters and vibrational spectra were reported in (Levy & Hargittai, 2000). However there is no information regarding the thermodynamic properties and relative concentration of the isomers in saturated vapour. Therefore, this work intends to verify the stable configurations of Ba_2X_4 isomers (X = F, Cl, Br or I), determine the thermodynamic properties and evaluate relative abundance of the isomers at different temperatures.

5.2 Computational details

The computations of geometrical parameters and vibrational frequencies were carried out using the methods and basis sets described in the previous chapters. For calculations that involved the MP2 method, no orbitals were frozen for Ba_2F_4, Ba_2Br_4 and Ba_2I_4 species, the script NCORE=0 was used while for Ba_2Cl_4 five orbitals were frozen for each chlorine atom and therefore the option NCORE=20 was used. The dissociation reactions $Ba_2X_4 = 2BaX_2$ were considered. The theoretical values of enthalpies of the reactions $\Delta_r H^o(0)$ and enthalpies of formation $\Delta_r H^o(0)$ of the dimers were computed following the procedure described in chapter two.

5.3 Results and discussion

5.3.1 Structural parameters and vibrational spectra of Ba_2X_4 isomers (X = F, Cl, Br or I)

Four different configurations of C_{3v}, C_{2v}, C_{2h} and D_{2h} (Fig. 5.1) were considered in the computation of the geometrical properties and vibrational frequencies of all dimer molecules. The results are shown in Table 5.1 for Ba_2F_4 (C_{3v}) and for other isomers in Appendix A2. A good agreement is observed between the results obtained by DFT/B3P86 and MP2 methods. It is therefore noted that the geometrical parameters and vibrational frequencies are not much sensitive to the computational method and basis set employed in the calculation. Our results for the Ba_2F_4 and Ba_2Cl_4 dimers are also compared with the data obtained by B3LYP method (Levy & Hargittai, 2000) as shown in Table 5.1 and in Appendix A2 for Ba_2F_4 and Ba_2Cl_4; a good agreement is observed between the respective parameters.

Table 5.1. Properties of the dimer Ba_2F_4 molecule (C_{3v} symmetry).

Property	DFT/B3P86 B2	MP2 B2	Literature data DFT/B3LYP (Levy & Hargittai, 2000)
$R_{e1}(Ba_1–F_b)$	2.616	2.611	2.626
$R_{e2}(Ba_2–F_b)$	2.357	2.362	2.371
$R_{e3}(Ba_1–F_t)$	2.278	2.294	2.288
$\alpha_e(F_t–Ba_1–F_b)$	138.4	138.6	138.6
$\beta_e(F_b–Ba_2–F_b)$	79.4	78.6	78.7
μ_e	11.2	11.9	11.4
$-E$	450.90140	450.10363	
$\omega_1 (A_1)$	409 (3.1)	405 (2.8)	409 (2.8)
$\omega_2 (A_1)$	391 (3.4)	392 (4.2)	387 (3.3)
$\omega_3 (A_1)$	261 (3.7)	265 (3.5)	263 (3.5)
$\omega_4 (A_1)$	124 (0.01)	127 (0.02)	128 (0.01)
$\omega_5 (E)$	312 (5.3)	329 (5.3)	324 (4.7)
$\omega_6 (E)$	180 (0.1)	195 (0.4)	188 (0.2)
$\omega_7 (E)$	146 (1.7)	148 (1.8)	148 (1.8)
$\omega_8 (E)$	32 (0.7)	38 (0.7)	29 (0.7)

Note: R_{e1}, R_{e2} and R_{e3} are the equilibrium internuclear distances, Å; α_e and β_e are the valence angles, degs; E is the total energy, au; ω_i are the vibrational frequencies, cm^{-1} and μ_e is the dipole moment, D. The values given in parenthesis near the frequencies are the intensities in IR spectrum in D^{2}amu^{-1}Å^{-2}.

Relative energies of the alternative structures were obtained as $\Delta E = E(\text{isomer}) - E(C_{3v})$ and the MP2 results are presented in Table 5.2 together with the number of imaginary frequencies (N_{imag}) for all isomers. The triple bridged isomer (C_{3v}) has the lowest energy of all isomers and thus the most favored configuration. On the basis of relative energies for the isomers, one can note the relative stability increasing in the order $D_{2h} < C_{2v} < C_{2h} < C_{3v}$. Among all alternative structures considered, the D_{2h} configuration was found to be nonequilibrium due to presence of two imaginary frequencies. The remaining configurations were confirmed to be equilibrium for all isomers except the Ba_2I_4, for which the C_{2v} structure displayed one imaginary frequency.

Table 5.2. Relative energies ($\Delta E = E(\text{isomer}) - E(C_{3v})$) in kJ mol^{-1} obtained at the MP2 computational level for possible dimer geometries.

Structures	Ba_2F_4		Ba_2Cl_4		Ba_2Br_4		Ba_2I_4	
	ΔE	N_{imag}	ΔE	N_{imag}	ΔE	N_{imag}	ΔE	N_{imag}
C_{3v}	0	0	0	0	0	0	0	0
C_{2v}	35.4	0	41.4	0	39.9	0	39.0	1
C_{2h}	27.6	0	38.4	0	38.3	0	38.9	0
D_{2h}	49.8	2	42.1	2	39.9	2	39.0	2

Our observations do not contradict with the results obtained by Hargittai and coworkers (Levy & Hargittai, 2000) and (Donald & Hoffmann, 2006), where two cyclic structures of C_{2h} and C_{2v} symmetry were shown to be higher in energy as compared to the C_{3v} isomer. The D_{2h}

configuration was identified to be nonequilibrium due to presence of imaginary frequencies; this D_{2h} structure was a saddle point between C_{2h} and C_{2v} configurations.

For the most stable C_{3v} isomer (bipyramid with a tail), we can suppose that it may be built of the $Ba_2X_3^+$ ion with X^- ion attached. The latter is rather loosely bound as in the vibrational spectrum of the Ba_2X_4 molecule, the lowest frequency, $\omega_8 = 38\ cm^{-1}$ (MP2), corresponds to the wagging mode of the terminal bond $Ba–X_t$. Alternatively, the bipyramidal configuration was suggested by (Levy & Hargittai, 2000) to be composed of the BaX^+ and BaX_3^- ionic species due to the relationship between the long bridged bonds $Ba_1−X_b$ and short terminal $Ba_1−X_t$ bond. Stability of Ba_2X_4 molecules regarding different decomposition channels are considered and analyzed in section 5.3.3.
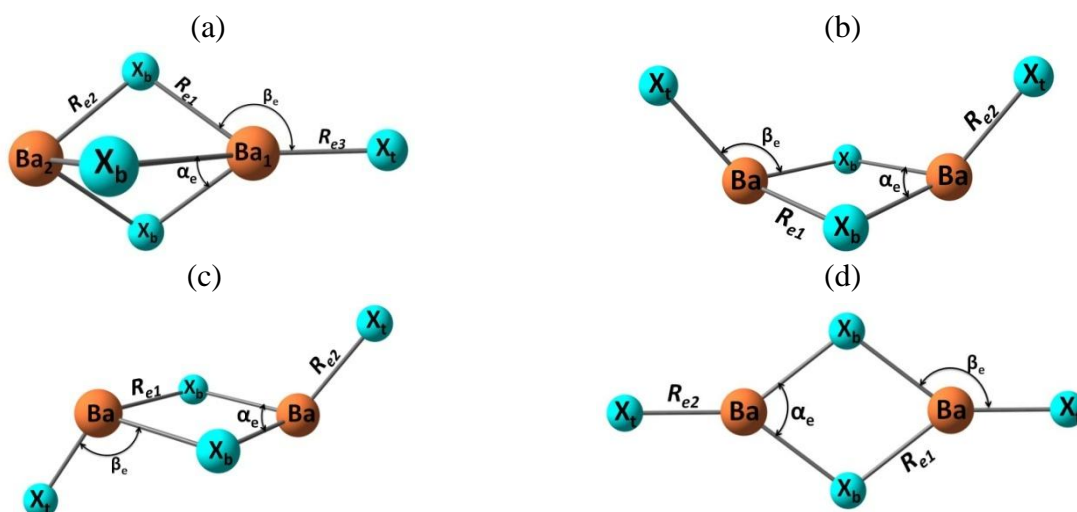
Figure 5.1. Equilibrium geometrical structures of the dimers Ba_2X_4 (X = F, Cl, Br or I): (a) C_{3v}, (b) C_{2v}, (c) C_{2h} and (d) D_{2h}.

5.3.2 Relative abundance of the isomers

We have analyzed the relative amount of the isomers in saturated vapours using the thermodynamic approach, following the procedure (Mwanga *et al.*, 2015). The pressure ratio between two isomers p_j/p_i has been calculated from the equation:

$$\Delta_r H^o(0) = T\Delta_r\Phi^o(T) − RTln(p_j/p_i) \tag{5.1}$$

where $\Delta_r H^\circ(0)$ is the enthalpy of isomerisation reaction; T is absolute temperature; $\Delta_r\Phi^\circ(T)$ is the reduced Gibbs energy of the reaction. The ratio p_j/p_i represents $p(C_{2v})/p(C_{3v})$, $p(C_{2h})/p(C_{3v})$, or $p(C_{2v})/p(C_{2h})$. The values of $\Delta_r H^\circ(0)$ have been obtained via energies $\Delta_r E_{iso}$ and ZPVE corrections ($\Delta_r\varepsilon_{iso}$) by Eqs. (2.1) – (2.3). The relative concentrations p_j/p_i have been calculated for

the temperature range $300 – 2000$ K; the selected results of p_j/p_i at $T = 1000$ K are given in Table 5.3 together with TD characteristics of the reactions. The predominant isomer is identified from the value of p_j/p_i: if the ratio $p_j/p_i > 1$ then the product j is dominant over the reactant i and vice versa.

Table 5.3. The isomerization reactions for the dimer Ba_2X_4 molecules, the energies $\Delta_r E_{iso}$, ZPVE corrections $\Delta_r\varepsilon_{iso}$, enthalpies $\Delta_r H°(0)$, and reduced Gibbs energies $\Delta_r\Phi°(T)$ of the reactions and relative abundances p_j/p_i of isomers ($T = 1000$ K) by MP2 method.

Isomerization Reaction	$\Delta_r E_{iso}$, kJ mol^{-1}	$\Delta_r\varepsilon_{iso}$, kJ mol^{-1}	$\Delta_r H°(0)$, kJ mol^{-1}	$\Delta_r\Phi°(T)$, J mol^{-1} K^{-1}	p_j/p_i
Ba_2F_4 (C_{3v}) $\rightleftarrows$ Ba_2F_4 (C_{2v})	35.40	−0.81	34.6	20.800	0.19
Ba_2F_4 (C_{3v}) $\rightleftarrows$ Ba_2F_4 (C_{2h})	27.56	−0.62	27.0	19.003	0.38
Ba_2F_4 (C_{2h}) $\rightleftarrows$ Ba_2F_4 (C_{2v})	7.84	−0.20	7.6	1.797	0.50
Ba_2Cl_4 (C_{3v}) $\rightleftarrows$ Ba_2Cl_4 (C_{2v})	41.4	−0.78	40.6	32.456	1.59
Ba_2Cl_4 (C_{3v}) $\rightleftarrows$ Ba_2Cl_4 (C_{2h})	38.4	−0.62	37.8	28.876	1.50
Ba_2Cl_4 (C_{2h}) $\rightleftarrows$ Ba_2Cl_4 (C_{2v})	2.98	−0.16	2.8	3.580	1.06
Ba_2Br_4 (C_{3v}) $\rightleftarrows$ Ba_2Br_4 (C_{2v})	39.89	−0.72	39.2	42.702	5.99
Ba_2Br_4 (C_{3v}) $\rightleftarrows$ Ba_2Br_4 (C_{2h})	38.33	−0.57	37.8	32.889	2.37
Ba_2Br_4 (C_{2h}) $\rightleftarrows$ Ba_2Br_4 (C_{2v})	1.56	−0.14	1.4	9.813	2.53
Ba_2I_4 (C_{3v}) $\rightleftarrows$ Ba_2I_4 (C_{2h})	38.95	−0.66	38.3	49.051	3.65

The fraction w_i of each Ba_2X_4 isomer, C_{3v}, (bipyramidal), C_{2v} (*cis-*) or C_{2h} (*trans-*), was also estimated; $w_i = p_i/P$, where P is the total pressure of three isomers for each dimer molecule (Eqns. 5.2 – 5.4). For the Ba_2F_4 dimers, the values of w_i are plotted versus temperature in Fig. 5.2. One can see the bipyramidal isomer is prevailing at $T < 1400$ K. At elevated temperatures (above 1400 K) all three isomers become comparable in their relative concentration; with temperature raise the *trans*-isomer becomes most abundant.

$$w_I = \frac{1}{1+x_1+x_2} \tag{5.2}$$

$$w_{II} = \frac{x_2}{1+x_2+x_3} \tag{5.3}$$

$$w_{III} = \frac{x_3}{1+x_2+x_3} \tag{5.4}$$

where w_I, w_{II} and w_{III} are the fractions of C_{3v}, C_{2v} and C_{2h} isomers respectively, the x_i are the ratios of pressure of the i-isomer p_i to the total pressure $P = p_1 + p_2 + p_3$ of three isomers, the numbers 1, 2 and 3 represent the respective isomers.

.
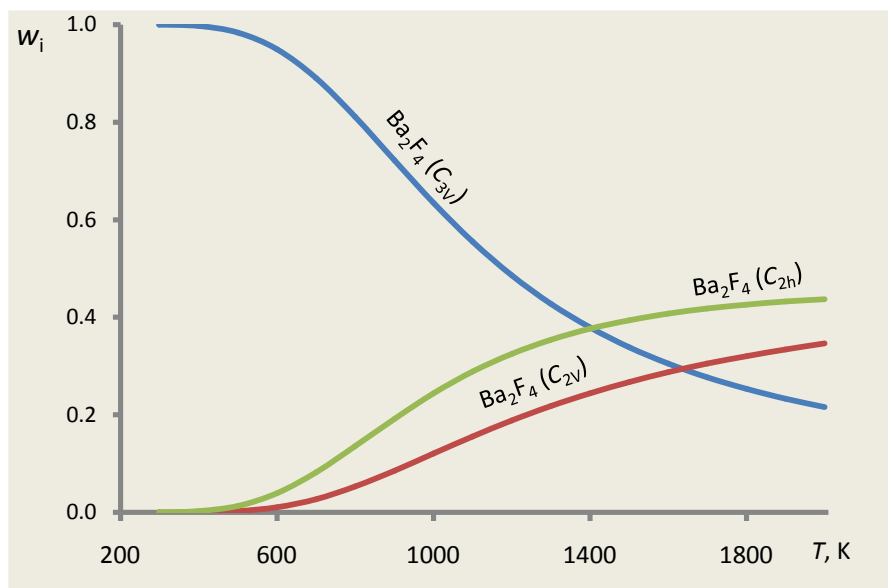
Figure 5.2. Fractions w_i of the Ba_2F_4 isomers versus temperature.

Similar to Ba_2F_4, the fractions of the Ba_2Cl_4 isomers were computed for the temperature range from 200 to 2000 K and plotted in Fig. 5.3. At lower temperatures < 900 K, the pyramidal isomer C_{3v} predominates. At a temperature of about 900 K, all three isomers coexist in equal proportions of $w_i \approx 0.34$. Above this temperature the *cis*-isomer (C_{2v}) starts to predominate followed by the *trans*-isomer (C_{2h}) while the pyramidal isomer (C_{3v}) continues decreasing gradually with increase in temperature.
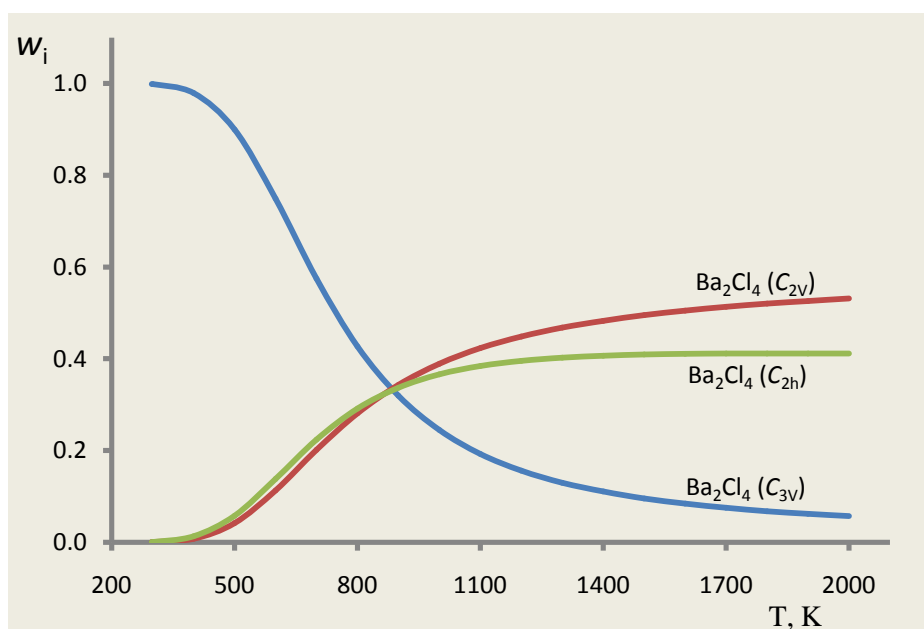
Figure 5.3. Fractions w_i of the Ba_2Cl_4 isomers versus temperature.

For the Ba_2Br_4, the fractions of the isomers are shown in Fig. 5.4. At temperatures lower than 600 K, the pyramidal isomer exists in larger proportions but at about 600 K, two isomers (C_{3v} and C_{2v}) coexist with equal fraction $w_i \approx 0.4$. At temperatures > 800 K, the *cis*-isomer predominates followed by the *trans*-isomer and then the pyramidal isomer. It should be noted that the coexistence of C_{3v} and C_{2v} isomers in equal fractions for the Ba_2F_4, Ba_2Cl_4 and Ba_2Br_4 is observed at temperatures 1650 K, 900 K and 600 K, respectively. Furthermore, one can note that at higher temperatures, the three isomers are comparable in their proportions for the Ba_2F_4 dimers two isomers (C_{2v} and C_{2h}) for Ba_2Cl_4, and two isomers (C_{2h} and C_{3v}) for Ba_2Br_4.
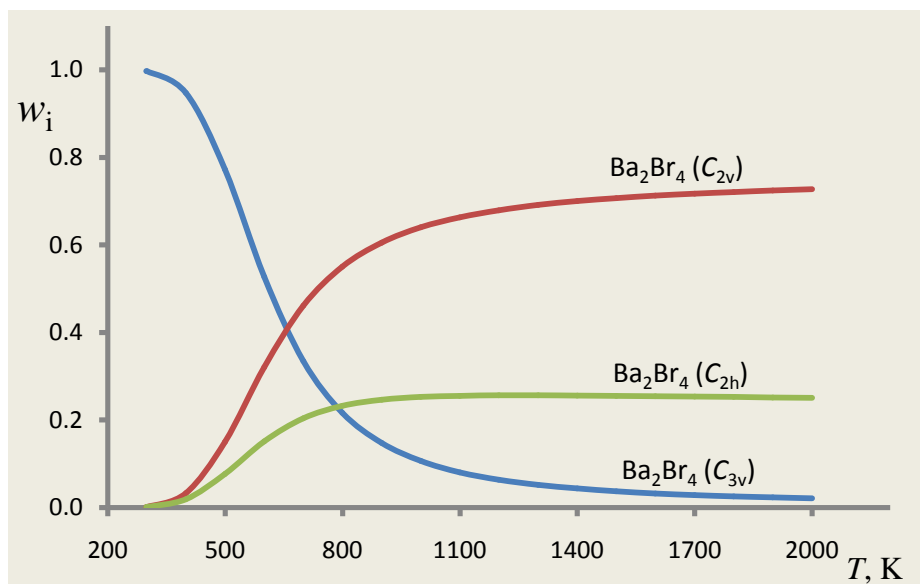
Figure 5.4. Fractions w_i of the Ba_2Br_4 isomers versus temperature.

The relative concentrations of the isomers of Ba_2I_4 are presented in Fig. 5.5. As discussed earlier in section 5.3.1, only two isomers (C_{3v} and C_{2h}) coexist. As seen from the plot, the pyramidal isomer dominates at temperatures less than 800 K, at about 800 K two isomers coexist in equal proportion, $w_i \approx 0.5$. At temperatures above 800 K, the fraction of the *trans*-isomer increases and thus this isomer predominates.

Generally the pyramidal isomer for all dimers is predominant at lower temperatures but its concentration lowers at elevated temperatures while the fraction of other isomers, C_{2v} and C_{2h} increases.
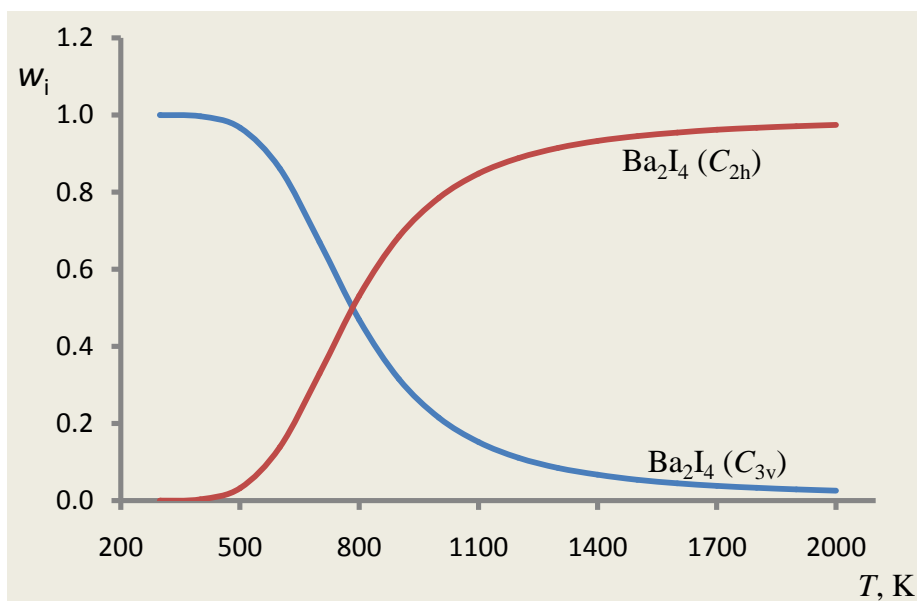
Figure 5.5. Fractions w_i of the Ba_2I_4 isomers versus temperature.

5.3.3 Enthalpies of dissociation reactions and formation of the isomers

The enthalpies $\Delta_r H°(0)$ of dissociation reactions

$$Ba_2X_4 = 2BaX_2$$
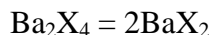
have been obtained through the energies $\Delta_r E_{iso}$ and ZPVE corrections $\Delta_r \varepsilon_{iso}$. Analysis of the dependence of $\Delta_r H°(0)$ values on methods of determination was done and the results are shown in Fig. 5.6. A similar trend is observed for all isomers and all halides: a leap from DFT to MP2 methods with gradual decrease followed by. There is a fair agreement in the results found by the MP methods, while the DFT results seem to be underrated essentially and therefore excluded from further consideration. Table 5.4 presents the accepted values of $\Delta_r H°(0)$ found as an average between the MP methods. Based on the accepted $\Delta_r H°(0)$, the enthalpies of formation of the dimers have been obtained.

The enthalpy of dissociation reaction of the pentaatomic positive ion $Ba_2X_3^+$ is worth to compare with that of the Ba_2X_4 molecule. The geometrical structure of the most favorable C_{3v} isomer of the Ba_2X_4 molecule is similar to that of the $Ba_2X_3^+$ ion, both having three bridged equilibrium structures (Figs. 5.1a and 2.3b). The species $Ba_2F_3^+$ and Ba_2F_4 (C_{3v}) are chosen to describe this comparison. All ten levels of computation were used to calculate the enthalpies of dissociation reaction $Ba_2F_4 = 2BaF_2$ (Fig. 5.7).
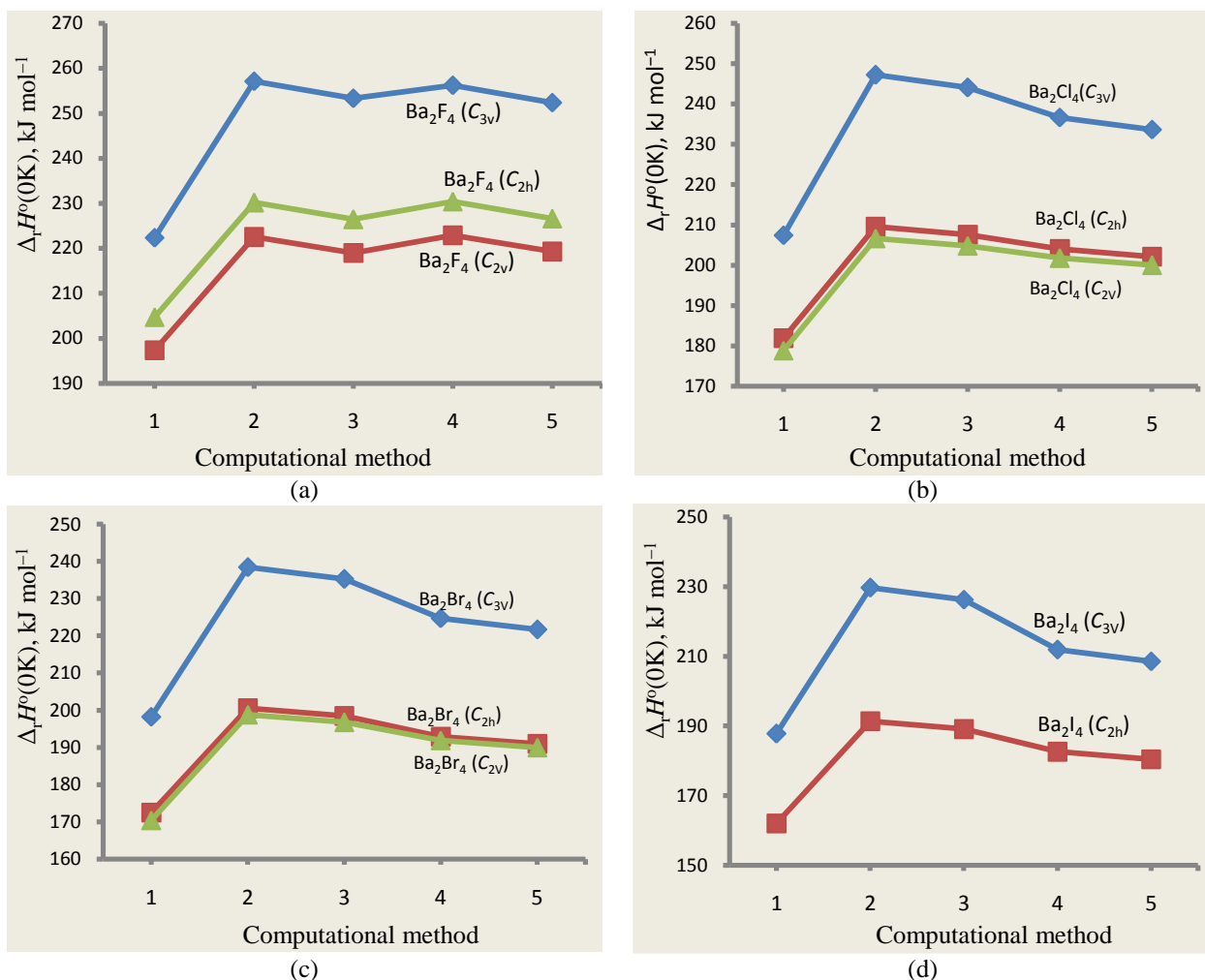
Figure 5.6. Enthalpies of dissociation reaction versus computational methods for the isomers of (a) Ba_2F_4, (b) Ba_2Cl_4, (c) Ba_2Br_4 and (d) Ba_2I_4: 1–DFT, 2–MP2, 3–MP2^{CP}, 4–MP4 and 5–MP4^{CP}.

The theoretical values of $\Delta_r H°(0)$ for the Ba_2F_4 molecule exhibit a similar behavior versus the level of calculation as for the cluster ion $Ba_2F_3^+$. The results by eight methods (MP2 B1, MP2^{CP} B1, MP4 B1, MP4^{CP} B1, MP2 B2, MP2^{CP} B2, MP4 B2 and MP4^{CP} B2) were taken into account to get the average value of $\Delta_r H°(0)$ for the Ba_2F_4 molecule, 240 ± 7 kJ mol^{-1}. In comparison, the enthalpy for the detachment of the BaF^+ from $Ba_2F_3^+$ is much higher, 359 ± 10 kJ mol^{-1}. This observation implies that the pentaatomic positive $Ba_2F_3^+$ ion is more strongly bonded than the dimer molecule Ba_2F_4. Two routes of dissociation of the dimer molecule $Ba_2F_4 = BaF^+ + BaF_3^-$ and $Ba_2F_4 = Ba_2F_3^+ + F^-$ may be considered. The enthalpies of these two reactions evaluated on the base of the obtained enthalpies of formation of the ions BaF_3^- and $Ba_2F_3^+$ (Table 2.8) and the reference data for the BaF^+ and F^- (Gurvich *et al*., 2000) are equal to 632 kJ mol^{-1} and 539 kJ

77

mol^{-1}, respectively. It is evident that these two channels of dissociation require much more energy than the decay into two monomers.
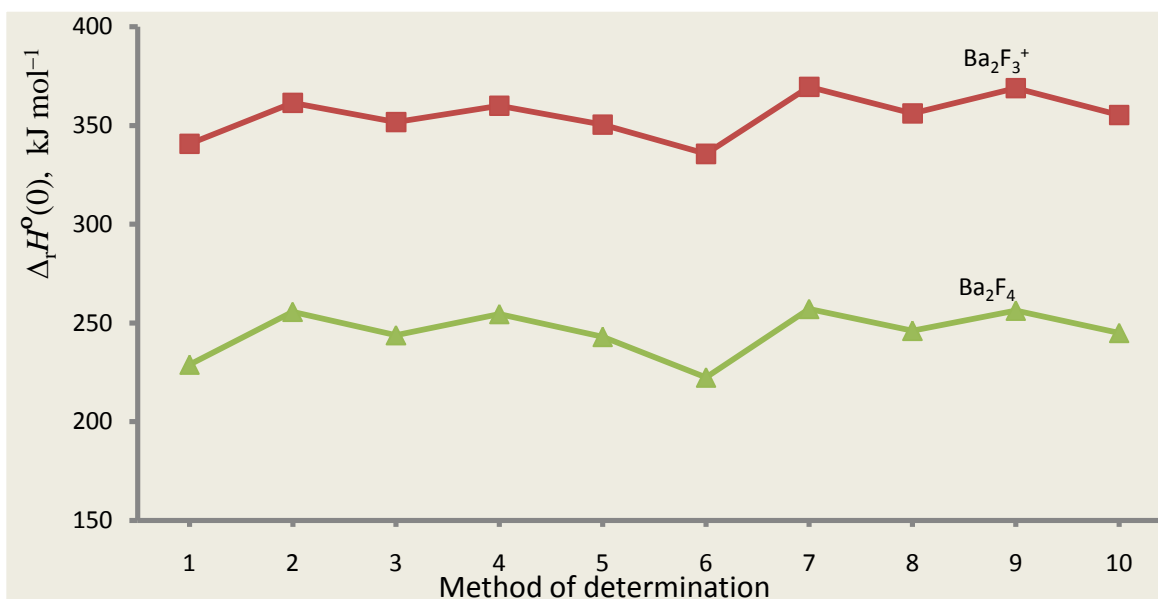
Figure 5.7. Enthalpies of dissociation reactions of the Ba$_2$F$_3^+$ ion and Ba$_2$F$_4$ molecule versus level of computation: 1 – DFT B1, 2 – MP2 B1, 3 – MP2^{CP} B1, 4 – MP4 B1, 5 – MP4^{CP} B1, 6 – DFT B2, 7 – MP2 B2, 8 – MP2^{CP} B2, 9 – MP4 B2, 10 – MP4^{CP} B2.

Table 5.4. Enthalpies of dissociation reactions and formation of the dimers Ba$_2$X$_4$, kJ mol^{-1} (X = F, Cl, Br or I).

	Enthalpies of dissociation, $\Delta_r H^o(0)$			Enthalpies of formation, $\Delta_f H^o(0)$		
	C_{3v}	C_{2h}	C_{2v}	C_{3v}	C_{2h}	C_{2v}
Ba$_2$F$_4$	240 ± 7	228 ± 2	221 ± 2	-1859 ± 7	-1848 ± 2	-1840 ± 2
Ba$_2$Cl$_4$	240 ± 7	206 ± 4	203 ± 3	-1236 ± 7	-1201 ± 4	-1199 ± 3
Ba$_2$Br$_4$	230 ± 8	196 ± 5	194 ± 4	-1023 ± 8	-989 ± 5	-987 ± 4
Ba$_2$I$_4$	219 ± 11	186 ± 5		-787 ± 11	-754 ± 5	

It is observed that for all isomers, the pyramidal isomer exhibits higher enthalpy of dissociation reaction than the *cis*- and *trans*-isomers. The stability of the isomers follows the trend: Ba$_2$X$_4$ (C_{3v}) > Ba$_2$X$_4$ (C_{2h}) > Ba$_2$X$_4$ (C_{2v}). Apparently, this trend relates to the relative energies of the isomers listed in Table 5.2. Furthermore, one can note that the magnitudes of enthalpies of dissociation reactions for the *cis*- and *trans*-isomers are close to one another, transformation between these two isomers may occur through D_{2h} configuration, and the transformation is easy provided there is low energy barrier. Considering the isomers of different halides, the tendency for formation of dimers follows the order Ba$_2$F$_4$ > Ba$_2$Cl$_4$ > Ba$_2$Br$_4$ > Ba$_2$I$_4$. It is worth to compare our results of dimerization energies with those reported earlier by (Donald & Hoffman, 2006) particularly for the C_{3v} isomers. The results are comparable, they both show similar trend.

78

However, for all halides our results are slightly higher in magnitude than those reported by Donald and Hoffman.

5.4 Conclusion

Theoretical study of the thermodynamic properties and relative abundance of isomers Ba_2F_4, Ba_2Cl_4, Ba_2Br_4 and Ba_2I_4 has been conducted employing DFT, MP2 and MP4 methods. It was observed that the first three molecules exhibit three isomeric structures (C_{3v}, C_{2h} & C_{2v}) while Ba_2I_4 exists in two isomeric forms (C_{3v} & C_{2h}). At low temperatures, the pyramidal configuration (C_{3v}) is most favored, as the temperature rises other isomers become significant. For the Ba_2Br_4 isomers, the fraction of the *cis-* isomer at higher temperatures is much higher than that of *trans-* and pyramidal isomers.

The enthalpies of dissociation reactions of the isomers have shown higher value for the pyramidal isomer, followed by the *trans-* and then *cis-*isomer. The stability of these isomers decreases in the order $C_{3v} \rightarrow C_{2h} \rightarrow C_{2v}$.

CHAPTER SIX

6.0   General Discussion, Conclusion and Recommendations

6.1   General Discussion

Structural properties

Structural parameters and vibrational frequencies are important in the computation of thermodynamic properties of cluster ions. Therefore, accurate determination of these parameters is inevitable in order to obtain valid results for thermodynamic properties. In this work, the results obtained by both DFT and MP2 methods for internuclear separations are in good agreement with each other and also correspond well with the reference data. The obtained results for internuclear separations for BaF, BaF^+, BaF_2 and $BaBr_2$ are in good agreement with the reference data (Herzberg & Huber, 1979; Kushawaha, 1973), (Jakubek et al., 1994), (Donald & Hoffmann, 2006; Levy & Hargittai, 2000) and (Hargittai et al., 2001) respectively as presented in Fig. 6.1. It is noted that for BaF_2, the average deviation from reference value of the results of R_e(Ba–F) is 0.01 Å and the maximum deviation is 0.02 Å. For $BaBr_2$ molecule, the average and maximum deviations are 0.01 Å and 0.02 Å respectively. Furthermore, the diatomic neutral BaF molecule has average and maximum deviation of 0.02 Å while the ion BaF^+ has 0.04 Å and 0.05 Å respectively. These results show high accuracy as regards the reference values. All species exhibit a similar trend across all computational methods and thus the geometrical parameters are not much sensitive to the methods of determination.

The calculated vibrational frequencies for the species BaF, BaF^+ and BaBr correspond well with the reference data by (Kushawaha, 1973), (Jakubek et al., 1994) and (Bradford, 1975) respectively (Fig. 6.2). There is no reliable experimental data for the vibrational frequency of $BaBr^+$. It is observed that there is a good agreement between the results obtained by DFT and MP2 methods. Also, all species show a similar trend across the methods of determination. The average and maximum deviation from reference values are 0.4% and 2.8% for BaF^+, 0.3% and 1.9% for BaF and 2.0% and 3.0% for BaBr respectively. Thus, these results are reliable and appropriate to use in the computation of thermodynamic properties of the cluster ions.
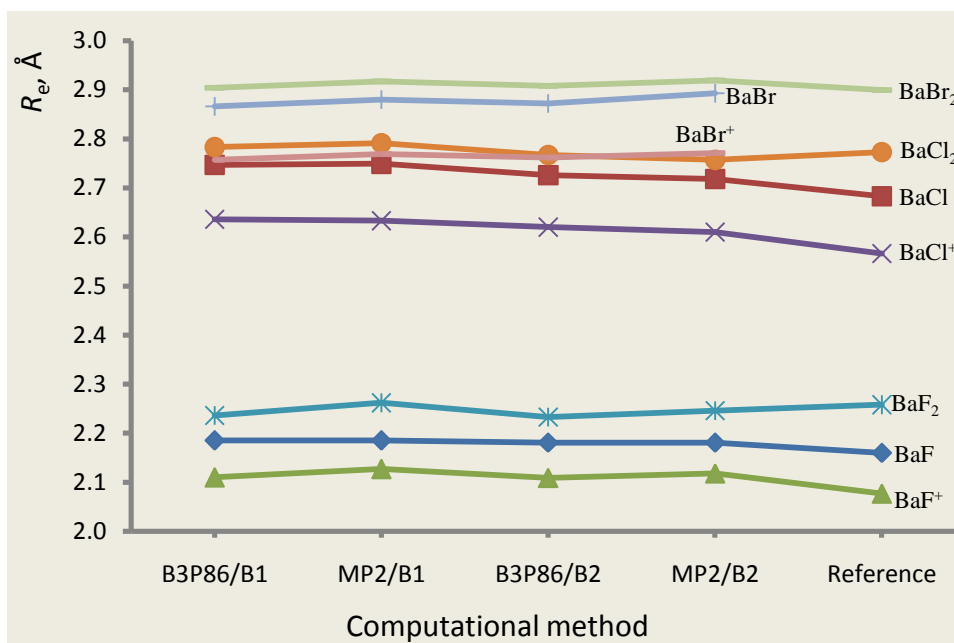
Figure 6.1. Internuclear distances Ba–X versus computational method.
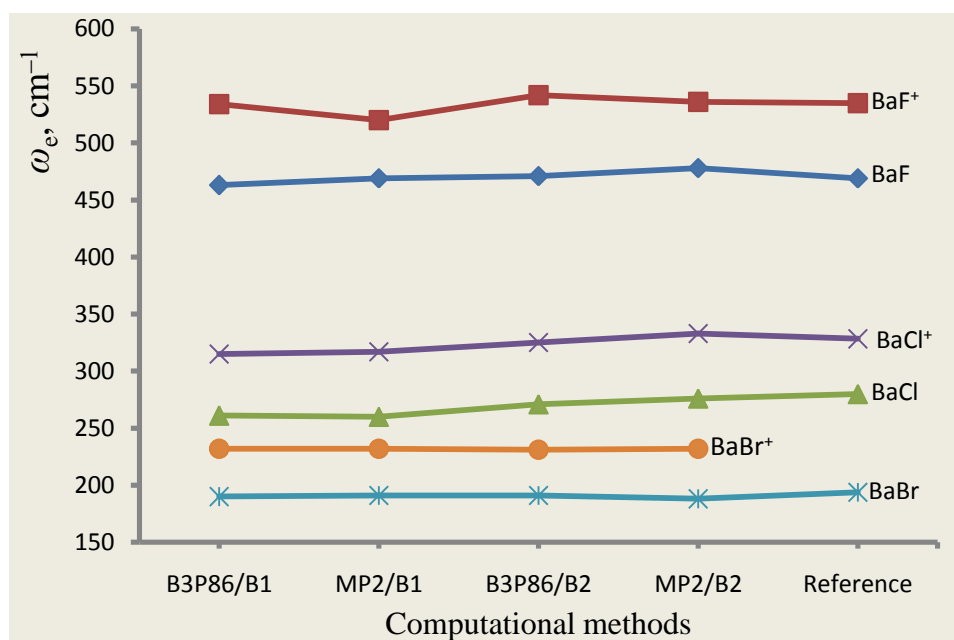
Figure 6.2. Vibrational frequencies ω_{str} (Ba–X) versus computational method.

Regarding the effect of the halogen nature, the magnitudes of internuclear separations in the BaX-species are observed to be directly related to the electronegativity of the corresponding halogens. The values of electronegativity of the halogens in Pauling units are 4.0 (F), 3.0 (Cl), 2.8 (Br) and 2.5 (I) (General Properties of Halogens, 2017). As is seen from Fig. 6.3 where the internuclear separation of the species BaX, BaX$^+$, BaX$_2$, BaX$_3^-$ and Ba$_2$X$_3^+$ are plotted against halogens, the order of increase of R_e(Ba–X) follows this trend: F < Cl < Br < I. This means, the

higher the electronegativity of halogen the shorter the Ba–X bond. Higher electronegativity implies stronger attraction between barium and halogen atom that results to shortening of the bond. It is also noted that the value of R_e(Ba–X) increases with increase in the size of the molecule and thus follows the order: $BaX^+ < BaX_2 < BaX_3^- < Ba_2X_3^+$.
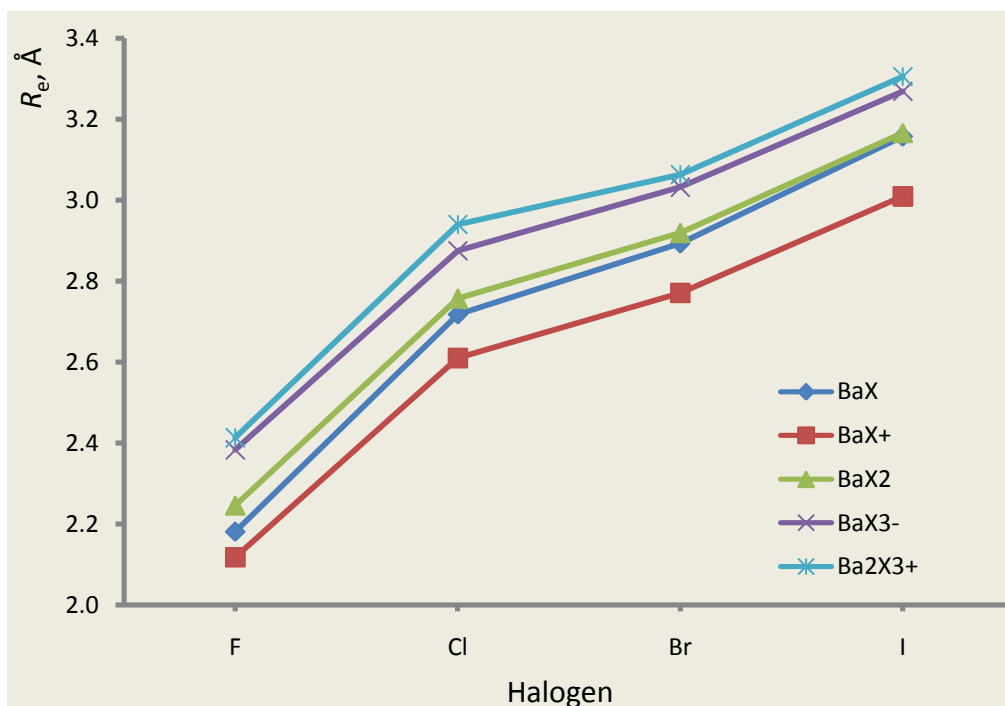
Figure 6.3. Internuclear separations Ba–X of the species BaX, BaX^+, BaX_2, BaX_3^- and $Ba_2X_3^+$ versus halogens (X = F, Cl, Br or I) at MP2 level.

Isomers Ba$_2$X$_4$

For the dimer molecules Ba_2X_4, different alternative structures were considered, bipyramidal (C_{3v}), cyclic planar (D_{2h}), cyclic nonplanar *cis-* (C_{2v}) and *trans-* (C_{2h}) isomeric forms were proved to exist for Ba_2F_4, Ba_2Cl_4 and Ba_2Br_4 while only C_{3v} and C_{2h} exist for Ba_2I_4. For all halides, the bipyramidal isomer possessed the lowest energy. The relative abundances of the isomers were evaluated in a broad temperature range. The C_{3v} isomer appeared predominant at lower temperatures. When the temperature increases other isomers become competitive as shown on Fig. 6.4.

For the Ba_2X_4 dimers, the isomers become comparable in amount at temperatures ~1400 K (Ba_2F_4), ~900 K (Ba_2Cl_4), ~600 – 800 K (Ba_2Br_4) and ~800 K (Ba_2I_4). Thus in series F→Cl→Br→I the temperatures at which the cyclic isomers become predominant decrease gradually.
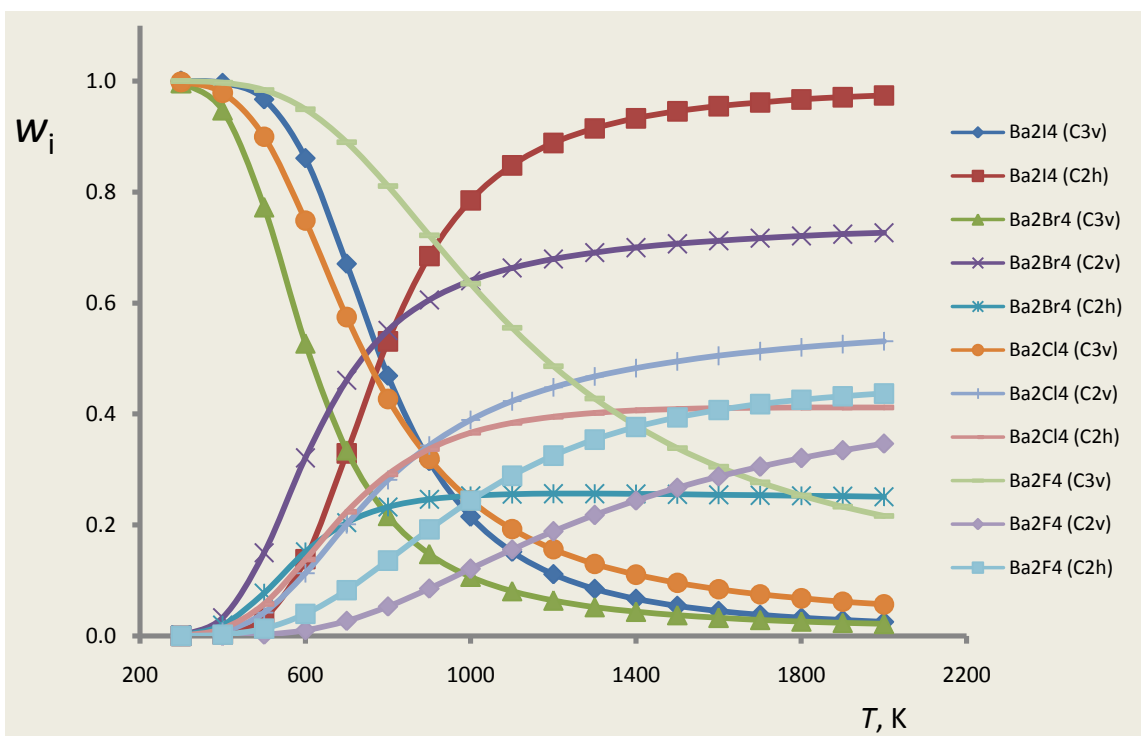
Figure 6.4. Fractions w_i of the Ba_2X_4 isomers versus temperature (X = F, Cl, Br or I).

Enthalpies of dissociation reactions

The geometrical parameters and vibrational frequencies were used in the computation of TD functions of the species given in Appendix. The TD functions were used for the treatment of the equilibrium constants measured previously. Dissociation reactions with elimination of BaX_2 molecules were considered. For calculation of the theoretical enthalpies of the reactions, the MP4 method was employed in addition to DFT and MP2 methods, BSSE was taken into account. Generally, the DFT method showed a poor agreement with values based on experiment, while the MP-methods provided reliable results.

The illustration of the computational method effect on theoretical values of $\Delta_r H°(0)$ is given in Fig. 6.5 in which the enthalpies of dissociation reactions of the Ba_2X_4 dimers are plotted against method. The DFT results deviated much from MP2, MP4 and CP corrections. Similar to the cluster ions, the magnitudes of $\Delta_r H°(0)$ depend on the nature of halogen: they decrease in the order $Ba_2F_4 \rightarrow Ba_2Cl_4 \rightarrow Ba_2Br_4 \rightarrow Ba_2I_4$.
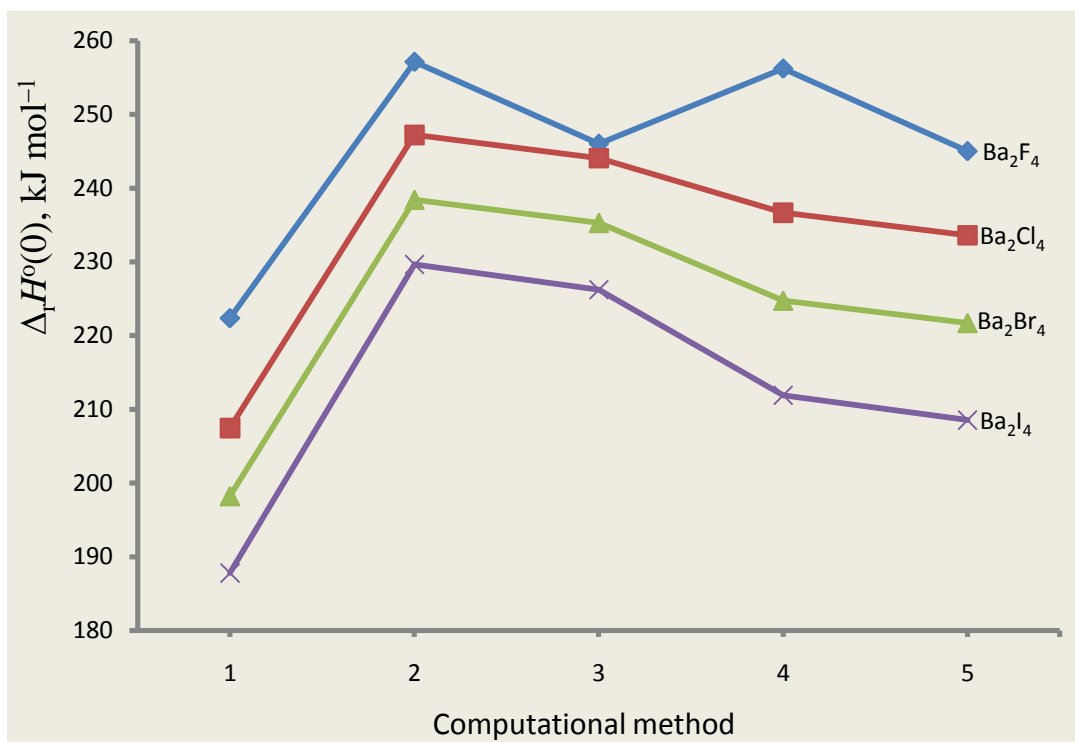
Figure 6.5. Enthalpies of dissociation reaction of Ba_2X_4, C_{3v} ($Ba_2X_4 = 2BaX_2$) versus computational method: 1 – DFT; 2 – MP2; 3 – MP2^{CP}; 4 – MP4; 5 – MP4^{CP}.

For the cluster ions, the enthalpies of dissociation reactions evidently relate both the nature of halogen and size of the cluster. As shown in Fig. 6.6, the values of $\Delta_r H^o(0)$ tend to decrease in the order F→Cl→Br→I. The trend is similar to that of the dimer molecules Ba_2X_4 (C_{3v}). This means that the BaF-species have the highest values of $\Delta_r H^o(0)$ while the respective BaI-species have lowest values. It can be related to the electronegativity values of the halogens: F > Cl > Br > I. It means the higher the electronegativity of the halogen the stronger the Ba–X bonds and therefore the higher the energy required to dissociate the ion. It is further noted that for positive cluster ions the stability is related to their size. As observed from Fig. 6.6, the smaller clusters have higher magnitudes of $\Delta_r H^o(0)$. Generally, stability of the ions follows the order $Ba_2X_3^+ > Ba_3X_5^+ > Ba_4X_7^+ > Ba_5X_9^+$. Exception was observed for $Ba_5X_9^+$ for fluorine and chlorine, the $Ba_5Cl_9^+$ ion unexpectedly has higher value of $\Delta_r H^o(0)$ than $Ba_5F_9^+$. We argue that this discrepancy may be attributed to the steric factor; chlorine atom has comparable size to barium atom dissimilar to fluorine atom. Comparable atomic sizes favour compactness and therefore high stability.

84
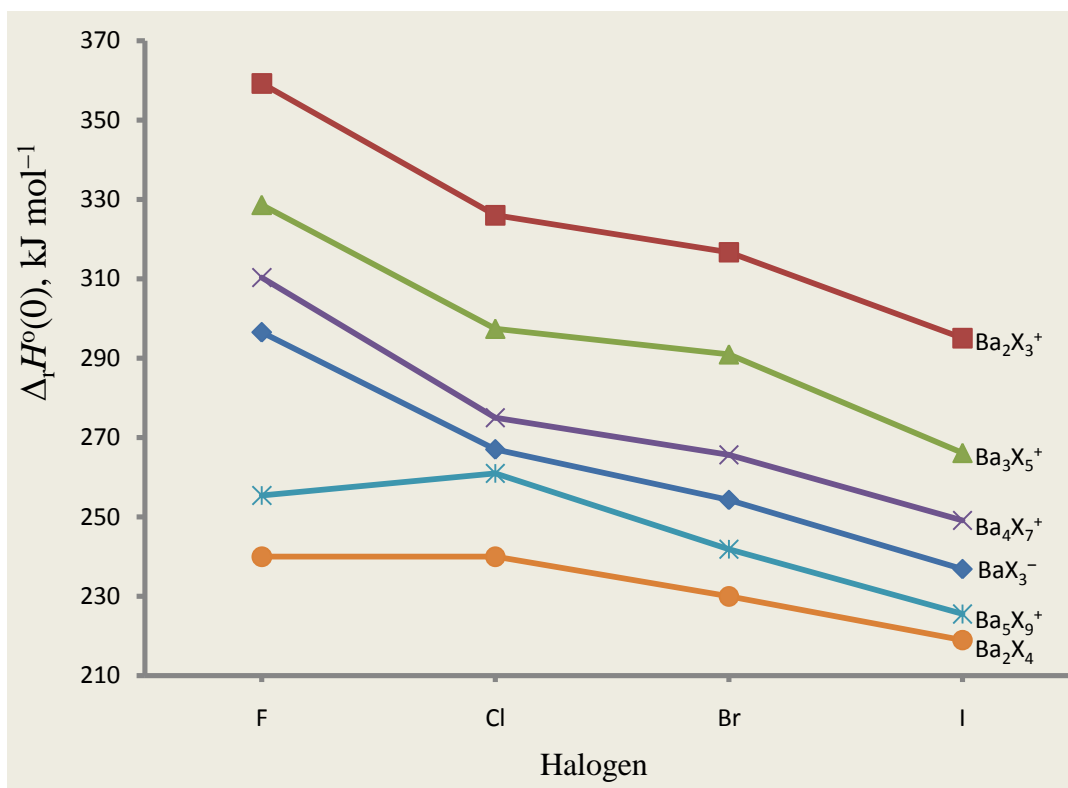
Figure 6.6. Enthalpies of dissociation reactions of the species ($BaI_3^- \rightleftarrows I^- + BaI_2$; $BaI^+(BaI_2)_n \rightleftarrows BaI^+(BaI_2)_{n-1} + BaI_2$; & $Ba_2X_4 \rightleftarrows 2BaX_2$) versus halogen (X = F, Cl, Br or I).

6.2   Conclusion

The structure, vibrational spectra and thermodynamic functions and enthalpies of dissociation reactions of the cluster ions detected earlier in saturated vapours over barium dihalides, BaX_2 (X = F, Cl, Br, I), have been studied theoretically. In addition, the dimer molecules of the corresponding barium dihalides were considered; their structure, vibrational spectra, thermodynamic properties and vapour compositions have been established.

The quantum chemical methods, DFT and MP2 with triple-ζ basis sets employed in this work were validated by computing the structural properties of the simple species BaX, BaX^+ and BaX_2 (X = halogen) and comparing the results with the available experimental and theoretical data.

For all cluster ions, alternative configurations were considered but no isomers were identified. The equilibrium configurations confirmed for the ions are D_{3h} for BaX_3^-, $Ba_2X_3^+$, $Ba_3X_5^+$ and $Ba_5X_9^+$ and C_{2v} for $Ba_4X_7^+$. It was observed that the structural parameters are not much sensitive to the method of determination and basis set used.

For the Ba_2X_4 dimer molecules, three isomeric forms of C_{3v}, C_{2v} and C_{2h} symmetry were confirmed for the molecules Ba_2F_4, Ba_2Cl_4 and Ba_2Br_4 while for Ba_2I_4 only two, C_{3v} and C_{2h} isomers. It was shown that for all halides, the bipyramidal C_{3v} isomers possessed the lowest energy, being predominant in saturated vapours at lower temperatures, whereas at higher temperatures, close to experimental, the relative amount of isomers appeared to be comparable.

The enthalpies of dissociation reactions and enthalpies of formation of the cluster ions were computed both theoretically and based on experiment. For the latter, the experimental equilibrium constants measured earlier were used. The theoretical methods employed were DFT, MP2, $MP2^{CP}$, MP4 and $MP4^{CP}$; the MP-results demonstrated a good agreement with the 'based on experiment' in oppose to the DFT. The magnitudes of $\Delta_r H°(0)$ were observed to depend on cluster size and nature of halogen; for positive cluster ions, the smaller the cluster ion the higher is the value of $\Delta_r H°(0)$. Regarding the nature of halogen, cluster ions of more electronegative halogen have higher values of $\Delta_r H°(0)$.

6.3 Recommendations

As continuation to this work, the following studies are recommended for future work:

1. In this work we compared our results for $Ba_2X_3^+$, $Ba_3X_5^+$ and $Ba_4X_7^+$ with the results obtained based on experimental equilibrium constants available. More up-to date experimental studies need to be conducted for other cluster ions like $Ba_5X_9^+$.

2. For the isomers of the dimer molecules, a theoretical study of the structural properties, thermodynamic properties and vapour compositions was done. We recommend experimental studies on the same at the temperatures considered in this work. Also application of more advanced method (CCSD), to study transition states and barriers along the $C_{3v} \rightarrow C_{2h}$ to verify the relative abundance of the isomers at different temperatures is recommended.

3. Theoretical studies of cluster ions of mixed halogens for example BaF_2Cl^-, $BaFCl_2^-$, $Ba_2F_2Cl^+$ and $Ba_2FCl_2^+$ is recommended.

4. We recommend similar studies to be conducted about the cluster ions existing in vapours over other alkaline earth metal dihalides.

References

Alkali Earth Metals. (2017). Retrieved January 10, 2017, from
https://www.learner.org/interactives/periodic/groups3.html.

Axten, J., Trachtman, M., & Bock, C. W. (1994). An *Ab Initio* Molecular Orbital Study of Small
Magnesium Dihalide Clusters. *The Journal of Physical Chemistry*, *98*(32), 7823–7831.
https://doi.org/10.1021/j100083a013.

Bode, B. M. & Gordon, M. S. (1998). MacMolPlt version 7.4.2. *Journal of Molecular Graphics
Modelling*. 133–138. http://www.scl.ameslab.gov/MacMolPlt/.

Baikov, V. I. (1968). Low-Frequency Vapor Spectra of Alkaline-Earth Metal Florides, *Optical
Spectroscopy*. Vol. 25, p.194.

Baikov, V. I. (1969). Stretching Vibration Frequencies of Free Molecules of the Group II A
Metal Halides, *Optical Spectroscopy*. Vol. 27, p.502.

Bartlett, R. J. (1989). Coupled-cluster approach to molecular structure and spectra: a step toward
predictive quantum chemistry. *The Journal of Physical Chemistry*, *93*(5), 1697–1708.
https://doi.org/10.1021/j100342a008.

Bartlett, R. J., & Purvis, G. D. (1978). Many-Body perturbation theory, Coupled-Pair Many-
Electron theory, and the importance of Quadruple Excitations for the Correlation Problem.
International Journal of Quantum Chemistry, *14*(5), 561–581.
https://doi.org/10.1002/qua.560140504.

Becke, A. D. (1988). Density-functional exchange-energy approximation with correct asymptotic
behavior. *Physical Review A*, *38*(6), 3098–3100.
https://doi.org/10.1103/PhysRevA.38.3098.

Becke, A. D. (1993a). A new mixing of Hartree–Fock and local density-functional theories. *The
Journal of Chemical Physics*, *98*(2), 1372. https://doi.org/10.1063/1.464304.

Becke, A. D. (1993b). Density-functional thermochemistry. III. The role of exact exchange. *The
Journal of Chemical Physics*, *98*(7), 5648. https://doi.org/10.1063/1.464913.

Becke, A. D. (1993). Density functional thermochemistry. III. The role of exact exchange Density-functional thermochemistry. III. The role of exact exchange. *Journal of Chemical Physics, Additional Information on Journal of Chemical Physics Journal Homepage*, *98*(5648). https://doi.org/10.1063/1.464913.

Becke, A. D. (2014). Perspective: Fifty years of density-functional theory in chemical physics. *Journal of Chemical Physics*. https://doi.org/10.1063/1.4869598.

Belyaev, V. N., Gotkis, I. S., Lebedeva, N. L. & Krasnov, K. S. (1990). Ionization potentials of MX molecules (M = Ca, Sr, Ba; X = F, Cl, Br, I, OH, O), *Russian Journal of Physical Chemistry*. 64:773.

Benson, S. W. & Patterson, M. J. (2008-2009), presented at the 31st International Electric Propulsion Conference, University of Michigan, Ann Arbor, MI, USA, September 20– 24. 2009. M. Patterson, NASA Glenn Research Center, Cleveland, 2008, Ohio 44135. http://www.nas.

Binnewies, M. (1998). Chemische Transportreaktionen. *Chemie in Unserer Zeit*, *1*, 15–21. https://doi.org/10.1002/ciuz.19980320104.

Bisseling, R., & Kosloff, R. (1985). The fast Hankel transform as a tool in the solution of the time dependent Schrödinger equation. *Journal of Computational Physics*, *59*(1), 136–151. https://doi.org/10.1016/0021-9991(85)90112-3.

Bode, B. M & Gordon, M. (1998). MacMolPlt version 7.4.2. *Journal of Molecular Graphics and Modelling*. Retrieved from http://www.scl.ameslab.gov/MacMolPlt/.

Boys, S., & Bernardi, F. (1970). The calculation of small molecular interactions by the differences of separate total energies. Some procedures with reduced errors. *Molecular Physics*, (May 2012), 553–566. https://doi.org/10.1080/00268977000101561.

Bradford, R. S. (1975). Production efficiencies of electronically excited states of barium monohalides. *The Journal of Chemical Physics*, *62*(6), 2060. https://doi.org/10.1063/1.430795.

Butman, M. F., Smirnov, A. A., Kudin, L. S. & Dabringhaus, H. (2002). Thermal ion emission

from crystalline SrCl$_2$ at the temperatures of phase transition to the superionic state, *Surface Science*. 511, 331–339.

Butman, M. F., Smirnov, A. A., Kudin, L. S. & Dabringhaus, H. (2001). Mass spectrometric study of the thermal ion emission from crystalline BaF$_2$ at the temperatures of phase transition to the superionic state, *Surface Science*. 489, 83–99.

Calder, V. (1969). Geometry and Vibrational Spectra of Alkaline-Earth Dihalides. II. CaF$_2$, SrF$_2$, and BaF$_2$. *The Journal of Chemical Physics*, *51*(5), 2093. https://doi.org/10.1063/1.1672304.

Castleman, A. W. & Khanna, S. N. (2007). Superatoms: building blocks of new materials, *Chemical Physics of Solid Surfaces*. 113, 2664–2675. doi:10.1016/S1571-0785(07)12010-1.

Čížek, J. (1966). On the Correlation Problem in Atomic and Molecular Systems. Calculation of Wavefunction Components in Ursell-Type Expansion Using Quantum-Field Theoretical Methods. *The Journal of Chemical Physics*, *45*(11), 4256. https://doi.org/10.1063/1.1727484.

Cramer, C. J. (2004). *Essentials of Computational Chemistry Theories and Models Second Edition*.

Dagdigian, P. J., Cruse, H. W. & Zare R. N. (1976). Vibrational state analysis of unrelaxed BaI from the reactions Ba + CH$_3$I and Ba + CH$_2$I$_2$, *Chemical Physics*. 15, 249–260. doi:10.1016/0301-0104(76)80158-9.

Devore, T. C., & Gole, J. L. (1999). Energetics, molecular electronic structure, and spectroscopy of forming Group IIA dihalide complexes. *Chemical Physics*, *241*(2), 221–238. https://doi.org/16/S0301-0104(98)00401-7.

Donald, K. J., & Hoffmann, R. (2006). Solid memory: Structural preferences in group 2 dihalide monomers, dimers, and solids. *Journal of the American Chemical Society*, *128*(34), 11236–11249. https://doi.org/10.1021/ja062817j.

Duncan, M. A. (2000). Frontiers in the spectroscopy of mass-selected molecular ions. *International Journal of Mass Spectrometry*, *200*(1-3), 545–569.

https://doi.org/10.1016/S1387-3806(00)00366-3.

Dunning Jr, T. H. (1989). Gaussian basis sets for use in correlated molecular calculations. I. The atoms boron through neon and hydrogen. *The Journal of Chemical Physics.*, *90*, 1007. https://doi.org/10.1063/1.456153.

Dunning T. H., J., Peterson, K. A., & Wilson, A. K. (2001). Gaussian basis sets for use in correlated molecular calculations. X. The atoms aluminum through argon revisited. *Journal of Chemical Physics*, *114*(21), 9244–9253. https://doi.org/10.1063/1.1367373.

Ehlert, T. C., Blue, G. D., Green, J. W., & Margrave, J. L. (1964). Mass Spectrometric Studies at High Temperatures. III. Dissociation Energies of the Alkaline Earth Monofluorides. *The Journal of Chemical Physics*, *41*(8), 2250. https://doi.org/10.1063/1.1726255.

Elliott, B. M., Koyle, E., Boldyrev, A. I., Wang, X-B. & Wang, L-S. (2005). MX_3^- Superhalogens (M = Be, Mg, Ca; X = Cl, Br): A Photoelectron Spectroscopic and *Ab Initio* Theoretical Study, *Journal of Physical Chemistry A*. 109, 11560–7. doi:10.1021/jp054036v.

Emons, V. H-H., Kiessling, D. & Horlbeck, W. (1982). Dampfdruckmessungen und massenspektrometrische untersuchungen der Gasphase uber Erdalkalimetallhalogeniden, Z. anorg. allg. Chem. 222 (1982) 3–6.

Environmental Molecular Sciences Laboratory, U.S. Retrieved from https://bse.pnl.gov/bse/portal.

Feller, D. (1996). The Role of Databases in Support of Computational Chemistry Calculations. *Journal of Computational Chemistry*. 17(13), 1571-1586.

Fontijn, A. (1998). Wide-temperature range observations on reactions of metal atoms and small radicals. *Pure and Applied Chemistry*, *70*(2), 469–476. https://doi.org/10.1351/pac199870020469.

Gigli, G. (1990). On the structure of the alkaline earth dihalides dimers. *The Journal of Chemical Physics*, *93*(7), 5224. https://doi.org/10.1063/1.459667

Girichev, A. G., Giricheva, N. I., Vogt, N., Girichev, G. V, & Vogt, J. (1996). Structural investigation of molecules in the vapour over beryllium dichloride using electron diffraction and mass spectrometric data. *Journal of Molecular Structure*. 384 (1996) 175-182.

Granovsky, A. A., Firefly version 8, www http://classic.chem.msu.su/gran/firefly/index.html.

Group 17: General Properties of Halogens. https://chem.libretexts.org/Core/Inorganic_Chemistry/Descriptive_Chemistry/Elements_Organized_by_Block/2_p-Block_Elements/Group_17%3A_The_Halogens/1Group_17%3A_General_Properties. Accessed 28 March, 2017.

Guido, M., & Gigli, G. (1976). Ion model and equilibrium configuration of the gaseous alkaline-earth dihalides. *The Journal of Chemical Physics*, *65*(4), 1397–1402. https://doi.org/10.1063/1.434468.

Gurvich, L. V., Yungman, V. S., Bergman, G. A., Veitz, I. V., Gusarov, A. V., Iorish, V. S., Leonidov, V. Y., Medvedev, V. A., Belov, G. V., Aristova, N. M., Gorokhov, L. N., Dorofeeva, O. V., Ezhov, Y. S., Efimov, M.E., Krivosheya, N. S., Nazarenko, I. I., Osina, E. L. (2000). Ivtanthermo for Windows Database on Thermodynamic Properties of Individual Substances and Thermodynamic Modeling Software Moscow Glushko Thermocenter of RAS.

Hargittai, M. (2000). Molecular structure of metal halides. *Chemical Reviews*. https://doi.org/10.1021/cr970115u.

Hargittai, M. (2005). High-temperature gas-phase electron diffraction: Unexpected dimer structures among metal halides. *Structural Chemistry*, *16*(1), 33–40. https://doi.org/10.1007/s11224-005-1078-z.

Hargittai, M., Kolonits, M. Â., & Schultz, G. È. (2001). The molecular structure of barium dibromide: an electron diffraction and quantum chemical study. *Journal of Molecular Structure*, 567-568, 241-246.

Hendricks, J. H., Aquino, M. I., Maslar, J. E., & Zachariah, M. R. (1998). Metal and ceramic thin

film growth by reaction of alkali metals with metal halides: A new route for low-temperature chemical vapor deposition. *Chemistry of Materials*, *10*(8), 2221–2229. https://doi.org/Doi 10.1021/Cm980161q.

Herzberg, G., & Huber, K. P. (1979). *Molecular Spectra and Molecular Structure. Nature*. https://doi.org/10.1007/978-1-4757-0961-2.

Hilpert, K., & Niemann, U. (1997). High temperature chemistry in metal halide lamps. *Thermochimica Acta*. https://doi.org/10.1016/S0040-6031(97)00136-6.

Huenecke, K. (2002). Experimental and Theoretical Investigation of Ion/Molecular Clusters in the Subsonic Turbulent Flow. (Daimler Chrysler Aerospace Airbus, Deutschland). <http://cordis.europa.eu/search/index.cfm?fuseaction=proj.document&PJ_RCN=5944267>.

Jacob, F., Pogrebnoi, A. M., & Pogrebnaya, T. P. (2016). Cluster ions in saturated vapor over barium difluoride: Structure and thermodynamic properties. *Computational and Theoretical Chemistry*. https://doi.org/10.1016/j.comptc.2016.07.011.

Jakubek, Z. J., Harris, N. A, Field, R. W., & Gardner, J. A. (1994). Ionization potentials of CaF and BaF. *Journal of Chemical Physics*, *100*(1), 622–627. https://doi.org/10.1063/1.466923.

Kaupp, M. (2001). "Non-VSEPR" Structures and Bonding in d^0 Systems. *Angewandte Chemie (International Ed. in English)*, *40*(19), 3534–3565. https://doi.org/10.1002/1521-3773(20011001)40:19<3534:AID-ANIE3534>3.0.

Kaupp, M., Schleyer, P. V. R., Stoll, H., & Preuss, H. (1991). Pseudopotential approaches to Ca, Sr, and Ba hydrides. Why are some alkaline earth MX_2 compounds bent? *The Journal of Chemical Physics*, *94*(2), 1360–1366. https://doi.org/10.1063/1.459993.

Kendall, R. A, Dunning Jr., T. H., & Harrison, R. J. (1992). Electron affinities of the first-row atoms revisited. Systematic basis sets and wave functions. *Journal of Chemical Physics*, *96*(May 2013), 6796. https://doi.org/10.1063/1.462569.

Khanna, S. N., & Jena, P. (1992). Assembling crystals from clusters. *Physical Review Letters*, *69*(11), 1664–1667. https://doi.org/10.1103/PhysRevLett.69.1664.

Khanna, S. N., & Jena, P. (1995). Atomic clusters: Building blocks for a class of solids. *Physical Review B*, *51*(19), 13705–13716. https://doi.org/10.1103/PhysRevB.51.13705.

Knight, L. B. (1971). Hyperfine Interaction and Chemical Bonding in MgF, CaF, SrF, and BaF molecules. *The Journal of Chemical Physics*, *54*(1), 322. https://doi.org/10.1063/1.1674610.

Kohn, W., & Sham, L. J. (1965). Self-Consistent Equations Including Exchange and Correlation Effects. *Physical Review*, *140*(4A), A1133–A1138. https://doi.org/10.1103/PhysRev.140.A1133.

Krasnov, K. S., Philippenko, N. V., Bobkova, V. A., Lebedeva, N. L., Morozov, E. V., Ustinova, T. I., & Romanova, G. A. (1979). *Handbook of Molecular constants of Inorganic constants*. (K. Krasnov, Ed.). Leningrad, Khimiya.

Kushawaha, V. S. (1973). The $C^2\pi$ and the $X^2\sigma$ States of BaF. *Spectroscopy Letters*, *6*(10), 633–645. https://doi.org/10.1080/00387017308060853.

Kudin, L. S., Burdukovskaya, G. G., Vorobev, O. V. & Bozhko, N. V. (1990). Mezhvuzovskii sbornik "Molekulyarnaya Struktura" ("Molecular Structure"), Ivanovo, p. 144.

Lau, K. H., Brittain, R. D., & Hildenbrand, D. L. (1989). High temperature thermodynamic studies of some gaseous thorium fluorides. *The Journal of Chemical Physics*, *90*(2), 1158. https://doi.org/10.1063/1.456171.

Leach, A. R. (2001). *Molecular Modelling: Principles and Applications, second edition*. Pearson Education EMA.

Lee, Yang, W., & Parr, R. (1988). Development of the Colle- Salvetti correlation energy formula into a functional of the electron density. *Physical Reviews B*, *37*(2), 785–789.

Lee, C., Yang, W., & Parr, R. G. (1988). Development of the Colle-Salvetti correlation-energy formula into a functional of the electron density. *Physical Review. B, Condensed Matter*, *37*(2), 785–789. https://doi.org/10.1103/PhysRevB.37.785.

Lee, E. P. F., & Potts, A. W. (1979). An Investigation of the Valence Shell Electronic Structure of Alkaline Earth Halides by Using *Ab Initio* s.c.f. Calculations and Photoelectron

Spectroscopy. *Proceedings of the Royal Society A: Mathematical, Physical and Engineering Sciences*. https://doi.org/10.1098/rspa.1979.0025.

Lesiecki M. L. and Nibler J. W. (1976). Infrared and Raman spectra and structures of matrix isolated magnesium dihalides: MgF_2, $MgCl_2$, $MgBr_2$, and MgI_2. *The Journal of Chemical Physics*, *64*(2), 871. https://doi.org/10.1063/1.432210.

Levy, J. B., & Hargittai, M. (2000). Unusual Dimer Structures of the Heavier Alkaline Earth Dihalides: A Density Functional Study. *Journal of Physical Chemistry A*, 104, 1950–1958. https://doi.org/10.1021/jp994339n.

Liu, Y., Zhao, J., Li, F., & Chen, Z. (2013). Appropriate description of intermolecular interactions in the methane hydrates: An assessment of DFT methods. *Journal of Computational Chemistry*, *34*(2), 121–131. https://doi.org/10.1002/jcc.23112.

Martin, J. M. L., & Sundermann, A. (2001). Correlation consistent valence basis sets for use with the Stuttgart-Dresden-Bonn relativistic effective core potentials: the atoms Ga-Kr and In-Xe. *Journal of Chemical Physics*, *114*(8), 3408–3420. https://doi.org/10.1063/1.1337864.

Michael, F.L. & Allan, J.L. (1994). Principles of Plasma Discharges and Materials Processing, 2nd ed. (Wiley, New York), p. 512.

Molntir, J., Marsden, C. J., & Hargittai, M. (1995). Molecular Structures and Force Fields of Monomeric and Dimeric Magnesium Dichloride from Electron Diffraction and Quantum Chemical Calculations, *Journal of Physical Chemistry*, 99 (22), 9062–9071.

Moustapher, I., Pogrebnaya, T., & Pogrebnoi, A. (2016). Cluster Ions in Vapour over Calcium Dichloride: Theoretical Study of Geometrical Structure and Vibrational Spectra. *British Journal of Applied Science & Technology*, *12*(3), 1–14. https://doi.org/10.9734/BJAST/2016/21810.

Murray, K. K., Boyd, R. K., Eberlin, M. N., Langley, G. J., Li, L., & Naito, Y. (2013). Definitions of terms relating to mass spectrometry (IUPAC Recommendations 2013). *Pure Applied Chemistry*, *85*(7), 1515–1609. https://doi.org/10.1351/PAC-REC-06-04-06.

Mwanga, S. F., Pogrebnaya, T. P., Pogrebnoi, A. M. (2015). Molecular and ionic clusters

existing in vapor over cesium chloride: Structure and thermodynamic properties. *Computational and Theoretical Chemistry*, *1078 (2016*, 47–54.

Mwanga, S. F., Pogrebnaya, T. P., & Pogrebnoi, A. M. (2015). Structure and properties of molecular and ionic clusters in vapour over caesium fluoride. *Molecular Physics*. https://doi.org/10.1080/00268976.2015.1007104.

Mwanga, S., Pogrebnaya, T., & Pogrebnoi, A. (2015). Theoretical Study of Cluster Ions Existing in Vapours over Cesium Bromide and Iodide. *British Journal of Applied Science & Technology*. https://doi.org/10.9734/BJAST/2015/17612.

National Institute of Standards and Technology, (NIST,US); www.nist.gov.

Ottosson, M., Andersson, T., Carlsson, J-O., Hårsta, A., Jansson, U., Norling, P., Niskanen, K. & Nordblad, P. (1989). Chemical vapor deposition of the superconducting $YBa_2Cu_3O_{7-x}$ phase using halides as metal sources. *Applied Physics Letters*, *54*(24), 2476. https://doi.org/10.1063/1.101540.

Parr, R. G., & Yang, W. (1989). *Density-functional theory of atoms and molecules*. Oxford University Press.

Perdew, J. P. (1986a). Density-functional approximation for the correlation energy of the inhomogeneous electron gas. *Physical Review B*, *33*(12), 8822–8824. https://doi.org/10.1103/PhysRevB.33.8822.

Perdew, J. P. (1986b). Erratum: Density-functional approximation for the correlation energy of the inhomogeneous electron gas. *Physical Review. B, Condensed Matter*, *34*(10), 7406. https://doi.org/10.1103/PhysRevB.33.8822.

Perdew, J. P. J., Chevary, J. A., Vosko, S. H., Jackson, K. K. A., Pederson, M. R., Singh, D. J., & Fiolhais, C. (1992). Atoms, molecules, solids, and surfaces: Applications of the generalized gradient approximation for exchange and correlation. *Physical Review. B, Condensed Matter*, *46*(11), 6671–6687. https://doi.org/10.1103/PhysRevB.46.6671.

Perdew, J. P., & Zunger, A. (1981). Self interaction correction to density functional approximations for many-electron systems. *Physical Review B*, *23*(10), 5048–5079.

https://doi.org/10.1103/PhysRevB.23.5048.

Perdew, Y., & Wang, J. P. (1992). Accurate and simple analytic representation of the electron-gas correlation energy. *Physical Review. B, Condensed Matter*, *45*(23), 13244–13249. https://doi.org/10.1103/PhysRevB.43.8911.

Pogrebnaya, T. P., Sliznev, V. V. & Solomonik, V. (1997). An *Ab Initio* study of the isomerism and vibrational spectra of the dimeric M_2F_4 and MM'F_4 molecules (M, M' = Be, Mg, Ca). *Koordinatsionnaya Khimiya*, *23*(7), 498-505.

Pogrebnaya, T. P., Hishamunda, J. B., Girabawe, C. & Pogrebnoi, A. M. (2012). Theoretical Study of Structure, Vibration Spectra and Thermodynamic Properties of Cluster Ions in Vapors over Potassium, Rubidium and Cesium Chlorides. https://doi.org/10.1007/978-90-481-8650-1.

Pogrebnaya, T. P., Pogrebnoi, A. M., & Kudin, L. S. (2008). Calculation of the thermodynamic characteristics of ions in vapor over sodium fluoride. *Russian Journal of Physical Chemistry A*, *82*(1), 75–82. https://doi.org/10.1134/S0036024408010111.

Pogrebnaya, T. P., Pogrebnoi, A. M., Kudin, L. S. (2007). Theoretical Study of the Structure and Stability of the Na_2Cl^+, $NaCl_2^-$, $Na_3Cl_2^+$ AND $Na_2Cl_3^-$. *Journal of Structural Chemistry*. *48*(6), 987–995.

Pogrebnoi, A. M., Mass Spectrometric Investigation of Ion Molecular Equilibria in vapours over alkali earth metal halides, Candidate's dissertation in chemistry, Ivanovo State University of Chemical Technology, Ivanovo, 1981.

Pogrebnoi, A. M., Kudin, L. S., and Krasnov, K. S (1984). Ion-Molecular Equilibrium in Vapours over Halogenides of Alkaline Earth Metals, *Russian Journal of Physical Chemistry*. 58, 2129.

Pogrebnoi, A. M., Pogrebnaya, T. P., Kudin, L. S., & Tuyizere, S. (2013). Structure and thermodynamic properties of positive and negative cluster ions in saturated vapour over barium dichloride. *Molecular Physics*, 111(21), 3234–3245. https://doi.org/10.1080/00268976.2013.776711.

Pople, J. A., Krishnan, R., Schlegel, H. B., & Binkley, J. S. (1978). Electron correlation theories and their application to the study of simple reaction potential surfaces. *International Journal of Quantum Chemistry*, *14*(5), 545–560. https://doi.org/10.1002/qua.560140503.

Purvis, G. D., & Bartlett, R. J. (1982). A full coupled-cluster singles and doubles model: The inclusion of disconnected triples. *The Journal of Chemical Physics*, *76*(1982), 1910–1918. https://doi.org/10.1063/1.443164.

Quantum Chemistry. (2016). Retrieved January 19, 2017, from https://en.wikipedia.org/wiki/Quantum_chemistry.

Rajagopal, A. K., & Callaway, J. (1973). Inhomogeneous electron gas. *Physical Review B*, *7*(5), 1912–1919. https://doi.org/10.1103/PhysRevB.7.1912.

Ramondo, F., Bencivenni, L., Nunziante Cesaro, S., & Hilpert, K. (1989). FTIR matrix isolation study on gaseous calcium dihalide molecules. *Journal of Molecular Structure*, *192*(1-2), 83–94. https://doi.org/10.1016/0022-2860(89)87008-5.

Ramondo, F., Bencivenni, L., & Spoliti, M. (1992). *Ab Initio* study on the Be_2F_4, Mg_2F_4 dimers, on the mixed dimers $BeMgF_4$ and $LiNaF_2$ and on the Li_2BeF_4, $LiBCl_4$ and $LiAlCl_4$ ion-pairs. *Journal of Molecular Structure (Theochem)*, 277, 171–184.

Ramondo, F., Rossi, V., & Bencivenni, L. (1988). Structure and vibrational frequencies of CaF_2 aggregates isolated in a low temperature matrix. *Molecular Physics*, *64*(3), 513–520. https://doi.org/10.1080/00268978800100363.

Rao, B. K., Khanna, S. N., & Jena, P. (2000). Designing New Materials Using Atomic Clusters, *Journal of Cluster Science*, *10*(4), 477–491.

Réffy, B., Kolonits, M., & Hargittai, M. (2005). Molecular structure of magnesium dibromide: An electron diffraction and quantum chemical study. *Journal of Physical Chemistry A*, *109*(37), 8379–8384. https://doi.org/10.1021/jp0530606.

Rosen, A. & Westin, E. (1988). Local Density Theory Calculations of the Ionization Energies and Optical Transitions in BaF and BaCl. *Chemical Physics Letters*. 149 (3).

Schmidt, M. W., Baldridge, K. K., Boatz, J. A., Elbert, S. T., Gordon, M. S., Jensen, J. H., Koseki, S., Matsunaga, N., Nguyen, K.A., Su, S., Windus, T.L., Dupuis, M. & Montgomery, J.A. (1993). General atomic and molecular electronic structure system. *Journal of Computational Chemistry*, *14*(11), 1347–1363. https://doi.org/10.1002/jcc.540141112.

Schuchardt, K.L., Didier, B.T., Elsethagen, T., Sun, L., Gurumoorthi, V., Chase, J., Li, J., & Windus, T.L. (2007). Basis Set Exchange: A Community Database for Computational Sciences. *Journal of Chemical Information and Modeling*, 47(3), 1045-1052. doi:10.1021/ci600510j.

Smirnov, B. M (2012). Fundamentals of Ionized Gases: Basic Topics in Plasma Physics. John Wiley & Sons, 19 Sep 2012 - Science - 450 pages.

Spoliti, M., De Maria, G., D'alessio, L., Maltese, M. (1980). Bonding in and Spectroscopic Propertes of Gaseous Triatomic Molecules; *Journal of Molecular Structure*, 67, 159-167.

Seijo, L., Barandiarán, Z., & Huzinaga, S. (1991). *Ab Initio* model potential study of the equilibrium geometry of alkaline earth dihalides: MX2 (M=Mg, Ca, Sr, Ba; X=F, Cl, Br, I). *The Journal of Chemical Physics*, *94*(5), 3762. https://doi.org/10.1063/1.459748.

Snelson, A. (1966). Infrared Spectra of Some Alkaline Earth Halides by the Matrix Isolation Technique. *The Journal of Physical Chemistry*. *63*(1), 3208–3217.

Snelson A., Cyvin B.N & Cyvin S.J (1974). The Infrared Matrix Isolation Spectrum and Normal Coordinate Analysis of the Beryllium Fluoride Dimer. *The Journal of Physical Chemstry*. 410, 206-212.

Solomonik, V. G., Smirnov, A. N., & Mileyev, M. A. (2005). Structure , Vibrational Spectra , and Energetic Stability of LnX_4^- Ions (Ln = La, Lu; X = F, Cl, Br, I), *Russian Journal of Coordination Chemistry*. *31*(3), 203–212.

Tokarev, K. L. (2007-2009). OpenThermo v.1.0 Beta 1 (C). Retrieved from http://openthermo.software.informer.com/.

Spiridonov, V .P., Gershikov, A.G., Altman, A.B., Romanov, G.V & Ivanov, A.A (1981). A new

approach to electron diffraction analysis of symmetric triatomic molecules with large amplitude bending motion the equilibrium geometry, force field and vibrational frequencies, *Chemical Physics Letters*, 77(1).

Varga, Z., Lanza, G., Minichino, C., & Hargittai, M. (2006). Quasilinear molecule par excellence, $SrCl_2$: Structure from high-temperature gas-phase electron diffraction and quantum-chemical calculations - Computed structures of $SrCl_2$.argon complexes. *Chemistry - A European Journal*, *12*(32), 8345–8357. https://doi.org/10.1002/chem.200600328.

Vasiliu, M., (2010). Computational Thermodynamic Studies of Alkali and Alkaline Earth Compounds, Olefin Metathesis Catalysts, and Borane – Azoles for Chemical Hydrogen Storage. Candidate's dissertation submitted to Unversity of Alabama.

Watts, J. D., Gauss, J., & Bartlett, R. J. (1993). Coupled-cluster methods with noniterative triple excitations for restricted open-shell Hartree–Fock and other general single determinant reference functions. Energies and analytical gradients. *The Journal of Chemical Physics*, *98*(11), 8718. https://doi.org/10.1063/1.464480.

Ystenes, M., & Westberg, N. (1995). *Ab Initio* quantum mechanical vibrational analysis of the dimeric molecules Mg_2F_4, Mg_2C1_4 and Mg_2Br_4. *Spectrochimica Acta Part A*, 51, 1501-1508.

Zatula, A. S. (2012). Experimental and Computational Studies of Dynamic processes in ionic water clusters. Candidate's dissertation submitted to University of Oslo, Norway.

Zhurko, G.A., & Zhurko, D. A. Chemcraft. Version 1.7 (build 132). Retrieved from HTML: www.chemcraftprog.com.

APPENDICES

Appendix A1: The thermodynamic functions of the cluster ions BaX_3^-, $Ba_2X_3^+$, $Ba_3X_5^+$, $Ba_4X_7^+$ and $Ba_5X_9^+$ and dimer molecules Ba_2X_4.

The thermodynamic functions of the species were obtained for 298.15 K and between 300 – 2000 K. The molar heat capacity (c_p°), reduced Gibbs free energy (Φ°), and entropy (S°) are given in $J\cdot mol^{-1}\cdot K^{-1}$ and the enthalpy increment ($H^\circ(T)–H^\circ(0)$) is given in $kJ\cdot mol^{-1}$. The reduced Gibbs free energy was calculated from: $\Phi^\circ(T) = -[H^\circ(T)–H^\circ(0) – TS^\circ(T)]/T$. The thermodynamic functions were calculated using parameters obtained at highest theoretical level available for each species and are presented in Tables A1.1 – A1.29.

Table A1.1. Thermodynamic functions of the BaF_3^- ions.

T	$c_p^\circ(T)$	$\Phi^\circ(T)$	$S^\circ(T)$	$H^\circ(T)–H^\circ(0)$
298.15	77.794	275.388	338.746	18.890
300	77.852	275.780	339.227	19.034
400	80.006	294.606	361.958	26.941
500	81.085	309.938	379.939	35.001
600	81.694	322.877	394.781	43.142
700	82.070	334.073	407.404	51.332
800	82.317	343.941	418.381	59.552
900	82.488	352.761	428.087	67.793
1000	82.611	360.736	436.784	76.048
1100	82.703	368.014	444.662	84.314
1200	82.773	374.705	451.862	92.588
1300	82.827	380.899	458.489	100.868
1400	82.871	386.663	464.629	109.153
1500	82.906	392.053	470.348	117.442
1600	82.935	397.116	475.699	125.734
1700	82.958	401.888	480.728	134.029
1800	82.978	406.401	485.470	142.325
1900	82.995	410.681	489.957	150.624
2000	83.010	414.753	494.215	158.924

Table A1.2. Thermodynamic functions of the $Ba_2F_3^+$ ions.

T	$c_p^\circ(T)$	$\Phi^\circ(T)$	$S^\circ(T)$	$H^\circ(T)–H^\circ(0)$
298.15	98.306	287.313	358.529	21.233
300	98.414	287.754	359.138	21.415
400	102.389	309.366	388.067	31.481
500	104.359	327.493	411.149	41.828
600	105.467	343.076	430.283	52.324
700	106.148	356.728	446.596	62.908
800	106.595	368.868	460.801	73.546
900	106.905	379.795	473.375	84.222
1000	107.127	389.726	484.651	94.924
1100	107.292	398.828	494.869	105.646
1200	107.418	407.226	504.210	116.381

100

1300	107.517	415.021	512.812	127.128
1400	107.595	422.295	520.783	137.884
1500	107.658	429.111	528.209	148.647
1600	107.710	435.524	535.159	159.415
1700	107.753	441.579	541.690	170.189
1800	107.789	447.313	547.850	180.966
1900	107.819	452.759	553.679	191.746
2000	107.845	457.945	559.210	202.529

Table A1.3. Thermodynamic functions of the $Ba_3F_5^+$ ions.

T	$c_p°(T)$	$\Phi°(T)$	$S°(T)$	$H°(T)–H°(0)$
298.15	177.260	384.256	511.592	37.965
300	177.260	384.256	511.592	37.965
400	177.430	385.045	512.689	38.293
500	183.350	423.730	564.676	56.378
600	185.760	456.184	605.886	74.851
700	186.860	484.050	639.864	93.489
800	187.430	508.422	668.715	112.205
900	187.770	530.059	693.766	130.966
1000	188.000	549.502	715.896	149.755
1100	188.150	567.149	735.713	168.564
1200	188.270	583.301	753.652	187.386
1300	188.350	598.190	770.037	206.216
1400	188.330	611.996	785.112	225.051
1500	188.320	624.866	799.069	243.884
1600	188.210	636.917	812.060	262.714
1700	188.190	648.249	824.208	281.535
1800	188.030	658.937	835.612	300.347
1900	187.980	669.054	846.357	319.146
2000	187.730	678.656	856.514	337.931

Table A1.4. Thermodynamic functions of the $Ba_4F_7^+$ ions.

T	$c_p°(T)$	$\Phi°(T)$	$S°(T)$	$H°(T)–H°(0)$
298.15	237.390	436.195	605.064	50.348
300	237.620	437.242	606.534	50.788
400	245.970	488.639	676.193	75.022
500	250.070	531.878	731.568	99.845
600	252.360	569.087	777.382	124.977
700	253.760	601.700	816.397	150.288
800	254.680	630.705	850.347	175.714
900	255.320	656.811	880.384	201.216
1000	255.780	680.537	907.309	226.772
1100	256.120	702.279	931.704	252.368
1200	256.390	722.340	954.001	277.993
1300	256.580	740.960	974.531	303.642
1400	256.740	758.331	993.551	329.308
1500	256.870	774.611	1011.270	354.988
1600	257.000	789.924	1027.850	380.681
1700	257.060	804.381	1043.430	406.383
1800	257.120	818.078	1058.130	432.093
1900	257.200	831.077	1072.030	457.810
2000	257.260	843.464	1085.230	483.533

Table A1.5. Thermodynamic functions of the $Ba_5F_9^+$ ions.

T	$c_p^\circ(T)$	$\Phi^\circ(T)$	$S^\circ(T)$	$H^\circ(T)-H^\circ(0)$
298.15	308.590	522.908	748.415	67.235
300	308.860	524.304	750.325	67.806
400	318.690	592.590	840.708	99.247
500	323.510	649.631	912.397	131.383
600	326.210	698.506	971.641	163.881
700	327.880	741.214	1022.060	196.592
800	328.970	779.123	1065.920	229.438
900	329.720	813.183	1104.710	262.374
1000	330.210	844.106	1139.480	295.374
1100	330.680	872.416	1170.980	328.420
1200	330.960	898.509	1199.760	361.501
1300	331.190	922.714	1226.260	394.610
1400	331.470	945.282	1250.810	427.739
1500	331.510	966.423	1273.680	460.886
1600	331.770	986.301	1295.080	494.047
1700	331.850	1005.062	1315.190	527.218
1800	331.870	1022.827	1334.160	560.400
1900	331.900	1039.685	1352.100	593.589
2000	331.700	1055.737	1369.130	626.786

Table A1.6. Thermodynamic functions of the $BaBr^+$ ions.

T	c_p°	Φ°	S°	$H^\circ(T)-H^\circ(0)$
298.15	36.598	228.775	262.386	10.021
300	36.608	228.983	262.613	10.089
400	36.949	238.775	273.198	13.769
500	37.113	246.516	281.462	17.473
600	37.204	252.922	288.237	21.189
700	37.259	258.387	293.977	24.913
800	37.295	263.154	298.955	28.640
900	37.320	267.381	303.349	32.371
1000	37.338	271.178	307.282	36.104
1100	37.351	274.624	310.841	39.839
1200	37.361	277.780	314.092	43.574
1300	37.369	280.689	317.082	47.311
1400	37.376	283.389	319.852	51.048
1500	37.381	285.907	322.431	54.786
1600	37.385	288.266	324.844	58.524
1700	37.388	290.485	327.110	62.263
1800	37.391	292.579	329.247	66.002
1900	37.394	294.563	331.269	69.741
2000	37.396	296.447	333.187	73.481

Table A1.7. Thermodynamic functions of the cluster ions $BaBr_3^-$.

T	c_p°	Φ°	S°	$H^\circ(T)-H^\circ(0)$
298.15	81.940	334.467	407.282	21.710
300	81.954	334.917	407.789	21.861
400	82.467	356.231	431.446	30.086
500	82.708	373.185	449.877	38.346
600	82.841	387.262	464.969	46.624
700	82.921	399.299	477.746	54.913
800	82.973	409.813	488.822	63.207
900	83.009	419.145	498.597	71.507

1000	83.034	427.535	507.344	79.809
1100	83.053	435.156	515.259	88.113
1200	83.068	442.137	522.486	96.419
1300	83.079	448.577	529.136	104.727
1400	83.088	454.553	535.293	113.035
1500	83.095	460.129	541.026	121.344
1600	83.101	465.355	546.389	129.654
1700	83.106	470.271	551.427	137.964
1800	83.110	474.913	556.177	146.275
1900	83.114	479.309	560.671	154.587
2000	83.117	483.485	564.934	162.898

Table A1.8. Thermodynamic functions of the cluster ions $Ba_2Br_3{}^+$.

T	$c°_p$	$\Phi°$	$S°$	$H°(T)–H°(0)$
298.15	105.978	347.093	436.442	26.640
300	106.004	347.646	437.098	26.836
400	106.904	374.017	467.735	37.487
500	107.326	395.238	491.640	48.201
600	107.558	412.986	511.230	58.946
700	107.698	428.237	527.822	69.710
800	107.789	441.604	542.209	80.484
900	107.851	453.501	554.909	91.266
1000	107.896	464.220	566.274	102.054
1100	107.929	473.973	576.559	112.845
1200	107.954	482.919	585.952	123.639
1300	107.974	491.181	594.593	134.436
1400	107.990	498.857	602.596	145.234
1500	108.002	506.024	610.047	156.034
1600	108.012	512.746	617.017	166.834
1700	108.021	519.074	623.566	177.636
1800	108.028	525.052	629.740	188.439
1900	108.034	530.717	635.581	199.242
2000	108.039	536.100	641.123	210.045

Table A1.9. Thermodynamic functions of the cluster ion $Ba_3Br_5{}^+$.

T	$c°_p$	$\Phi°$	$S°$	$H°(T)–H°(0)$
298.15	179.749	453.813	604.277	44.861
300	179.787	454.744	605.389	45.193
400	181.143	499.200	657.323	63.249
500	181.777	535.022	697.820	81.399
600	182.124	565.003	730.995	99.595
700	182.334	590.774	759.087	117.819
800	182.470	613.369	783.444	136.060
900	182.564	633.484	804.941	154.312
1000	182.631	651.608	824.180	172.572
1100	182.680	668.100	841.589	190.837
1200	182.718	683.230	857.486	209.107
1300	182.748	697.204	872.112	227.381
1400	182.771	710.187	885.656	245.657
1500	182.790	722.310	898.267	263.935
1600	182.805	733.680	910.064	282.214
1700	182.818	744.385	921.147	300.496
1800	182.829	754.498	931.597	318.778
1900	182.838	764.082	941.482	337.061
2000	182.845	773.188	950.861	355.345

Table A1.10. Thermodynamic functions of the cluster ions $Ba_4Br_7^+$.

T	c°_p	Φ°	S°	$H^{\circ}(T)-H^{\circ}(0)$
298.15	253.484	573.607	786.075	63.348
300	253.535	574.922	787.644	63.817
400	255.360	637.683	860.868	89.274
500	256.213	688.237	917.952	114.857
600	256.680	730.537	964.710	140.504
700	256.962	766.890	1004.301	166.187
800	257.146	798.759	1038.626	191.893
900	257.271	827.127	1068.921	217.615
1000	257.362	852.686	1096.032	243.347
1100	257.428	875.941	1120.565	269.086
1200	257.479	897.273	1142.966	294.832
1300	257.519	916.976	1163.577	320.582
1400	257.550	935.280	1182.662	346.335
1500	257.575	952.371	1200.432	372.091
1600	257.596	968.400	1217.057	397.850
1700	257.613	983.491	1232.674	423.611
1800	257.628	997.747	1247.399	449.373
1900	257.640	1011.257	1261.329	475.136
2000	257.650	1024.094	1274.544	500.901

Table A1.11. Thermodynamic functions of the cluster ions $Ba_5Br_9^+$.

T	c°_p	Φ°	S°	$H^{\circ}(T)-H^{\circ}(0)$
298.15	327.189	674.463	949.098	81.883
300	327.254	676.163	951.123	82.488
400	329.559	757.268	1045.630	115.345
500	330.638	822.577	1119.298	148.361
600	331.228	877.210	1179.638	181.457
700	331.584	924.156	1230.725	214.599
800	331.816	965.307	1275.019	247.769
900	331.976	1001.934	1314.111	280.959
1000	332.090	1034.931	1349.094	314.163
1100	332.174	1064.953	1380.750	347.376
1200	332.238	1092.491	1409.655	380.597
1300	332.288	1117.925	1436.251	413.824
1400	332.328	1141.553	1460.877	447.054
1500	332.360	1163.614	1483.807	480.289
1600	332.386	1184.304	1505.258	513.526
1700	332.408	1203.782	1525.409	546.766
1800	332.426	1222.183	1544.410	580.008
1900	332.441	1239.620	1562.383	613.251
2000	332.455	1256.188	1579.436	646.496

Table A1.12. Thermodynamic functions of the BaI^+ ions.

T	c°_p	Φ°	S°	$H^{\circ}(T)-H^{\circ}(0)$
298.15	36.895	235.956	270.233	10.220
300	36.901	236.168	270.462	10.288
400	37.121	246.135	281.112	13.991
500	37.225	253.991	289.408	17.708
600	37.283	260.477	296.200	21.434
700	37.318	266.001	301.950	25.164
800	37.340	270.813	306.935	28.897
900	37.356	275.076	311.334	32.632
1000	37.367	278.902	315.270	36.368

1100	37.375	282.373	318.832	40.105
1200	37.382	285.548	322.085	43.843
1300	37.386	288.476	325.077	47.582
1400	37.390	291.190	327.848	51.321
1500	37.394	293.721	330.427	55.060
1600	37.396	296.091	332.841	58.799
1700	37.398	298.320	335.108	62.539
1800	37.400	300.424	337.246	66.279
1900	37.402	302.416	339.268	70.019
2000	37.403	304.307	341.186	73.759

Table A1.13. Thermodynamic functions of the BaI_3^- ions.

T	c_p°	Φ°	S°	$H^\circ(T)-H^\circ(0)$
298.15	82.358	356.812	431.605	22.299
300	82.367	357.275	432.114	22.452
400	82.704	379.094	455.863	30.708
500	82.861	396.363	474.336	38.987
600	82.947	410.656	489.452	47.278
700	82.999	422.850	502.243	55.575
800	83.033	433.482	513.328	63.877
900	83.056	442.908	523.109	72.181
1000	83.073	451.373	531.861	80.488
1100	83.085	459.056	539.779	88.796
1200	83.095	466.088	547.009	97.105
1300	83.102	472.572	553.661	105.415
1400	83.108	478.587	559.819	113.725
1500	83.112	484.196	565.553	122.036
1600	83.116	489.450	570.917	130.348
1700	83.119	494.392	575.956	138.659
1800	83.122	499.057	580.707	146.972
1900	83.124	503.473	585.202	155.284
2000	83.126	507.667	589.466	163.596

Table A1.14. Thermodynamic functions of the $Ba_2I_3^+$ ions.

T	c_p°	Φ°	S°	$H^\circ(T)-H^\circ(0)$
298.15	106.716	370.277	463.143	27.688
300	106.733	370.851	463.803	27.886
400	107.320	398.120	494.601	38.592
500	107.595	419.902	518.581	49.340
600	107.745	438.034	538.213	60.107
700	107.835	453.562	554.829	70.887
800	107.894	467.141	569.233	81.673
900	107.935	479.204	581.943	92.465
1000	107.964	490.057	593.317	103.260
1100	107.985	499.919	603.608	114.057
1200	108.002	508.957	613.005	124.857
1300	108.014	517.298	621.650	135.658
1400	108.024	525.041	629.655	146.460
1500	108.032	532.267	637.108	157.262
1600	108.039	539.039	644.081	168.066
1700	108.045	545.413	650.631	178.870
1800	108.049	551.432	656.806	189.675
1900	108.053	557.133	662.649	200.480
2000	108.056	562.548	668.191	211.286

Table A1.15. Thermodynamic functions of the $Ba_3I_5^+$ ions.

T	c°_p	Φ°	S°	$H^\circ(T)–H^\circ(0)$
298.15	180.643	485.135	640.439	46.304
300	180.670	486.097	641.557	46.638
400	181.646	531.784	693.686	64.761
500	182.101	568.372	734.274	82.951
600	182.350	598.875	767.499	101.174
700	182.500	625.024	795.620	119.417
800	182.597	647.906	819.996	137.673
900	182.664	668.245	841.507	155.936
1000	182.712	686.551	860.756	174.205
1100	182.748	703.192	878.172	192.478
1200	182.775	718.446	894.074	210.754
1300	182.796	732.526	908.705	229.033
1400	182.813	745.600	922.252	247.313
1500	182.826	757.802	934.865	265.595
1600	182.837	769.241	946.665	283.878
1700	182.846	780.007	957.750	302.162
1800	182.854	790.175	968.201	320.448
1900	182.860	799.807	978.088	338.733
2000	182.866	808.958	987.467	357.020

Table A1.16. Thermodynamic functions of the $Ba_4I_7^+$ ions.

T	c°_p	Φ°	S°	$H^\circ(T)–H^\circ(0)$
298.15	255.074	627.917	849.418	66.041
300	255.106	629.288	850.996	66.512
400	256.254	694.344	924.566	92.089
500	256.789	746.324	981.811	117.744
600	257.081	789.594	1028.658	143.439
700	257.257	826.650	1068.301	169.156
800	257.372	859.051	1102.661	194.888
900	257.450	887.836	1132.980	220.629
1000	257.507	913.731	1160.108	246.377
1100	257.548	937.262	1184.653	272.130
1200	257.580	958.826	1207.064	297.887
1300	257.605	978.724	1227.683	323.646
1400	257.624	997.197	1246.774	349.407
1500	257.640	1014.435	1264.549	375.171
1600	257.653	1030.592	1281.177	400.935
1700	257.664	1045.797	1296.798	426.701
1800	257.673	1060.154	1311.525	452.468
1900	257.680	1073.754	1325.457	478.236
2000	257.687	1086.673	1338.675	504.004

Table A1.17. Thermodynamic functions of the $Ba_5I_9^+$ ions.

T	c°_p	Φ°	S°	$H^\circ(T)–H^\circ(0)$
298.15	329.300	756.009	1043.349	85.670
300	329.340	757.787	1045.386	86.279
400	330.747	842.118	1140.352	119.293
500	331.403	909.425	1214.235	152.404
600	331.760	965.417	1274.691	185.564
700	331.976	1013.346	1325.850	218.752
800	332.117	1055.242	1370.189	251.957
900	332.213	1092.452	1409.312	285.174

1000	332.282	1125.919	1444.318	318.399
1100	332.333	1156.327	1475.991	351.630
1200	332.372	1184.188	1504.909	384.865
1300	332.402	1209.896	1531.514	418.104
1400	332.426	1233.759	1556.149	451.345
1500	332.446	1256.025	1579.085	484.589
1600	332.461	1276.894	1600.541	517.834
1700	332.475	1296.531	1620.697	551.081
1800	332.486	1315.073	1639.701	584.329
1900	332.495	1332.636	1657.677	617.578
2000	332.503	1349.318	1674.732	650.828

Table A1.18. Thermodynamic functions of the $Ba_5Cl_9^+$ ions.

T	c°_p	Φ°	S°	$H^\circ(T)–H^\circ(0)$
298.15	322.669	616.604	873.639	76.635
300	322.786	618.196	875.635	77.232
400	326.988	694.780	969.154	109.749
500	328.975	757.240	1042.357	142.558
600	330.066	809.916	1102.442	175.515
700	330.728	855.436	1153.375	208.558
800	331.159	895.501	1197.568	241.653
900	331.456	931.274	1236.591	274.785
1000	331.668	963.583	1271.525	307.942
1100	331.825	993.038	1303.144	341.117
1200	331.945	1020.100	1332.022	374.306
1300	332.038	1045.130	1358.595	407.505
1400	332.112	1068.410	1383.205	440.713
1500	332.172	1090.169	1406.120	473.927
1600	332.221	1110.593	1427.560	507.147
1700	332.261	1129.837	1447.702	540.371
1800	332.295	1148.028	1466.694	573.599
1900	332.324	1165.277	1484.661	606.830
2000	332.349	1181.676	1501.708	640.063

Table A1.19. Thermodynamic functions of the Ba_2F_4 (C_{3v}) isomer.

T	$c_p^\circ(T)$	$\Phi^\circ(T)$	$S^\circ(T)$	$H^\circ(T)–H^\circ(0)$
298.15	122.420	333.458	425.650	27.487
300	122.535	334.029	426.408	27.714
400	126.815	361.802	462.323	40.208
500	128.953	384.860	490.875	53.008
600	130.160	404.555	514.502	65.968
700	130.904	421.735	534.627	79.024
800	131.394	436.964	552.140	92.141
900	131.732	450.639	567.637	105.298
1000	131.976	463.046	581.530	118.484
1100	132.157	474.398	594.117	131.691
1200	132.296	484.861	605.623	144.914
1300	132.404	494.563	616.217	158.149
1400	132.490	503.607	626.032	171.394

1500	132.559	512.077	635.175	184.647
1600	132.616	520.041	643.732	197.906
1700	132.663	527.556	651.774	211.170
1800	132.703	534.670	659.357	224.438
1900	132.736	541.423	666.533	237.710
2000	132.765	547.850	673.342	250.985

Table A1.20. Thermodynamic functions of the Ba_2F_4 (C_{2v}) isomer.

T	$c_p°(T)$	$\Phi°(T)$	$S°(T)$	$H°(T)-H°(0)$
298.15	122.473	352.268	447.309	28.337
300	122.586	352.856	448.067	28.563
400	126.789	381.338	483.982	41.058
500	128.918	404.820	512.527	53.854
600	130.128	424.796	536.148	66.811
700	130.877	442.176	556.268	79.864
800	131.371	457.556	573.779	92.978
900	131.714	471.347	589.273	106.134
1000	131.960	483.846	603.164	119.318
1100	132.144	495.274	615.750	132.524
1200	132.284	505.800	627.254	145.745
1300	132.394	515.555	637.847	158.979
1400	132.481	524.645	647.662	172.223
1500	132.551	533.155	656.805	185.475
1600	132.609	541.153	665.361	198.733
1700	132.657	548.698	673.402	211.997
1800	132.697	555.839	680.986	225.264
1900	132.731	562.616	688.161	238.536
2000	132.760	569.065	694.970	251.810

Table A1.21. Thermodynamic functions of the Ba_2F_4 (C_{2h}) isomer.

T	$c_p°(T)$	$\Phi°(T)$	$S°(T)$	$H°(T)-H°(0)$
298.15	122.314	350.864	445.402	28.187
300	122.428	351.449	446.159	28.413
400	126.697	379.801	482.040	40.895
500	128.858	403.200	510.568	53.684
600	130.086	423.119	534.180	66.637
700	130.846	440.457	554.294	79.686
800	131.347	455.804	571.801	92.797
900	131.695	469.570	587.293	105.950
1000	131.945	482.049	601.182	119.133
1100	132.131	493.460	613.767	132.337
1200	132.274	503.972	625.270	145.558
1300	132.385	513.715	635.862	158.791
1400	132.473	522.795	645.676	172.034
1500	132.545	531.295	654.818	185.285
1600	132.603	539.285	663.374	198.543
1700	132.652	546.824	671.415	211.805
1800	132.692	553.958	678.998	225.073
1900	132.727	560.730	686.174	238.344
2000	132.756	567.173	692.982	251.618

Table A1.22. Thermodynamic functions of the Ba_2Cl_4 (C_{3v}) isomer.

T	$c_p°(T)$	$\Phi°(T)$	$S°(T)$	$H°(T)-H°(0)$
298.15	128.567	372.514	477.389	31.268
300	128.620	373.163	478.184	31.506
400	130.495	404.292	515.480	44.474
500	131.392	429.558	544.706	57.574
600	131.886	450.809	568.709	70.740
700	132.187	469.142	589.064	83.944
800	132.383	485.261	606.729	97.174
900	132.518	499.641	622.329	110.419
1000	132.615	512.620	636.297	123.676
1100	132.687	524.447	648.940	136.941
1200	132.742	535.310	660.488	150.213
1300	132.784	545.353	671.114	163.489
1400	132.818	554.692	680.956	176.769
1500	132.846	563.418	690.121	190.053
1600	132.868	571.608	698.695	203.338
1700	132.886	579.323	706.751	216.626
1800	132.902	586.615	714.347	229.916
1900	132.915	593.529	721.533	243.206
2000	132.926	600.101	728.351	256.499

Table A1.23. Thermodynamic functions of the Ba_2Cl_4 (C_{2v}) isomer.

T	$c_p°(T)$	$\Phi°(T)$	$S°(T)$	$H°(T)-H°(0)$
298.15	128.633	403.157	510.595	32.032
300	128.684	403.822	511.391	32.270
400	130.524	435.590	548.699	45.243
500	131.408	461.241	577.930	58.344
600	131.896	482.749	601.936	71.512
700	132.194	501.266	622.292	84.717
800	132.389	517.523	639.958	97.947
900	132.522	532.010	655.559	111.193
1000	132.618	545.076	669.527	124.450
1100	132.690	556.973	682.170	137.716
1200	132.744	567.894	693.718	150.988
1300	132.786	577.987	704.345	164.264
1400	132.820	587.369	714.187	177.545
1500	132.847	596.132	723.351	190.828
1600	132.869	604.354	731.926	204.114
1700	132.888	612.098	739.981	217.402
1800	132.903	619.415	747.578	230.691
1900	132.916	626.352	754.764	243.982
2000	132.927	632.944	761.582	257.274

Table A1.24. Thermodynamic functions of the Ba_2Cl_4 (C_{2h}) isomer.

T	$c_p°(T)$	$\Phi°(T)$	$S°(T)$	$H°(T)-H°(0)$
298.15	128.543	399.911	506.907	31.900
300	128.595	400.573	507.702	32.138
400	130.473	432.228	544.990	45.104
500	131.374	457.808	574.212	58.201
600	131.873	479.268	598.212	71.366
700	132.177	497.751	618.565	84.570
800	132.375	513.981	636.229	97.798
900	132.512	528.448	651.829	111.043

1000	132.610	541.496	665.796	124.299
1100	132.683	553.380	678.438	137.564
1200	132.738	564.290	689.986	150.835
1300	132.781	574.373	700.612	164.111
1400	132.815	583.746	710.454	177.391
1500	132.843	592.502	719.618	190.674
1600	132.866	600.717	728.192	203.959
1700	132.885	608.455	736.248	217.247
1800	132.900	615.768	743.844	230.536
1900	132.914	622.699	751.030	243.827
2000	132.925	629.288	757.848	257.119

Table A1.25. Thermodynamic functions of the Ba$_2$Br$_4$ (C_{3v}) isomer.

T	$c_p°(T)$	$\Phi°(T)$	$S°(T)$	$H°(T)-H°(0)$
298.15	130.750	411.387	523.615	33.460
300	130.777	412.081	524.424	33.702
400	131.749	445.109	562.199	46.835
500	132.206	471.580	591.653	60.036
600	132.456	493.663	615.781	73.270
700	132.608	512.605	636.211	86.524
800	132.707	529.188	653.926	99.790
900	132.775	543.933	669.560	113.064
1000	132.823	557.208	683.552	126.344
1100	132.859	569.278	696.213	139.628
1200	132.886	580.345	707.775	152.916
1300	132.908	590.562	718.412	166.205
1400	132.925	600.050	728.263	179.497
1500	132.938	608.907	737.434	192.790
1600	132.949	617.211	746.014	206.085
1700	132.959	625.027	754.074	219.380
1800	132.966	632.409	761.674	232.676
1900	132.973	639.404	768.863	245.973
2000	132.979	646.049	775.684	259.271

Table A1.26. Thermodynamic functions of the Ba$_2$Br$_4$ (C_{2v}) isomer.

T	$c_p°(T)$	$\Phi°(T)$	$S°(T)$	$H°(T)-H°(0)$
298.15	130.840	452.447	566.985	34.149
300	130.866	453.155	567.794	34.391
400	131.798	486.760	605.588	47.531
500	132.237	513.580	635.051	60.735
600	132.478	535.896	659.184	73.972
700	132.624	555.006	679.617	87.227
800	132.719	571.714	697.333	100.495
900	132.784	586.557	712.969	113.770
1000	132.831	599.910	726.962	127.051
1100	132.865	612.045	739.624	140.336
1200	132.892	623.165	751.185	153.624
1300	132.912	633.428	761.823	166.914
1400	132.928	642.955	771.674	180.206
1500	132.942	651.845	780.845	193.500
1600	132.952	660.179	789.426	206.794
1700	132.961	668.021	797.486	220.090
1800	132.969	675.427	805.086	233.386
1900	132.975	682.442	812.276	246.684
2000	132.981	689.105	819.096	259.981

Table A1.27. Thermodynamic functions of the Ba_2Br_4 (C_{2h}) isomer.

T	$c_p°(T)$	$\Phi°(T)$	$S°(T)$	$H°(T)-H°(0)$
298.15	130.814	442.952	557.045	34.016
300	130.841	443.658	557.854	34.258
400	131.783	477.151	595.643	47.396
500	132.228	503.903	625.102	60.599
600	132.471	526.175	649.234	73.835
700	132.619	545.251	669.666	87.090
800	132.715	561.935	687.382	100.357
900	132.781	576.759	703.018	113.632
1000	132.828	590.097	717.010	126.913
1100	132.863	602.219	729.672	140.197
1200	132.890	613.329	741.233	153.485
1300	132.911	623.582	751.871	166.775
1400	132.927	633.102	761.721	180.067
1500	132.941	641.986	770.893	193.361
1600	132.951	650.313	779.473	206.655
1700	132.960	658.150	787.534	219.951
1800	132.968	665.552	795.134	233.247
1900	132.974	672.563	802.323	246.544
2000	132.980	679.223	809.144	259.842

Table A1.28. Thermodynamic functions of the Ba_2I_4 (C_{3v}) isomer.

T	$c_p°(T)$	$\Phi°(T)$	$S°(T)$	$H°(T)-H°(0)$
298.15	131.471	441.646	557.482	34.536
300	131.490	442.363	558.296	34.779
400	132.157	476.311	596.228	47.966
500	132.470	503.355	625.755	61.199
600	132.640	525.830	649.924	74.456
700	132.743	545.056	670.379	87.725
800	132.811	561.854	688.109	101.003
900	132.857	576.769	703.754	114.287
1000	132.890	590.180	717.754	127.574
1100	132.914	602.362	730.421	140.864
1200	132.933	613.523	741.987	154.157
1300	132.947	623.819	752.628	167.451
1400	132.959	633.376	762.481	180.746
1500	132.968	642.292	771.654	194.042
1600	132.976	650.648	780.236	207.340
1700	132.982	658.511	788.298	220.637
1800	132.987	665.934	795.899	233.936
1900	132.992	672.965	803.089	247.235
2000	132.995	679.644	809.911	260.534

Table A1.29. Thermodynamic functions of the Ba_2I_4 (C_{2h}) isomer.

T	$c_p°(T)$	$\Phi°(T)$	$S°(T)$	$H°(T)-H°(0)$
298.15	131.564	489.178	607.147	35.172
300	131.582	489.908	607.961	35.416
400	132.208	524.389	645.913	48.609
500	132.502	551.756	675.450	61.847
600	132.663	574.447	699.623	75.106
700	132.760	593.828	720.081	88.377
800	132.823	610.742	737.813	101.656
900	132.867	625.748	753.460	114.941

1000	132.898	639.231	767.461	128.229
1100	132.921	651.473	780.129	141.520
1200	132.938	662.684	791.695	154.813
1300	132.952	673.022	802.336	168.108
1400	132.963	682.615	812.190	181.404
1500	132.972	691.563	821.363	194.700
1600	132.979	699.946	829.945	207.998
1700	132.985	707.833	838.007	221.296
1800	132.990	715.278	845.609	234.595
1900	132.994	722.328	852.799	247.894
2000	132.997	729.024	859.621	261.194

Appendix A2: The structural properties for the isomers of Ba_2F_4, Ba_2Cl_4, Ba_2Br_4 and Ba_2I_4 and the cluster ion $Ba_5Cl_9^+$.

The internuclear separations, valence angles, dipole moments, total energies and frequencies of normal vibration for the isomers of Ba_2F_4, Ba_2Cl_4, Ba_2Br_4 and Ba_2I_4 and the cluster ion $Ba_5Cl_9^+$ were calculated and presented in Tables A2.1 – A2.12. Note: R_{e1}, R_{e2}, R_{e3} and R_{e4} are the equilibrium internuclear distances, Å; α_e, β_e and γ_e are the valence angles, degs; E is the total energy, au; ω_i are the vibrational frequencies, cm^{-1} and μ_e is the dipole moment, D. The values given in parenthesis near the frequencies are the intensities in IR spectrum in D^{2}amu^{-1}Å^{-2}.

Table A2.1. Properties of the dimer Ba_2F_4 molecule (C_{2v} symmetry).

Property	DFT/B3P86	MP2	Literature data DFT/B3LYP (Levy & Hargittai, 2000)
R_{e1}(Ba–F$_b$)	2.468	2.472	2.479
R_{e2}(Ba–F$_t$)	2.238	2.251	2.244
α_e(F$_b$–Ba–F$_b$)	73.1	72.4	72.6
β_e(F$_t$–Ba–F$_b$)	120.4	121.1	
γ_e(Ba–Ba–F$_t$)	125.6	125.7	126
μ_e	10.5	11.4	10.4
$-E$	450.89174	450.09014	
ω_1 (A_1)	439 (4.2)	436 (4.5)	440
ω_2 (A_1)	299 (0.1)	299 (0.1)	300
ω_3 (A_1)	124 (1.0)	124 (1.1)	124
ω_4 (A_1)	110 (0.01)	111 (0)	111
ω_5 (A_1)	33 (0.1)	34 (0.1)	32
ω_7 (A_2)	252 (0)	265 (0)	256
ω_8 (A_2)	53 (0)	53 (0)	51
ω_9 (B_1)	270 (2.9)	271 (3.0)	268
ω_{10} (B_1)	80 (0.3)	79 (0.3)	77
ω_{11} (B_2)	430 (1.6)	426 (1.6)	432
ω_{12} (B_2)	329 (7.8)	335 (7.9)	331
ω_{13} (B_2)	42 (0.6)	40 (0.7)	36

Table A2.2. Properties of Ba_2F_4 (C_{2h}) isomer.

Property	DFT	MP2	Literature data DFT/B3LYP (Levy & Hargittai, 2000)
R_{e1}(Ba–F$_b$)	2.458	2.462	2.468
R_{e2}(Ba–F$_t$)	2.239	2.252	2.245
α_e(F$_b$–Ba–F$_b$)	73.3	72.6	72.8
β_e(F$_t$–Ba–F$_b$)	114.7	115.2	
γ_e(Ba–Ba–F$_t$)	121.4	121.9	113.3
μ_e	0.0	0.0	

$-E$	450.89467	450.09313	
$\omega_1\,(A_g)$	437 (0)	431 (0)	436
$\omega_2\,(A_g)$	303 (0)	302 (0)	303
$\omega_3\,(A_g)$	115 (0)	115 (0)	116
$\omega_4\,(A_g)$	54 (0)	50 (0)	50
$\omega_5\,(B_g)$	258 (0)	269 (0)	260
$\omega_6\,(B_g)$	92 (0)	89 (0)	88
$\omega_7\,(A_u)$	272 (2.9)	274 (3.0)	270
$\omega_8\,(A_u)$	57 (1.0)	54 (1.0)	54
$\omega_9\,(B_u)$	434 (5.7)	428 (5.9)	434
$\omega_{10}\,(B_u)$	335 (8.0)	341 (8.2)	336
$\omega_{11}\,(B_u)$	130 (1.0)	129 (1.1)	129
$\omega_{12}\,(B_u)$	31 (0.7)	26 (0.7)	18

Table A2.3. Properties of Ba_2F_4 (D_{2h}) isomer.

Property	DFT	MP2	Literature data DFT/B3LYP (Levy & Hargittai, 2000)
$R_{e1}(Ba–X_b)$	2.500	2.504	2.510
$R_{e2}(Ba–X_t)$	2.264	2.278	2.270
$\alpha_e(X_b–Ba–X_b)$	75.1	74.2	74.8
$\beta_e(X_t–Ba–X_b)$	142.4	142.9	
μ_e	0.0	0.0	
$-E$	450.88492	450.08467	
$\omega_1\,(A_g)$	430 (0)	425 (0)	429
$\omega_2\,(A_g)$	290 (0)	288 (0)	292
$\omega_3\,(A_g)$	95 (0)	96 (0)	97
$\omega_4\,(B_{2g})$	52i	47i (0)	63i
$\omega_5\,(B_{3g})$	238 (0)	252 (0)	242
$\omega_6\,(B_{3g})$	43 (0)	42 (0)	36
$\omega_7\,(B_{1u})$	417 (6.5)	412 (6.3)	416
$\omega_8\,(B_{1u})$	308 (8.1)	316 (8.2)	310
$\omega_9\,(B_{2u})$	280 (3.0)	278 (3.1)	277
$\omega_{10}\,(B_{2u})$	39 (1.0)	37 (1.0)	31
$\omega_{11}\,(B_{3u})$	92 (1.0)	93 (1.0)	91
$\omega_{12}\,(B_{3u})$	44i	38i (1.7)	54i

Table A2.4. Properties of the dimer Ba_2Cl_4 molecule (C_{3v} symmetry).

Property	DFT/B3P86	MP2	Literature data DFT/B3LYP (Levy & Hargittai, 2000)
$R_{e1}(Ba_1–X_b)$	3.106	3.091	3.137
$R_{e2}(Ba_2–X_b)$	2.854	2.854	2.881
$R_{e3}(Ba_1–X_t)$	2.777	2.789	2.798
$\alpha_e(X_t–Ba_1–X_b)$	134.0	134.3	134.3
$\beta_e(X_b–Ba_2–X_b)$	85.3	84.3	84.9
μ_e	13.1	14.5	13.4
$-E$	1892.36350	1889.94801	
$\omega_1\,(A_1)$	255 (2.3)	256 (2.2)	251 (2.2)
$\omega_2\,(A_1)$	238 (1.1)	240 (1.4)	234 (1.0)
$\omega_3\,(A_1)$	160 (1.6)	167 (1.4)	157 (1.6)

ω_4 (A_1)	85 (0.03)	86 (0.03)	86 (0.02)
ω_5 (E)	214 (3.0)	217 (3.0)	209 (2.9)
ω_6 (E)	120 (0.02)	132 (0.2)	117 (0.1)
ω_7 (E)	83 (0.7)	82 (0.7)	84 (0.8)
ω_8 (E)	30 (0.2)	31 (0.2)	30 (0.2)

Table A2.5. Properties of the dimer Ba_2Cl_4 molecule (C_{2v} symmetry).

Property	DFT/B3P86	MP2	Literature data DFT/B3LYP (Levy & Hargittai, 2000)
$R_{e1}(Ba–X_b)$	2.976	2.976	3.003
$R_{e2}(Ba–X_t)$	2.750	2.761	2.769
$\alpha_e(X_b–Ba–X_b)$	81.5	80.5	81.2
$\beta_e(X_t–Ba–X_b)$	129.6	130.7	
$\gamma_e(Ba–Ba–X_t)$	144.5	144.9	145.0
μ_e	9.0	9.5	9.0
$-E$	1892.35232	1889.93224	
ω_1 (A_1)	271 (1.0)	269 (1.1)	266
ω_2 (A_1)	189 (0.0003)	189 (0.0002)	185
ω_3 (A_1)	69 (0.2)	70 (0.1)	70
ω_4 (A_1)	60 (0.5)	61 (0.6)	62
ω_5 (A_1)	16 (0.2)	11 (0.2)	10
ω_6 (A_2)	163 (0)	170 (0)	158
ω_7 (A_2)	37 (0.2)	36 (0)	35
ω_8 (B_1)	186 (1.6)	187 (1.6)	181
ω_9 (B_1)	38 (0)	37 (0.3)	35
ω_{10} (B_2)	262 (3.5)	261 (3.6)	258
ω_{11} (B_2)	195 (2.9)	199 (2.8)	190
ω_{12} (B_2)	17 (0.2)	13 (0.2)	11

Table A2.6. Properties of Ba_2Cl_4 (C_{2h}) isomer.

Property	DFT	MP2	Literature data DFT/B3LYP (Levy & Hargittai, 2000)
$R_{e1}(Ba–X_b)$	2.966	2.966	2.994
$R_{e2}(Ba–X_t)$	2.746	2.757	2.765
$\alpha_e(X_b–Ba–X_b)$	81.5	80.6	81.3
$\beta_e(X_t–Ba–X_b)$	123.5	124.7	
$\gamma_e(Ba–Ba–X_t)$	136.8	138.4	137.4
μ_e	0.0	0.0	
$-E$	1892.35355	1889.93338	
ω_1 (A_g)	270 (0)	268 (0)	265
ω_2 (A_g)	191 (0)	192 (0)	187
ω_3 (A_g)	71 (0)	73 (0)	72
ω_4 (A_g)	25 (0)	23 (0)	25
ω_5 (B_g)	166 (0)	172 (0)	159
ω_6 (B_g)	47 (0)	46 (0)	47
ω_7 (A_u)	187 (1.6)	188 (1.6)	181

ω_8 (A_u)	30 (0.4)	30 (0.5)	32
ω_9 (B_u)	264 (4.3)	262 (4.5)	260
ω_{10} (B_u)	200 (3.1)	203 (2.9)	193
ω_{11} (B_u)	64 (0.6)	65 (0.7)	66
ω_{12} (B_u)	14 (0.3)	13 (0.4)	14

Table A2.7. Properties of Ba_2Cl_4 (D_{2h}) isomer.

Property	DFT	MP2	Literature data DFT/B3LYP (Levy & Hargittai, 2000)
R_{e1}(Ba–X_b)	2.988	2.988	3.015
R_{e2}(Ba–X_t)	2.759	2.771	2.779
α_e(X_b–Ba–X_b)	82.1	80.6	81.7
β_e(X_t–Ba–X_b)	139.0	139.9	
μ_e	0.0	0.0	
$-E$	1892.35149	1889.93199	
ω_1 (A_g)	268 (0)	268 (0)	264
ω_2 (A_g)	188 (1.6)	189 (1.6)	183
ω_3 (A_g)	62 (0)	66 (0)	65
ω_4 (B_{2g})	22i (0)	17i (0)	22
ω_5 (B_{3g})	161 (0)	170 (0)	156
ω_6 (B_{3g})	36 (0)	35 (0)	37
ω_7 (B_{1u})	259 (5.3)	259 (5.4)	255 (5.1)
ω_8 (B_{1u})	190 (2.6)	196 (2.4)	185 (2.6)
ω_9 (B_{2u})	185 (0)	188 (0)	183 (1.6)
ω_{10} (B_{2u})	27 (0.4)	27 (0.5)	28 (0.4)
ω_{11} (B_{3u})	53 (0.7)	56 (0.8)	55 (0.8)
ω_{12} (B_{3u})	13i (0.7)	7i (0.6)	12 (0.7)

Table A2.8. Properties of the dimer Ba_2X_4 (X = Br or I) molecule (C_{3v} symmetry).

Property	Ba_2Br_4		Ba_2I_4	
	DFT	MP2	DFT	MP2
R_{e1}(Ba_1–X_b)	3.265	3.257	3.497	3.481
R_{e2}(Ba_2–X_b)	3.013	3.020	3.247	3.252
R_{e3}(Ba_1–X_t)	2.933	2.940	3.166	3.183
α_e(X_t–Ba_1–X_b)	132.7	132.6	131.0	131.3
β_e(X_b–Ba_2–X_b)	87.2	86.8	89.4	88.3
μ_e	13.3	14.7	13.6	15.3
$-E$	105.21149	104.36901	97.35592	96.43000
ω_1 (A_1)	185 (1.2)	225 (1.3)	152 (1.0)	155 (1.0)
ω_2 (A_1)	167 (1.0)	166 (1.4)	131 (0.8)	135 (0.9)
ω_3 (A_1)	106 (0.5)	100 (0.06)	79 (0.2)	81 (0.2)
ω_4 (A_1)	68 (0.03)	65 (0.008)	53 (0.02)	53 (0.02)
ω_5 (E)	151 (1.7)	152 (1.8)	122 (1.3)	125 (1.4)
ω_6 (E)	86 (0.1)	89 (0.1)	71 (0.1)	77 (0.1)
ω_7 (E)	54 (0.3)	54 (0.3)	38 (0.2)	37 (0.2)
ω_8 (E)	22 (0.05)	20 (0.06)	16 (0.02)	16 (0.03)

Table A2.9. Properties of the dimer Ba_2X_4 (X = Br or I) molecule (C_{2v} symmetry).

Property	Ba_2Br_4		Ba_2I_4	
	DFT	MP2	DFT	MP2
$R_{e1}(Ba–X_b)$	3.138	3.139	3.374	3.376
$R_{e2}(Ba–X_t)$	2.908	2.925	3.143	3.164
$\alpha_e(X_b–Ba–X_b)$	84.3	83.2	87.9	86.6
$\beta_e(X_t–Ba–X_b)$	131.4	137.5	134.0	136.7
μ_e	7.7	3.3	4.6	0.5
$–E$	105.20063	104.35382	97.34550	96.41516
ω_1	194 (0.4)	195 (0.06)	160 (0.1)	162 (0.001)
ω_2	185 (3.2)	186 (3.9)	152 (3.1)	154 (3.3)
ω_3	134 (1.0)	136 (1.0)	111 (0.7)	115 (0.7)
ω_4	126 (0.9)	125 (0.5)	91 (0)	97 (0)
ω_5	125 (0.02)	120 (0.006)	91 (0.01)	91 (0.0002)
ω_6	113 (0)	118 (0)	89 (0.3)	91 (0.2)
ω_7	52 (0.1)	49 (0.05)	37 (0.1)	38 (0.003)
ω_8	39 (0.3)	38 (0.5)	27 (0.3)	30 (0.4)
ω_9	27 (0)	27 (0)	21 (0)	20 (0)
ω_{10}	23 (0.1)	17 (0.2)	14 (0.1)	13 (0.1)
ω_{11}	8 (0.1)	3i (0.01)	6 (0.1)	4 (0.1)
ω_{12}	7 (0.1)	11i (0.02)	4i (0.007)	5i (0.0002)

Table A2.10. Properties of Ba_2X_4 (X = Br or I) molecule (C_{2h}) isomer.

Property	Ba_2Br_4		Ba_2I_4	
	DFT	MP2	3.366	3.374
$R_{e1}(Ba–X_b)$	3.128	3.124	3.140	3.162
$R_{e2}(Ba–X_t)$	2.905	2.915	87.8	86.7
$\alpha_e(X_b–Ba–X_b)$	84.3	83.2	129.0	134.2
$\beta_e(X_t–Ba–X_b)$	125.1	127.4	0.0	0.0
μ_e	0.0	0.0	97.34585	96.41517
$–E$	105.20148	104.35442	158 (0)	161 (0)
ω_1	191 (0)	194 (0)	151 (3.0)	154 (3.2)
ω_2	185 (3.3)	188 (3.4)	111 (0.7)	114 (0.7)
ω_3	134 (1.0)	136 (1.0)	95 (0)	97 (0)
ω_4	131 (1.1)	134 (1.0)	94 (0.5)	94 (0)
ω_5	128 (0)	127 (0)	92 (0)	93 (0.3)
ω_6	114 (0)	120 (0)	39 (0)	39 (0)
ω_7	55 (0)	53 (0)	30 (0.3)	30 (0.4)
ω_8	42 (0.4)	43 (0.4)	22 (0)	20 (0)
ω_9	31 (0)	29 (0)	13 (0.1)	12 (0.1)
ω_{10}	20 (0.2)	18 (0.2)	11 (0)	7 (0)
ω_{11}	18 (0)	14 (0)	6 (0.1)	4 (0.1)
ω_{12}	9 (0.2)	10i (0)	3.366	3.374

Table A2.11. Properties of Ba_2X_4 (X = Br or I) molecule (D_{2h}) isomer.

Property	Ba$_2$Br$_4$		Ba$_2$I$_4$	
	DFT	MP2	DFT	MP2
R_{e1}(Ba–X$_b$)	3.146	3.140	3.376	3.377
R_{e2}(Ba–X$_t$)	2.915	2.925	3.145	3.164
α_e(X$_b$–Ba–X$_b$)	84.8	83.2	88.1	86.7
β_e(X$_t$–Ba–X$_b$)	137.6	138.4	136.0	136.7
μ_e	0.0	0.0	0.0	0.0
$-E$	105.20031	104.35383	97.34548	96.41516
ω_1	194 (0)	195 (0)	159 (0)	162 (0)
ω_2	185 (4.0)	186 (4.1)	151 (3.3)	154 (3.3)
ω_3	136 (0.9)	136 (1.0)	111 (0.7)	115 (0.7)
ω_4	122 (0.7)	124 (0.5)	91 (0)	97 (0)
ω_5	122 (0)	120 (0)	89 (0)	90 (0.2)
ω_6	113 (0)	118 (0)	87 (0.3)	90 (0)
ω_7	48 (0)	47 (0)	36 (0)	36 (0)
ω_8	37 (0.5)	39 (0.5)	26 (0.4)	30 (0.4)
ω_9	27 (0)	26 (0)	21 (0)	20 (0)
ω_{10}	19 (0.2)	16 (0.2)	13 (0.1)	12 (0.1)
ω_{11}	4i (0.3)	11 (0.3)	4i (0.2)	6i (0.1)
ω_{12}	14i (0)	10 (0)	12i (0)	6i (0)

Table A2.12. Properties of the positive cluster ion $Ba_5Cl_9^+$ (D_{3h}).

Property	DFT/B3P86	Property	DFT/B3P86
R_{e1}(Ba–Cl$_h$)	3.405	ω_7 (A_1')	49 (0)
R_{e2}(Ba$_h$–Cl$_h$)	3.131	ω_8 (A_1')	43 (0)
R_{e3}(Ba$_h$–Cl)	2.955	ω_9 (A_2'')	208 (6.7)
R_{e4}(Ba–Cl)	3.022	ω_{10} (A_2'')	172 (0.00)
α_e(Cl$_h$-Ba-Cl$_h$)	71.1	ω_{11} (A_2'')	112 (0.6)
β_e(Cl-Ba$_h$-Cl)	157.2	ω_{12} (A_2'')	62 (0.3)
γ_e(Cl–Ba–Cl)	119.5	ω_{13} (E')	211 (5.1)
$-E$	4269.67061	ω_{14} (E')	179 (5.1)
q(Ba$_h$)	0.932	ω_{15} (E')	165 (0.04)
q(Ba)	0.877	ω_{16} (E')	106 (0.9)
$-q$(Cl$_h$)	0.331	ω_{17} (E')	79 (0.8)
$-q$(Cl)	0.417	ω_{18} (E')	55 (0.7)
ω_1 (A_1')	192 (0)	ω_{19} (E')	38 (0.1)
ω_2 (A_1')	172 (0)	ω_{20} (E'')	200 (0)
ω_3 (A_1')	153 (0)	ω_{21} (E'')	163 (0)
ω_4 (A_1')	142 (0)	ω_{22} (E'')	112 (0)
ω_5 (A_1')	96 (0)	ω_{23} (E'')	62 (0)
ω_6 (A_1')	49 (0)	ω_{24} (E'')	41 (0)